AD-A143 277 EXPERIMENTS ON INTERACTION OF KEV PARTICLE BEAMS WITH THE IONOSPHERE(U) PHOTOMETRICS INC WOBURN MA I L KOFSKY ET AL. 31 AUG 83 PHM-TR-83-01 1/2

UNCLASSIFIED AFGL-TR-83-0316 F19628-80-C-0133 F/G 4/1 NL

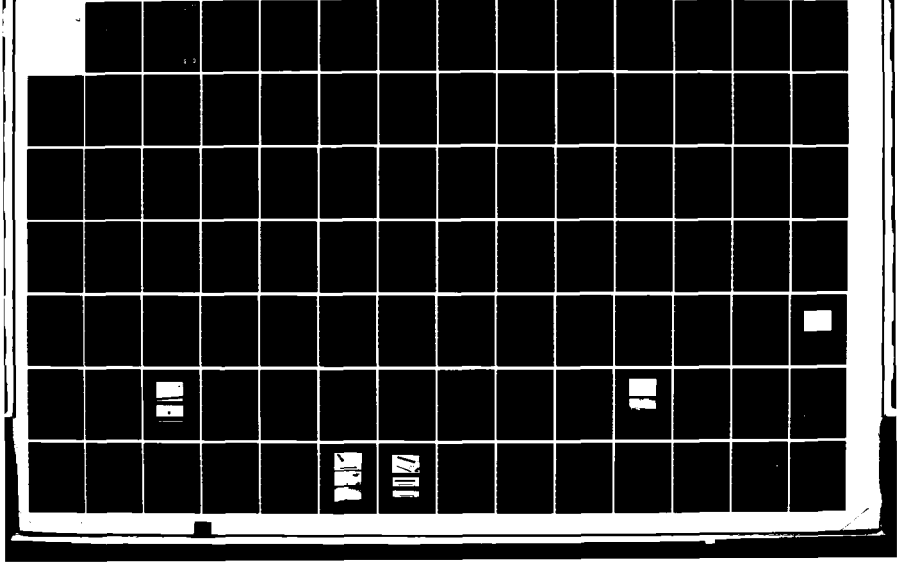

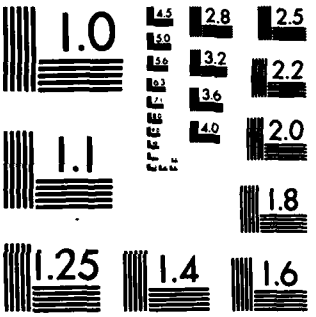

12

AFGL-TR-83-0316

EXPERIMENTS ON INTERACTION OF keV PARTICLE BEAMS WITH THE IONOSPHERE

I.L. Kofsky
D.P. Villanucci
J.L. Barrett
M.T. Chamberlain
R.B. Sluder

PhotoMetrics, Inc.
4 Arrow Drive
Woburn, MA 01801

31 August 1983

Final Report
1 August 1980 - 31 July 1983

Approved for public release; distribution unlimited

Prepared for

AIR FORCE GEOPHYSICS LABORATORY
AIR FORCE SYSTEMS COMMAND
UNITED STATES AIR FORCE
HANSCOM AFB, MASSACHUSETTS 01731

This report has been reviewed by the ESD Public Affairs Office (PA) and is releasable to the National Technical Information Service (NTIS).

This technical report has been reviewed and is approved for publication.

HERBERT A. COHEN
Contract Manager

IRVING MICHAEL, Acting Chief
Space Plasmas and Fields Branch

FOR THE COMMANDER

RITA C. SAGALYN, Director
Space Physics Division

Qualified requestors may obtain additional copies from the Defense Technical Information Center. All others should apply to the National Technical Information Service.

If your address has changed, or if you wish your name to be removed from the mailing list, or if the addressee is no longer employed by your organization, please notify AFGL/DAA, Hanscom AFB, MA 01731. This will assist us in maintaining a current mailing list.

Do not return copies of this report unless contractual obligation or notices on a specific document requires that it be returned.

Unclassified

SECURITY CLASSIFICATION OF THIS PAGE (When Data Entered)

REPORT DOCUMENTATION PAGE		READ INSTRUCTIONS BEFORE COMPLETING FORM
1. REPORT NUMBER AFGL-TR-83-0316	2. GOVT ACCESSION NO. AD-A143 277	3. RECIPIENT'S CATALOG NUMBER
4. TITLE (and Subtitle) EXPERIMENTS ON INTERACTION OF keV PARTICLE BEAMS WITH THE IONOSPHERE		5. TYPE OF REPORT & PERIOD COVERED Final 1 Aug 80 - 31 July 83 6. PERFORMING ORG. REPORT NUMBER PhM-TR-83-01
7. AUTHOR(s) I.L. Kofsky M.T. Chamberlain D.P. Villanucci R.B. Sluder J.L. Barrett		8. CONTRACT OR GRANT NUMBER(s) F19628-80-C-0133
9. PERFORMING ORGANIZATION NAME AND ADDRESS PhotoMetrics, Inc. 4 Arrow Drive Woburn, MA 01801		10. PROGRAM ELEMENT, PROJECT, TASK AREA & WORK UNIT NUMBERS 62101F 760114AC
11. CONTROLLING OFFICE NAME AND ADDRESS Air Force Geophysics Laboratory Hanscom AFB, Massachusetts 01731 1Lt. William K. Kaneshiro/PHG/Monitor		12. REPORT DATE 31 August 1983 13. NUMBER OF PAGES 144
14. MONITORING AGENCY NAME & ADDRESS(if different from Controlling Office)		15. SECURITY CLASS. (of this report) Unclassified 15a. DECLASSIFICATION/DOWNGRADING SCHEDULE N/A

16. DISTRIBUTION STATEMENT (of this Report)

Approved for public release; distribution unlimited

17. DISTRIBUTION STATEMENT (of the abstract entered in Block 20, if different from Report)

18. SUPPLEMENTARY NOTES

19. KEY WORDS (Continue on reverse side if necessary and identify by block number)

Electron beams in space
Ion beams in space
Beam plasma interactions
Rocket photometry
Air fluorescence
Upper atmosphere

20. ABSTRACT (Continue on reverse side if necessary and identify by block number)

Design and construction of photometric instruments for the SCEX and BERT-1 upper-atmospheric energetic particle injection experiments is described, and results of a preliminary analysis of N_2 Second Positive band irradiances measured at SCEX are presented. The ∿keV electron and ion beams ejected from BERT-1 (Beam Emission Rocket Test, scheduled for launch in 1985) will

DD FORM 1 JAN 73 1473 EDITION OF 1 NOV 65 IS OBSOLETE

Unclassified

SECURITY CLASSIFICATION OF THIS PAGE (When Data Entered)

20. Abstract (continued)

lie in the wide fields of radiometrically-calibrated low-light level video cameras and photometers, and a narrow-field photometer will measure air fluorescence in the space plasma surrounding the vehicle. The SCEX (Several Compatible [beam interaction] Experiments) rocket data show the volume excitation by 1-100 milliampere beams of 2-8 keV electrons to be virtually independent of ambient atmospheric density above ∿180 km altitude (in agreement with results from previous experiments), and also of the electrons' kinetic energy (a new finding); both observations are inconsistent with independent, linear propagation of the beam particles. The complete set of irradiances measured by SCEX's 3805Å-band photometer has been put on computer tape in a form suitable for determining their dependence on single and multiple experiment variables, for detailed analysis of the collective interactions of the beam with the ionospheric and induced plasma.

FOREWORD

This is the Final Report on a program of optical diagnosis of the interaction with the ionosphere of beams of keV charged particles ejected from AFGL and NASA rockets. A preliminary analysis of photometer data on fluorescence excited by electrons injected between 170 and 250 km (in the SCEX experiment) is reported, and design and construction of an optical remote-sensing system for Air Force Geophysics Laboratory's BERT-1 program is described and the individual instruments documented.

The SCEX data have been put in a form suitable for detailed computer-assisted analysis of the information they contain about beam interactions and propagation, and three instruments have been calibrated and delivered for further environmental testing and installation on the BERT-1 sounding rocket.

The SCEX and BERT-1 projects are described in Sections II and III, and further theoretical contributions to AFGL's particle beam- and vehicle-interactions program made during the course of the work appear in Appendixes I-IX. Earlier work for AFGL by PhotoMetrics on rocket photometry of injected particle beams is reported in Ref's 2,20, and AFGL-TR-78-0082, AD A058469 ("Photographic Measurements of Electrical Discharges," (1978) by R.B. Sluder), and AFGL-TR-79-0195, AD A092705 ("Data Analysis of Films from AFGL Rocket A32.603," (1979) by M.T. Chamberlain).

The authors were assisted by J.J. Costa, who was responsible for much of the mechanical design of the instruments, and Mrs. C.C. Rice, who typed the manuscript. The support and encouragement of H.A. Cohen and his colleagues of AFGL/PHG Branch is gratefully acknowledged.

TABLE OF CONTENTS

LIST OF ILLUSTRATIONS

LIST OF ILLUSTRATIONS (concluded)

LIST OF TABLES

SECTION I

INTRODUCTION AND SUMMARY

PURPOSE

The purpose of the program reported here is to study the interaction of beams of energetic (several keV's) electrons and ions with the upper atmosphere by optical sensing from onboard the rocket from which they are injected. Particle trajectories, return current paths, development of plasma sheaths, and other collective (beam-plasma) interactions that result in instabilities and discharge phenomena in the vehicle's vicinity are considered. The photometric and imaging instruments complement those making direct in situ measurements of particle densities and energy distributions, rocket potential, and spectrums of electromagnetic radiation in the charge-injection experiments.

PROJECTS

The work consisted of operating and analyzing the data from air fluorescence photometers and a video camera on an electron-injection rocket that was flown in January 1982, and specifying and constructing a system of photometers and low light level video camera for a more sophisticated follow-on experiment to be performed by Air Force Geophysics Laboratory in Fall 1984. These efforts are described in Sections II and III respectively. Supporting theoretical work on excitation of the thermosphere by charged-particle beams (and related technical issues), which has been submitted to AFGL during the course of the program, is included as a series of appendixes to this report.

RESULTS

The SCEX rocket, flown to an apogee of 241 km on the night of 26 Jan 1982 at Churchill Research Range, MB (Canada), returned irradiance data from a photometer sensitive to a Second Positive fluorescence band of N_2 that was pointed to intercept the air volumes excited by narrow beams of 1-100 milliampere, 2-8 kilovolt electrons ejected from the rocket. We analyzed the signal intensities at the higher altitudes of the trajectory (above 168 km on upleg) with the aid of a computer program that quantitatively takes into account the effects of ambient N_2 density, beam current and voltage (which determine the volume rates of ionization and excitation), and paths of the geomagnetically-guided primary particles through the instrument's field of view. The measured radiant intensities are found to be not consistent with a model of independently-acting electrons dissipating their kinetic energy in the undisturbed ambient atmosphere. (Similar nonlinear effects with virtual independence of the radiation on local air density have been observed in other charge-injection experiments.) Further interpretation of the SCEX photometer data, with inclusion of results from the lower downleg altitudes, is expected to indicate the role of collective interactions of the beam with the ionospheric and induced plasma and the (related) effect of outgassing from the rocket body.

An optical remote sensing system consisting of an ISIT (ultrasensitive, essentially photon noise limited) video camera, two wide-field fast response air fluorescence photometers, and a photometer pointed to measure the radiance of plasma sheaths developing near the rocket body has been specified, constructed, and calibrated. The instruments are designed for integration into AFGL's BERT-1 vehicle, which will inject beams of 1/2 - 2 keV electrons and 0.1 - 5 keV

positive monatomic ions at altitudes to 250 km (and from which various other probes will measure beam interaction properties). The optical system is intended (principally) to determine the onset of air breakdown associated with neutralization of the charged beam and rocket, from its measurements of the spatial distribution and total intensity of N_2 fluorescence at wavelengths below ~5500Å. This hardware, which is documented in this report, is now undergoing vibration, vacuum, and other rocket environment qualification tests at AFGL.

SECTION II

THE SCEX PROGRAM

CONTEXT

SCEX (Several Compatible Experiments Using a Rocketborne Electron Accelerator) was sponsored jointly by the National Aeronautics and Space Administration and Canada's National Research Council, with Prof. Paul J. Kellogg of the University of Minnesota's School of Physics and Astronomy as Principal Investigator. Its objectives included study of the beam-plasma discharge (Ref's 1,2,3,4) in the near space environment, vehicle neutralization, and radiofrequency wave emission stimulated in the ionosphere by the injected beam (and also magnetospheric and auroral-ionospheric phenomena to whose understanding optical measurements make no substantive contribution). Six individual scientific groups, including AFGL, provided instrumentation for the rocket experiment, with a separate engineering group responsible for telemetry of the data and other teams operating groundbased equipment to characterize auroral conditions and monitor RF emissions.

PhotoMetrics, under Air Force Geophysics Laboratory contract and technical direction, integrated and operated two filter photometers and a low light level video camera. Other diagnostic instrumentation, much of which was on platforms separated from the electron ejection ("mother") rocket, included energetic-particle spectrometers, a low energy electron spectrometer (retarding potential analyzer), Langmuir probe, vehicle potential monitor, electric field probes, and radiofrequency receivers. This rocket experiment (for which an experimenters' data package has been prepared by the Minnesota group, but

which has not been referenced in the journal literature at the time of this report) was one of a NASA/NRC beam injection series that included launches on 08 Apr 78 (27.010AE) and 03 Dec 79 (results from which are analyzed in Ref 5).

ROCKET VEHICLE, ELECTRON INJECTION

Launch of the Black Brant VC rocket (27.045UE) took place at 0352:20.8 UT on 27 January 1982, at Churchill Research Range. A moderately strong auroral arc system was reported south of the station (that is, in the direction of the trajectory), and was seen as a modulation of the photometer's signal as the instrument's field of view slowly swept in elevation and azimuth. The trajectory plane was at 140°T (southeastward), mean horizontal velocity was 0.6 km/sec, and apogee of 241 km was reached at 255 sec after launch. Data were taken between 168 km altitude on upleg (127 sec) and 82 km on downleg (416 sec).

The 900-lb payload rocket consisted of an aft section that carried the accelerator and the optical and some of the other instruments, a forward section which was separated about 2 min after launch, and four so-called throw-away detector packages. Instrumentation on these outlying platforms, measured the spatial distribution of induced-plasma properties (at distances that increase with time after their separation). The pitch, roll, and yaw motion of the aft section caused the pitch angle of the electron beam relative to the geomagnetic field to cycle between 8° and 140°, as shown in Figure 1.

The electron beam was ejected at 45° from the rocket's long axis (in the direction away from the optical instruments) in the plane defined by this axis and the optic axes of the photometers. Its initial total divergence is estimated at less than 10° full angle. The accelerator sequences three currents at 1.9 kV, 4 kV, and 8 kV anode cathode potential difference, in the following program:

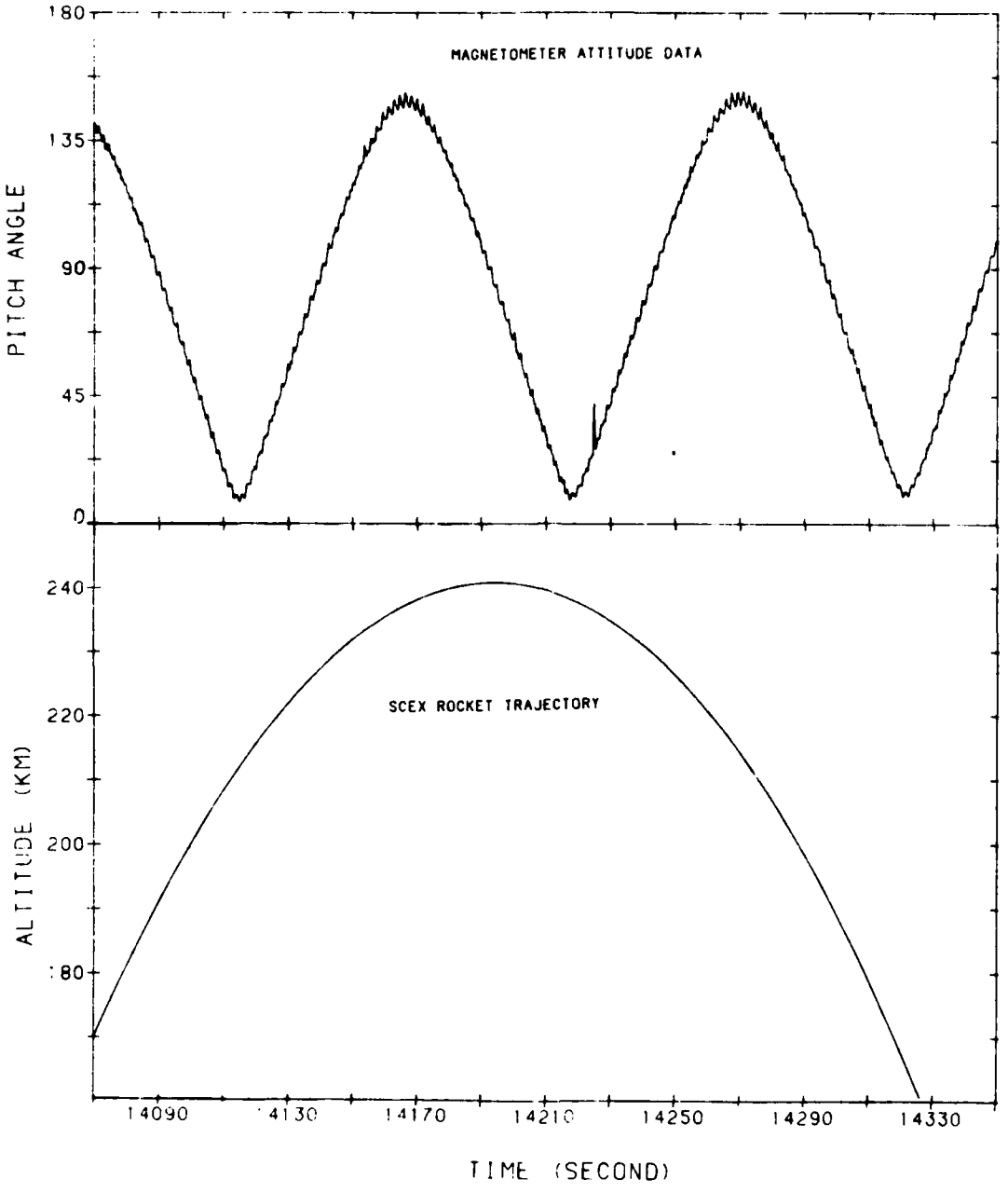

Figure 1. Altitude and pitch angle of SCEX's ejected electron beam. Launch is at 13940.8 sec UT.

100 millisec off (after the voltage is turned on)
50 msec 1 milliampere
100 msec off
50 msec 10 ma
100 msec off
50 msec maximum achievable current
(repeat at next accelerating voltage).

Thus beam electrons with the same kinetic energy are ejected over 0.45 sec, with a full voltage cycle repeated each 1.35 sec. Maximum current from the electron accelerator varied between 43 and 87 milliamps during flight, which provides further opportunity for determining the dependence of the optical signal on injected current. The accelerator currents and voltages were monitored and telemetered as part of the experiment.

PROGRAM TIMETABLE AND PARTICIPATION

PhotoMetrics' work on SCEX began 01 August 1980. At that time payload integration was scheduled to start on 01 December at Goddard Space Flight Center, with launch planned for early 1981. Two recently-built photometers with 30° nominal field of view were GFE'd to PhotoMetrics by AFGL in November 1980, and PhotoMetrics placed on order a ITT (Fort Wayne, IN) F4546 low light-level video camera just after the program started. As delivery of this camera was promised for February 1981, a similar but low-sensitivity dummy camera (GE TN2500, unintensified) was obtained to assist mechanical and electrical interfacing of the on-order camera to the rocket.

At this phase of the program the optic axes of the photometers had been scheduled to point at 20° and 70° elevation from the payload's forward (long) axis, in the plane formed

by this axis and that of the ejected electron beam, with the photometers' objective lenses 1-1/4 m from the accelerator anode. Both instruments were to be sensitive to the (0,0) band of the N_2^+ First Negative (B→X) system, which extends ~15 Å below its P branch head at 3914 Å. The rate of excitation of this band, as is well known, remains very closely proportional to the rate of ionizations from N_2 by electrons of energy greater than 28 eV. The rationale for using two essentially-identical photometers, only one of whose fields would intercept the initial (undeflected) beam axis was, that the ratio of signals would in some way indicate the onset of a collective interaction of the beam with the ambient atmosphere, which is known (Ref 4) to spread the beam laterally. That is, the photometers would serve as a "camera" having two relatively wide-angle and non-touching picture elements.

Insofar as the primary electron beam is guided through their fields of view by the earth's magnetic field, the ratio of photometer signals is by no means an unambiguous measure of interaction/energy dissipation nonlinearities. Further, the video camera is available to measure the spatial distribution of atmospheric excitation, which is one of the characteristic signatures of beam-plasma discharge. Hence we suggested that the two photometers be applied to measure a spectroscopic signature of the discharge, the magnitudes and (in particular) ratio of intensities in two air fluorescence features. Serving as a "spectrometer" with two sensitivity bands, the instruments would determine an effective temperature of the beam from the relative rates of emission of nitrogen molecule bands having known (energy-dependent) impact excitation cross-sections; the absolute intensities are a further indication of discharge initiation (as in the experiments reported in Ref 1).

The second fluorescence band selected was the 0,2 transition of the N_2 Second Positive (C→B) system below 3805Å.

We specified an interference filter isolating this band, and installed it in one of the photometers. The photometers were coaligned to point at 20° elevation, mounted at a point 119 cm from the accelerator and so that the optical and ejected-beam axes intercept some 75 cm from the electron accelerator (refer to Figure 3, shown later). This change required some mechanical reconfiguration of the rocket. The expected 3805Å/3914Å intensity ratios are discussed in a later subsection of Section II.

A change in the pointing direction of the video camera was suggested by Prof. Kellogg on the basis of computer-assisted calculations of the trajectories the 2,4, and 8 keV electrons through its field of view as a function of their injection pitch angle. With the assistance of Dr. Charles K. Crawford of Kimball Physics (Wilton, NH) we repeated these calculations and submitted to AFGL the program developed for plotting model beam images. The video's optic axis was lowered to 30° elevation from its original 35°, with its field extending 47° in elevation and 37° in azimuth from the initial beam direction. For mechanical reasons its axis was placed 9° clockwise in rocket azimuth from the initial beam direction (when viewed along the payload's forward axis).

We took the photometers and F4546 video camera to NASA-Goddard Space Flight Center, MD, for preliminary integration into the SCEX payload 5-11 Mar 1981. (Dummy photometer units had been earlier provided for mechanical integration.) Between 26 Mar and 9 Apr we tested the instruments, installed as for the actual flight, in the 30-meter vacuum tank (Chamber A) at NASA-Johnson Space Center, TX. We found that the camera provided images having adequate signal/noise of fluorescence excited by a 2 ma beam of 1-1/2 keV electrons at a tank pressure equivalent to that at 130 km atmospheric altitude

(with no evidence from other instrumentation of discharge effects). The equipment's telemetrylines were also checked out in the JSC chamber tests. Persistent difficulties with performance of the photometers, which had been delivered to AFGL in Fall 1980, were encountered during these test periods and later recalibrations at PhotoMetrics' laboratory.

Following a hiatus due to lack of funds between August and October, we performed a post-vibration test checkout at NASA/Goddard 17-18 Nov 1981. Problems with sensitivity and noise of the photometers remained; and noise that developed in the video camera's automatic gain control monitor installed by PhotoMetrics was removed by RC-filtering. We then recalibrated the equipment. It was then shipped by AFGL to Churchill, under ground transport conditions where it was exposed to temperatures of -45°C. PhotoMetrics participated in the rocket buildup and launch 4-28 Jan 1982. After the video was reinstalled on the rocket alternate picture elements were found to be dropping out between turnon and 15-20 min warmup time, which resulted in images having half the specified resolution during that period. The fault was identified as originating in the camera head, which was not accessible for field repair. The problem was avoided by cycling the camera on and off each 10-15 min during the prelaunch hold periods.

During flight the N_2 Second Positive band photometer operated as planned, showing signal on each accelerator pulse and the about-expected modulation from the aurora. (Quantitative comparison of the auroral emission intensities measured by the rocket photometer and groundbased photometers and cameras is not practical because of the greatly different projections of these instruments' field of view.) The 3914Å photometer, however, returned no data, with the telemetry trace flat throughout the flight. The failure mode of the instrument,

which had performed poorly throughout the test and buildup period, has not been identified. The video images failed to show any aurora or fluorescence excited by the ejected electron beam even though the raster scan lines were present on the groundbased monitors during the experiment. As the signal strength of the video telemetry was much less than predicted (~15 dB), this data loss is currently ascribed to inadequate signal/noise in the downlink, most probably due to loss of the rocket transmitter's final stage. The SCEX instrument payload was not recovered for post-flight examination.

Following a further four-month hiatus in early 1982 due to lack of contract funding, we started analysis of the Second Positive band data. AFGL reduced the telemetry voltages to average radiance within the instrument's field of view, using PhotoMetrics' calibration. AFGL also developed a program for calculating the relative irradiance at the photometer that would result from the trajectory of the geomagnetically-deflected electron beam through its field of view (Ref 6), expanding on the (unpublished) beam-image calculations previously performed by Minnesota and PhotoMetrics/Kimball Physics. We review the status of this preliminary analysis after the documentation below of the video camera and photometer.

VIDEO CAMERA

The ITT F-4546 system (S/N 9445212) consists of a General Electric Company (Syracuse, NY) TN2500 CID (charge injection device) solid state digital camera modified by the addition of a proximity focussed microchannel-plate image intensifier (ITT Model F-4111). It has S-20 (extended red) spectral sensitivity, and used without a filter (as in the experiment) nominal threshold sensitivity of 10^{-6} ft candles (we discuss the actual calibration later). The camera was fitted with a 13 mm focal

length, f/1.5 objective lens (Canon VF 1315) to provide an angular field of view of 37° x 47°.

On its receipt we ruggedized the camera's electronics by conformal potting (with Emerson-Cumming coating), strengthening the mechanical monitoring of the circuit cards with nylon spacers, and fastening loose wires with Super-glue. In addition we tapped into the video amplifiers to monitor the voltage applied to the camera's automatic gain control and automatic light control circuits as the irradiance at its faceplate changes. Adding a similar monitor to the automatic brightness control of the image intensifier proved impractical. The completed arrangement allowed monitoring of the system's self-adjusting sensitivity at the high end of the intensifier's dynamic range (that is, for the expected weak light levels). These gain signals were telemetered from the rocket along with the image data flow.

The TN2500 camera outputs the video voltages in a TTL-compatible 8 bit parallel format at 4.5 MHz word rate. Its RS170 composite analog video signal is suitable for display on standard closed circuit TV monitors. The camera was used at 244 vertical lines across the field, 248 pixels per line. The TN2500 consists of a 28 x 21 x 6.7 cm control box weighing 900 g, and a 5.5 x 7.9 x 7.9 cm head weighing 340 g without lens, connected by a 50 cm cable. The intensifier section (ITT F-4111) and its high voltage power supply were potted in Conothane EN-11 by the manufacturer to prevent sparking and outgassing at rocket altitudes.

The lens for the camera was selected to provide a field of view comparable to the expected diameter of beam-associated discharges, which would be a few primary electron gyroradii, that is, several meters [at the mean range of the beam]. A Canon 13 mm focal length lens was selected on the basis of its

having higher aperture ratio than similar Nikon or Tamron lenses. This lens, which weighs 240 g, fits the camera's C mount and extends 6.4 cm from its front plate. The camera was mounted on the payload with its lens 185 cm from the accelerator, offset 9° in payload azimuth from the port (viewing forward along the rocket's long axis). Its optic axis was pointed at 30° elevation, 0° azimuth from this axis, with the long dimension of its angular field in the beam direction. When the electron beam is injected parallel or antiparallel to a geomagnetic field line, it passes near the center of the camera field at a range of 5 m from the camera (4-1/2 m from the accelerator anode), making an angle of about 15° with the camera axis.

We vacuum tested the camera in an AFGL bell jar at pressures to 10^{-6} torr, finding its sensitivity to be the same within measurement accuracy before and after the exposure. This threshold sensitivity was measured using a uniform-brightness area 15 cm square (AFGL Low-Brightness Source) filtered to 70 Å FWHM at 4280 Å. Scene brightnesses as low as 5×10^{-4} erg/(cm^2 sec ster) produced adequate output voltage signal over noise in single frames at full system gain. The camera's response was radiometrically calibrated against this light source, with the automatic gain control and automatic light control voltages recorded.

As noted, the video camera was operated in Johnson Space Center's Chamber A against several-milliampere beams of 1-4 keV electrons at ambient N_2 molecule densities down to those at 130 km altitude (the chamber's limit), and found to produce useful images. Scene radiances in these images were of the order of a few kilorayleighs. As noted the telemetry link for the video faceplate signal and the gain controllers (provided by another group) was also checked out during this test period. This video telemetry downlink used a 10-watt S-band (2215.5 MHz)

FM transmitter and two redundant wideband Microdyne 100 LS receivers driving two Panasonic WV 5400 monitors and MV-9200 video cassette recorders. A parallel BCD time code was fed into one of the two monitors and recorders to identify time-after-launch of each image. These recorders have 3/4 inch cassettes with 1 hr recording capability.

The radiofrequency signal intensity from this video image telemetry system was expected to be 20 dB above noise, but was observed to be only 5 dB above noise during actual rocket flight. No image contrast was detectable in the video playback, although the raster was visible. An attempt made to enhance with low pass filters the signal expected from the periodically-pulsing beam also failed to provide any useful information. As mentioned above the loss of data from the video camera has been provisionally ascribed to failure of the telemetry transmitter's final amplification stage.

PHOTOMETER PROPERTIES, OPTICAL AND ELECTRONIC

The optical and other characteristics of the two photometers are listed in Table 1. Further documentation and identification of mechanical interface, electrical interface, and schematic drawings is provided by their manufacturer in Ref 7.

As a critical rather than Koehler illumination system is employed, sensitivity in the photometer's field of view varies with the local conversion efficiency of the photocathode (the solid angle element at each el, az being imaged onto a patch on the cathode). Vignetting by the lens barrel reduces the effective angular field (from that otherwise defined by the photocathode area and the lens focal length) to approximately 24° full conical angle, as we will show presently. The current output from the electron multiplier is fed through a through a

Table 1. SCEX Photometers

Optical system:	1.9 cm diameter photocathode critically illuminated by a 3.7 cm focal length silica objective lens; barrel with interference filter extends 1.5 cm into object space from front surface of lens.
Phototube:	C31016F end-on, S/N's F2C2 and F1C51, nominal cathode quantum conversion efficiency 0.22 at 3900Å.
Clear aperture:	3.8 cm^2, 2.2 cm diameter objective lens.
Angular field:	30° circular nominal, vignetted by lens barrel to 24° effective (see text).

Spectral sensitivity:

Measurement	N_2 1st Negative (0,0) band	N_2 2nd Positive (0,2) band
	Normal incidence, manufacturer	10° incidence, PhotoMetrics
Max xmission	0.46	0.40
Peak wavelength	3933Å	3797Å
Half-power	3890,3976Å	3780,3811Å
FWHM	86Å	31Å
Tenth-power	3555,4034Å	3770,3826Å
Hundredth-power	3790,4075Å	3760,3848Å

Response:	Analog logarithmic, 2/3 decade per volt output.
Calibration:	Continuum low-brightness uniform-radiance source (3805Å filter measured separately).
Dimensions:	Optics box 22 x 3.1 x 3.1 cm. Electronics box 13.5 (including connector) x 3.1 x 3.1 cm, mounted to rear of one face of optics box.
Rocket mounting projection:	Refer to text and Figure 3.

logarithmetic amplifier to compress the planned wide dynamic range of scene brightnesses to the 0-5 volt range of the rocket's data telemetry system. High voltage applied to the photomultiplier tube was held constant at about 1100 V by a regulator circuit, and monitored during flight.

PhotoMetrics replaced the 3914Å-band interference filter initially in one photometer with a filter for the 0,2 transition of the N_2 Second Positive system. We specified that the filter be manufactured to transmit optimally the 3805Å-band's profile in the expected 15° half-angle illumination cone. We measured the as-received filter's transmission at 23°C temperature to a parallel light beam incident at 10° from its surface normal, which accurately simulates the passband-shifting and -broadening effect of a uniform light source filling the photometer's field of view (Ref 8). The spectral response of the 3914Å filter had been measured by its manufacturer, in normal-incident light. In practice this latter filter's wide wavelength response, 86 Å FWHM at normal incidence, obviates the need for detailed calculation of its mean tranmission of the band's P and R branches even when its effective spectral shift due to incidence of off-axis rays is considered. (Half of the photons are in the ~4Å-wide P branch, and the R branch extends ~10Å further toward the violet.) Such a calculation was, however, necessary for the 3805Å band, which we assumed to originate from N_2 molecules at 300 K uniformly radiating within the photometer instrument's field of view. This assumption of a constant local N_2 rotational temperature over the rocket's trajectory has the effect of underestimating slightly the band radiances at the higher altitudes, where broader rotational development resulting from the higher ambient temperatures moves some of the radiation further into the wings of the interference filter's transmission profile.

We calibrated the continuum response of the photometers with a spatially-uniform light source (originally of AFGL design and construction, unit D5) whose spectral radiance calibration is traceable to the National Bureau of Standards and whose brightness is adjustable over three decades. In practice a continuum scene brightness of 100 rayleighs within the passband resulted in a signal of 1/2 volt (below the dark reading of 5.0 volts) from the 3805 Å photometer. It should be noted that the measured radiance response can be converted to a a SCEX incident-irradiance calibration, as discussed later.

We estimated the effect of vignetting of the photometer's field by its lens support ring by tracing rays on its assembly diagram. The instrument's response falls to 80% of its paraxial value at 7° off axis, 50% at 12°, and zero at 14°. The dependence expected from geometric-optics considerations is [cos (off-axis angle)]^4 x [physical vignetting factor], the first term being the usual thin-simple-lens vignetting factor and the second term of course also decreasing with the light bundle's angle from the optical axis (in a complex way; some increases due to internal reflections in the unbaffled photometer could also be expected). As mentioned above, the photometer fields are therefore much better represented by a 12° half-angle cone than the original design goal of 15°.

Construction of the photometers had been completed about three months into PhotoMetrics' program, and substantial debugging and repair of the two units turned out to be required. Although the difficulties (principally broken electrical connections, marginally operative amplifiers, and incorrectly-trimmed applied voltages) identified in the course of PhotoMetrics' calibration and payload integration were corrected in a timely

way by the instrument's supplier, they nevertheless resulted in program delays.

THE SPECTROSCOPIC-RATIOS METHOD

The method for determining an effective temperature of the electrons in the beam region applies the well-known principle that the triplet states of N_2 are most efficiently excited by ~10-30 eV electrons (by electron-exchange collisions) while the electronic states of the N_2^+ ion are efficiently directly collisionally excited by electrons with energies >~19 eV. Thus the ratios of column intensities in emission bands provide a measure of the energy distribution of the plasma electrons. This physical situation is illustrated in Figure 2, which shows the energy dependence of the excitation cross-sections of the upper states of two major features in each system, the N_2 Second Positive ($C^3\pi_u \rightarrow B^3\pi_g$) 0,1 and N_2^+ First Negative ($B^2\Sigma_u \rightarrow X^2\Sigma_g^+$) 0,0 bands. Superposed on the cross-sections are the energy distributions of the electrons at four temperatures and those measured in the Echo III upper-atmospheric electron-injection experiment (Ref 9), with the resulting band intensity ratios calculated as described below. Oscillating electric fields associated with collective interactions of charged beams with plasmas heat the plasma electrons (Ref's 1,4), so that their energy distribution becomes different from that of the secondaries that are produced in impact ionizations by the primary injected electrons. (The latter are given in Ref 10 in the context of excitation by auroral particles having similar keV's energy.) In particular substantial fluxes of electrons near the 16 eV ionization threshold of N_2 would be present, enhancing the relative excitation of the Second Positive bands (and other N_2 triplet systems, not shown in Fig 2 for clarity).

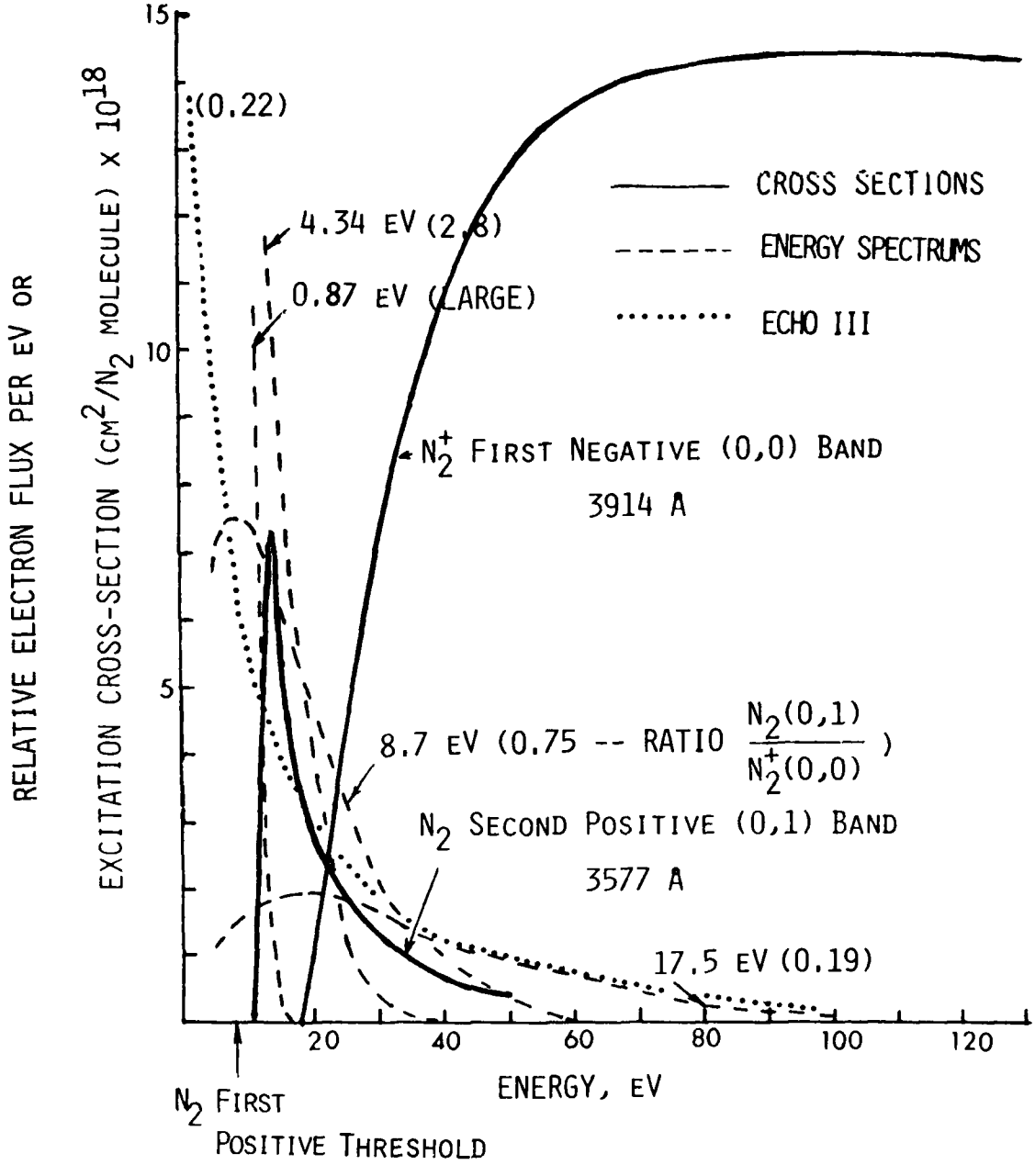

Figure 2. Excitation cross-sections of N_2 and energy spectra of thermal electrons at temperatures 0.87 to 17.5 eV. The spectrum measured on the Echo III rocket (Ref 9) is also shown. Ratios of emission intensity in the features indicated are in parentheses. The N_2 Second Positive (0,2) band intensity is 0.40 x that shown for the (0,1) band.

As interference filters for the 0,1 Second Positive band's wavelengths extending below 3577Å are difficult and expensive to fabricate, we chose to measure instead the intensity of the 0,2 band with head at 3805Å, whose emission probability is 0.40x that in the 0,1 band (as is known from the state's Franck-Condon branching factors). Like the 3914Å band, this band is well spectrally isolated from other upper-air fluorescence features (more on this later) and thus its intensity lends itself to measurement with interference-filter photometers of the design on hand. The 3805Å/3914Å band column intensities are therefore 0.4 times those listed in Figure 2, varying from 1.12 at 4.34 eV electron temperature (and very much higher at lower temperatures, as the electron energy distribution for 0.87 eV clearly shows) to 0.31 at 17.5 eV.

In contrast the calculated ratio at 120 km altitude from an electron energy spectrum that results from single particle energy dissipation is 0.13 (Ref 10, with the input from Ref 11 that 6.6% of the N_2 C → B system photons are in the 0,2 band); and the measured ratio viewing the ~100-150 km-altitude auroral excitation column from ground stations is also 0.13 (Ref 11). We applied our calculational model to the auroral energy distribution Ref 12, again getting a ratio of 0.13. Hence the emission ratio appears to be a sensitive function of the onset of discharges, with the proviso that account is taken of direct excitation of the two features by the primary beam electrons and that the instrument field of view encompasses the region outside the beam path excited by the laterally-scattered secondaries as well as the heated-plasma electrons (the discharge is confined principally within the injected beam's gyroradius).

We selected a band originating from the C state of N_2 because this state is known to be populated almost exclusively by direct electron impact on ground-state N_2 molecules. The

lower-lying $B(^3\pi_g)$ state, from which originate the even stronger $B \rightarrow A(^3\Sigma_u^+)$ First Positive bands, is to a large extent populated by cascade from the C, A and higher states (and perhaps also by atomic collisions), and the still lower-lying A state is metastable with a lifetime (~2 sec) much longer than the dwell time of the onboard photometers on the volume excited by the rocket's electron beams (as well as being in large part populated by cascade).

We derived the ratios shown in Fig 2 using a specially-developed digital computer program (SPECRAT) that calculates the electron energy spectrum at given temperatures (some of which are plotted in Fig 2) and folds this distribution into tabulated excitation cross-sections. For the N_2 X → C cross-sections, about which there had been earlier measurement disagreements, we used the recent results of Cartwright et al. (Ref 13). The $N_2(X) \rightarrow N_2^+(B)$ cross-sections, measurements of which are currently in good agreement, were taken from Ref's 14 and 15.

PHOTOMETER DATA ANALYSIS

The fact that the electron beam current and energy were independently varied, with injection at a series of altitudes and pitch angles to the geomagnetic field, provides an opportunity to investigate the dependence of the beam's interaction with the atmosphere on these parameters. The basic data, which are on the telemetry record as a function of time during flight, are

1a. Beam current I
1b. Accelerator anode-cathode potential difference V
2. 3805Å photometer signal, hereinafter labeled PHOT when calibrated and

corrected for the sky background due to aurora.

Further information needed for the analysis is

3. An ambient atmospheric species concentration profile.
4. Model irradiance at the photometer produced by the beam particles, which varies with the the beam's trajectory through the photometer's field of view (determined by the angles between the beam's axis and the geomagnetic field) as well as items 1) and 3).

PHOT could also depend directly on the pitch angle to the field, as well as through the trajectory calculation 4); on whether the beam was injected into the upper or lower hemisphere, that is, on the fraction of the primary electrons that escape the atmosphere (large when injection is upward from above 130 km); and/or time after launch, on which the rate of outgassing (principally of water vapor) would depend.

A flow chart of the data reduction and analysis is shown in Table 2. V,I, and the photometer's output voltage were sampled each 5 msec, or 9-10 times per current pulse, in a data file labeled SSS. We arithmetically averaged I,V, and PHOT (in program READ) to produce a single mean reading within individual beam pulses. The standard deviation of the individual voltage samplings is <1%, but the current fluctuations were substantially higher (20-50% standard deviation). The photometer signal varies by 30-90% within the pulses, without correlation with these current fluctuations. (This noise may be associated with instabilities in the interaction of the beam with the atmosphere.)

Table 2. Flow Chart for SCEX Data Analysis

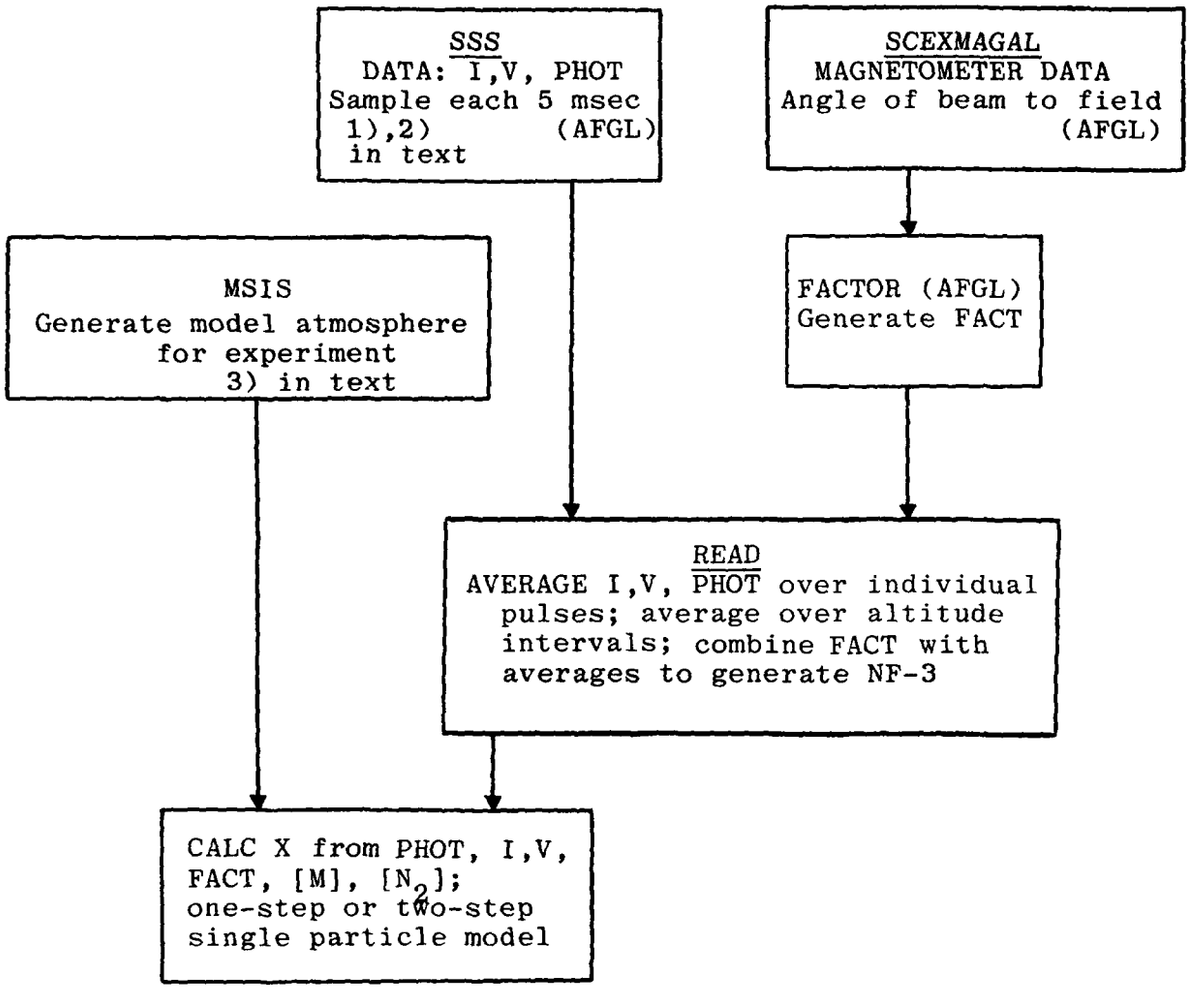

AFGL removed the slowly-varying photometer background due to aurora by spline fitting with a cubic polynomial function, in SSS. That this automatic subtraction procedure can lead to large errors, particularly when only 1 ma was injected, is evidenced by the occasional negative values of PHOT, which we omitted from the data reduction. (PhotoMetrics provided the telemetry voltage level to radiance transfer calibration for SSS.) The error in PHOT is relatively large because PHOT's value is the difference between two logarithmically recorded radiances. Irradiances within the photometer's ~14°-full cone field can be found from its radiance sensitivity (which was measured with the field uniformly filled) integrated over its aforementioned angular sensitivity. A manual summation shows this irradiance to be 0.10_5 times the as-calibrated radiance, in units photons/cm^2 sec when the radiance is in photons/cm^2 sec ster (= $(10^6/4\pi)$ x number of rayleighs).

For the atmosphere into which the beam was injected (Item 3 above), PhotoMetrics applied the MSIS model (Ref 16) appropriate to the conditions of the SCEX experiment, which are

Year/Day	82/027
Local standard time	21.64 hrs
Latitude/Longitude	58.8°N, 265.8°E
10.7 cm flux average	196.1
10.7 cm flux local	182.7
Ap	7.

The solar flux and magnetic activity index for the launch period were taken from Ref 17. Results, shown in Table 3, were put in program MSIS.

We calculated the irradiances that would result from impact excitation of ambient N_2 by the primary beam particles only (Item 4) using the beam geometry factors derived with AFGL's program FACTOR (described in Ref 6), taking initial

Table 3. MSIS Model Atmosphere for SCEX Trajectory Conditions

ALT *	T-EX **	TEMP **	N2 †	O2	O	AR	HE	H	TOTAL	KG.M-3
120.0	1078.4	372.4	2.383E+17	3.051E+16	1.170E+17	1.675E+15	5.682E+13	9.775E+10	3.876E+17	1.592E-14
125.0	1078.4	464.6	1.306E+17	1.584E+16	7.547E+16	7.799E+14	4.713E+13	8.445E+10	2.227E+17	8.968E-15
130.0	1078.4	544.6	8.133E+16	9.429E+15	5.379E+16	4.244E+14	4.096E+13	7.591E+10	1.450E+17	5.738E-15
135.0	1078.4	614.1	5.487E+16	6.118E+15	4.080E+16	2.547E+14	3.665E+13	6.994E+10	1.021E+17	3.976E-15
140.0	1078.4	674.5	3.908E+16	4.207E+15	3.229E+16	1.633E+14	3.345E+13	6.554E+10	7.578E+16	2.909E-15
145.0	1078.4	726.9	2.895E+16	3.018E+15	2.584E+16	1.098E+14	2.808E+13	6.216E+10	5.795E+16	2.200E-15
150.0	1078.4	772.5	2.207E+16	2.233E+15	2.120E+16	7.652E+13	2.435E+13	5.948E+10	4.561E+16	1.713E-15
155.0	1078.4	812.1	1.721E+16	1.692E+15	1.772E+16	5.480E+13	2.166E+13	5.732E+10	3.671E+16	1.365E-15
160.0	1078.4	846.5	1.366E+16	1.307E+15	1.504E+16	4.010E+13	1.965E+13	5.553E+10	3.007E+16	1.107E-15
165.0	1078.4	876.4	1.100E+16	1.025E+15	1.293E+16	2.985E+13	1.810E+13	5.403E+10	2.500E+16	9.111E-16
170.0	1078.4	902.5	8.955E+15	8.142E+14	1.122E+16	2.254E+13	1.687E+13	5.276E+10	2.103E+16	7.592E-16
175.0	1078.4	925.1	7.361E+15	6.531E+14	9.825E+15	1.722E+13	1.588E+13	5.166E+10	1.787E+16	6.390E-16
180.0	1078.4	944.8	6.098E+15	5.283E+14	8.663E+15	1.328E+13	1.507E+13	5.071E+10	1.532E+16	5.426E-16
185.0	1078.4	962.0	5.085E+15	4.304E+14	7.683E+15	1.032E+13	1.438E+13	4.987E+10	1.322E+16	4.641E-16
190.0	1078.4	976.9	4.264E+15	3.527E+14	6.849E+15	8.080E+12	1.378E+13	4.913E+10	1.149E+16	3.995E-16
195.0	1078.4	989.9	3.593E+15	2.905E+14	6.132E+15	6.361E+12	1.327E+13	4.847E+10	1.004E+16	3.458E-16
200.0	1078.4	1001.2	3.039E+15	2.403E+14	5.511E+15	5.033E+12	1.281E+13	4.787E+10	8.808E+15	3.008E-16
205.0	1078.4	1011.0	2.580E+15	1.995E+14	4.969E+15	3.999E+12	1.240E+13	4.733E+10	7.764E+15	2.628E-16
210.0	1078.4	1019.6	2.196E+15	1.662E+14	4.493E+15	3.189E+12	1.203E+13	4.684E+10	6.870E+15	2.305E-16
215.0	1078.4	1027.1	1.874E+15	1.388E+14	4.072E+15	2.551E+12	1.169E+13	4.638E+10	6.099E+15	2.029E-16
220.0	1078.4	1033.6	1.603E+15	1.162E+14	3.699E+15	2.047E+12	1.138E+13	4.596E+10	5.432E+15	1.791E-16
225.0	1078.4	1039.3	1.374E+15	9.754E+13	3.366E+15	1.646E+12	1.108E+13	4.556E+10	4.850E+15	1.586E-16
230.0	1078.4	1044.3	1.180E+15	8.200E+13	3.068E+15	1.326E+12	1.081E+13	4.520E+10	4.342E+15	1.408E-16
235.0	1078.4	1048.6	1.015E+15	6.904E+13	2.801E+15	1.071E+12	1.054E+13	4.485E+10	3.896E+15	1.254E-16
240.0	1078.4	1052.4	8.735E+14	5.822E+13	2.560E+15	8.661E+11	1.030E+13	4.452E+10	3.503E+15	1.118E-16
245.0	1078.4	1055.6	7.530E+14	4.915E+13	2.343E+15	7.015E+11	1.006E+13	4.421E+10	3.156E+15	9.994E-17
250.0	1078.4	1058.5	6.497E+14	4.155E+13	2.146E+15	5.689E+11	9.834E+12	4.391E+10	2.848E+15	8.951E-17
255.0	1078.4	1061.0	5.612E+14	3.515E+13	1.967E+15	4.619E+11	9.616E+12	4.362E+10	2.574E+15	8.030E-17
260.0	1078.4	1063.2	4.851E+14	2.977E+13	1.805E+15	3.755E+11	9.407E+12	4.334E+10	2.330E+15	7.217E-17

*Altitude, km **Temperature, K †Species concentrations, m^{-3}

angles to the geomagnetic field from AFGL's flight record SCEXMAGAL. The irradiances due to excitation by the secondary electrons require considerably more complex calculations, a point we shall discuss shortly. The geometric factor FACT, which changes with the orientation of the beam axis to the earth's magnetic field, is a relative irradiance

$$\Sigma(\text{beam path element within the field of view})/(\text{distance from element to photometer})^2,$$

with summation over the photometer's 30° field of view. FACT will be recognized as directly proportional to the integral of primary excitation rate at points along the beam (in a uniform atmosphere, that is, without outgassing from the rocket) divided by the solid angle subtended from these points by the objective lens, which is in effect the fraction of this (isotropically) emitted radiation that the photometer collects; in simple qualitative terms, it is a correction for the injected electron beam's deflection by the earth's magnetic field.

Note that the program FACTOR makes the assumption that the photometer's response is constant at all angles within a 30° conical field of view; that the primary beam has negligible angular divergence at all currents and voltages; and that Coulomb scattering of the beam electrons can be neglected (this last assumption breaks down below ~95 km, where the electrons' collision mean free path becomes less than their Larmor radius). FACTOR explicitly assumes single-particle transport, and thus can be considered as a means of testing for the collective beam-interaction processes inferred from an experiment that used the same electron accelerator at essentially the same atmosphere densities (Ref 5) and were also inferred from the flight of Ref 3. Reference is made to our comments above on the earlier iterations of the geometry-factor calculation, which considered only the image of the beam within camera

fields; the present calculation figures also in the distance from the instrument to line elements along the beam path, to determine irradiances (as was suggested by PhotoMetrics).

In practice FACT varies only over a range of about 2 for all the injection pitch angles encountered in flight. The reason is, that the primary electrons' gyroradius is typically a few times the transverse dimension of the angular field at close range to the photometer, where the major fraction of the irradiance sum originates because the $(\text{distance})^{-2}$ term is large. This is illustrated in Figure 3 (further projections of the beam-field geometry are shown in Ref 6). The separation of the photometer and accelerator is 1.19 m, while the gyroradius of electrons injected perpendicular to the 0.52-gauss field (an average over the trajectory altitudes at Churchill) is 2.85 m at 1.9 keV and 5.8 m at 8 keV. Figure 3 shows a worst case deflection, at the lowest electron momentum perpendicular to the earth's field. Thus the beam close to the photometer is not deflected "out" of the instrument's field of view, and when the beam is fortuitously bent to spiral within the field those path elements beyond about 3 m range contribute little to the total irradiance (refer again to Fig 3).

We calculated (in program SCEXC) the irradiances at the photometer that result from the primary beam only by multiplying the FACT outputs by $[N_2]$ (from Table 2) x (beam current I) x ([energy-dependent] impact excitation cross-section σ). To do this we first generated a new data tape NFS-3 by merging the averaged-over-pulses I,V, and PHOT with FACT. The cross-sections for direct excitation of 3805Å radiation were taken from Ref 18 (earlier laboratory data had been contaminated by the much greater excitation by secondary electrons), and are 5.2×10^{-22} cm^2/N_2 molecule at keV electron energy, 1.55×10^{-2} cm^2 at 4 keV, and 0.68×10^{-22} cm^2 at 8 keV.

Figure 3. Side projection of the photometer field and ejected electron beam. The actual beam is diverging in a cone angle of a few degrees. The curved trajectory refers to a 1.9 keV electron beam perpendicular to the magnetic field directed into the plane of the paper. See Ref 6 for further views of the beam-photometer geometry.

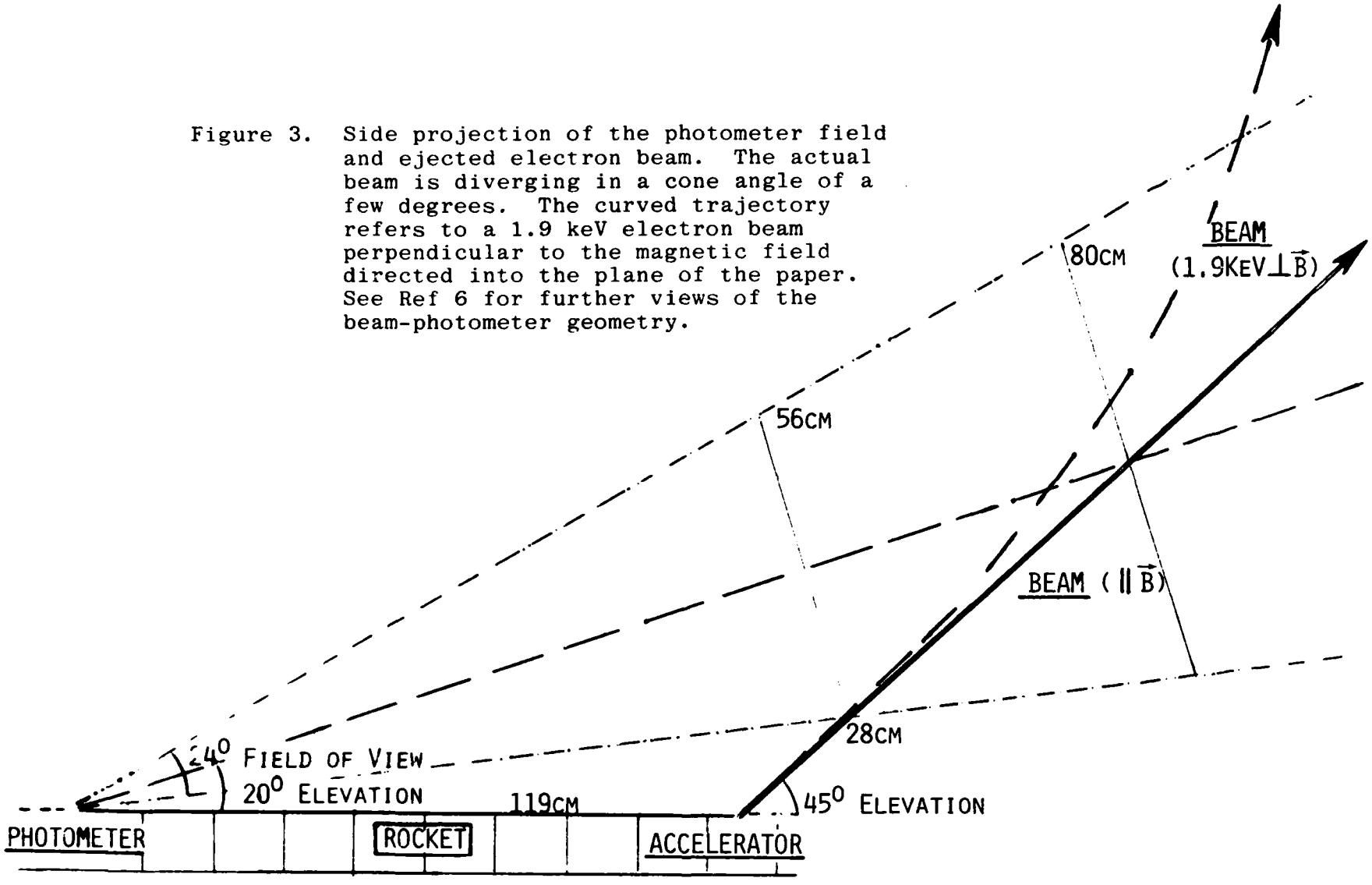

The resulting irradiance

$$\text{FACT} \times [N_2] \times \sigma(V) \times I$$

refers of course to direct excitations by the primary electron beam. It neglects the contribution of excitation by the secondary electrons produced in collisions of these beam electrons with air, radiation due to enhanced local molecule density from rocket outgassing, and radiation excited by collective interactions of the beam with the ionospheric plasma.

As noted above the FACTOR concept provides a test for the large number of backscattered ~keV electrons within the photometer's field of view that was reported in Ref 5 under what were interpreted as strong collective interaction conditions. Where outgassing and collective effects are negligible, and the irradiance component resulting from collisions of the secondaries within the photometer field remains strictly proportional to that from the primaries, these model irradiances would be proportional to the absolute photometer signals measured (equal to them if secondaries can be neglected), within the error due to the assumptions about the photometer's angular response. We return to this important issue shortly.

The final program SCEXC, a copy of which is included as Table 4, reads the READ tape until it reaches a pulse, uses the time of this pulse and the rocket trajectory parameters to generate the ejection altitude, and interpolates number densities of N_2 and other species at this altitude from MSIS. It then calculates a normalized photometer signal

$$X = \text{PHOT}/\sigma \cdot [N_2] \cdot \text{FACT} \cdot I$$

and otherwise manipulates the input parameters (including time after launch, on which all other parameters depend) to explore the dependence of this normalized output signal.

We have so far reduced the data for the upleg segment of the SCEX flight. As X appeared to be varying within very

Table 4. Listing of the SCEXC merge/X-calculation program

```
100=       PROGRAM SCEX (TAPE1, TAPE2, OUTPUT, TAPE3)
110=       DIMENSION A(3), SIG(3), H(29),DN2(29), DO2(29), DO(29),
                                                          DHE(29)
120=       DIMENSION HEAD(8), RI(4), YY(11), NK(3,11)
130=       DIMENSION XX(3,11), XXV(3,11), RN2(11)
140=       DATA SIG /5.4E-22,1.5E-22,6.8E-23/
150=       DATA RN2/1.37E16,1.04E16,7.88E15,5.99E15,4.55E15,
160=      1 3.46E15,2.62E15,1.99E15,1.51E15,1.15E15,8.73E14/
170=       DATA A /-4.5994535E-3, 2.3245382, -52.896149/
180=       DATA RI / 1.0, 1.3, 0.49, 0.37/
190=       DK=1.
200=       TL = 13940.8
210=       DO 999 KK=1,3
220=       DO 999 LL=1,10
230=       NK(KK,LL)=0
240=       XX(KK,LL)=0.
250=   999 XXV(KK,LL)=0.
260=       REWIND 1
270=       REWIND 2
280=       REWIND 3
290=       READ (2,2) HEAD
300=     1 FORMAT (/,A10)
310=     2 FORMAT (10(/), 8(A10))
320=     3 FORMAT (2X, F6.0, 16X, 3(2X, F10.0), 14X, F10.0)
330=     4 FORMAT ( /, 6(2X, 1PG11.4), 2X, I3, 2X, 1PG11.4)
340=     9 FORMAT (2X, F6.1, 16X, 3(2X, 1PG10.3), 14X, 1PG10.3)
350=       DO 10 I = 1, 29
360=       READ (2,3) H(I), DN2(I), DO2(I), DO(I), DHE(I)
370=    10 CONTINUE
380=       DO 190 K=1,300
390=       READ (1) T1, T2, R, C, V, G
400=    51 FORMAT(1X,"DATA IN",3X,4(E10.3,2X))
410=       IF (EOF(1)) 200, 19
420=    19 V=V/1000
430=       WRITE (3,4) T1, T2, R, C, V, G
440=       TA = (T1 + T2)*0.5 - TL
450=       IV = 2
460=       J=1
```

Table 4. Continued

```
      IF ( V .GT. 6.) IV = 3
      IF ( V .LT. 3.) IV = 1
   52 FORMAT(2X,2(I4,2X))
      ALT = A(1)*TA**2 + A(2)*TA + A(3)
      CALL INTERP (H, DN2, 29, 3, ALT, AN2)
   45 FORMAT(1X,E10.3)
      PROD=G*C*DK*SIG(IV)
      RR=R
      IF (RR.LT.0.)  R=0.
      X=R/(PROD*AN2)
      X=X*AN2
      GN2=AN2
      DO 87 JJ=1,10
      IF ((GN2.LT.RN2(JJ)).AND.(GN2.GE.RN2(JJ+1))) GO TO 85
      GO TO 87
   85 YY(JJ)=X
      J=JJ
   87 CONTINUE
      NK(IV,J)=NK(IV,J)+1
      XX(IV,J)=XX(IV,J)+YY(J)
      VB=V*C
      XXV(IV,J)=XXV(IV,J)+YY(J)/VB
   53 FORMAT(3X,E10.3)
   78 FORMAT(2X,I5)
      WRITE (3,6) TA, ALT, AN2, AO2, AO, AHE
      WRITE (3,7) SUM, PROD, IV, X
    6 FORMAT (10(1X, 1PG11.4))
    7 FORMAT (2(1X, 1PG11.4), 2X, I2, 2X, 1PG11.4)
  190 CONTINUE
   77 FORMAT(2X,3(E10.3,2X))
      DO 998 KK=1,3
      DO 998 LL=1,10
      IF(NK(IV,J).EQ.0) NK(IV,J)=1
      XX(IV,J)=XX(IV,J)/NK(IV,J)
      XXV(IV,J)=XXV(IV,J)/NK(IV,J)
  998 CONTINUE
      PRINT 76,NK
   76 FORMAT(2X,3(I4,2X))
      PRINT 77,XX
      PRINT 77,XXV
  200 STOP  $  END
      SUBROUTINE INTERP (X, Y, NPTS, NTERMS, XIN, YOUT)
      DIMENSION X(1), Y(1), DELTA(10), A(10)
   11 DO 19 I = 1,NPTS
```

Table 4. Concluded

```
 910=       IF (XIN - X(I)) 13, 17, 19
 920=    13 I1 = I - NTERMS/2
 930=       IF (I1) 15, 15, 21
 940=    15 I1 = 1
 950=       GOTO 21
 960=    17 YOUT = Y(I)
 970=    18 GOTO 61
 980=    19 CONTINUE
 990=       I1 = NPTS - NTERMS + 1
1000=    21 I2 = I1 + NTERMS - 1
1010=       IF (NPTS -I2) 23, 31, 31
1020=    23 I2 = NPTS
1030=       I1 = I2 -NTERMS + 1
1040=    25 IF (I1) 26, 26, 31
1050=    26 I1 = 1
1060=    27 NTERMS = I2 - I1 + 1
1070=    31 DENOM = X(I1+1) - X(I1)
1080=       DELTAX = (XIN - X(I1)) / DENOM
1090=       DO 35 I = 1,NTERMS
1100=       IX = I1 + I - 1
1110=    35 DELTA(I) = (X(IX) - X(I1)) / DENOM
1120=    40 A(1) = Y(I1)
1130=    41 DO 50 K = 2,NTERMS
1140=       PROD = 1.
1150=       SUM = 0.
1160=       IMAX = K - 1
1170=       IXMAX = I1 + IMAX
1180=       DO 49 I = 1,IMAX
1190=       J = K - 1
1200=       PROD = PROD * (DELTA(K) - DELTA(J))
1210=    49 SUM = SUM - A(J)/PROD
1220=    50 A(K) = SUM + Y(IXMAX)/PROD
1230=    51 SUM = A(1)
1240=       DO 57 J = 2,NTERMS
1250=       PROD = 1.
1260=       IMAX = J - 1
1270=       DO 56 I = 1,IMAX
1280=    56 PROD = PROD * (DELTAX - DELTA(I))
1290=    57 SUM = SUM + A(J)*PROD
1300=    60 YOUT = SUM
1310=    61 RETURN
1320=       END
```

narrow ranges of I,V, and $[N_2]$ we averaged X at fixed I and V, applying ten logarithmically-decreasing atmospheric density intervals over the 168 to 241 km (apogee) altitude range (in SCEXC). The data partially evaluated to date do not include those lower injection altitudes where 1) the upward-directed electron beam is almost totally contained by the atmosphere, with only a small fraction of the primaries and energetic secondaries escaping to the conjugate hemisphere (below ~130 km), and 2) no nonlinear beam-plasma interactions are expected in SCEX's current-voltage range (below ~120, km, Ref 1).

PRIMARY AND SECONDARY EXCITATION, COLLECTIVE INTERACTIONS

As noted, if secondaries, plasma interactions resulting in avalanche or heating of the ambient plasma, and outgassing can be neglected X would be both quantitatively predictable and constant throughout the experiment. If the irradiance from the secondaries is strictly proportional to (and at least comparable to) that from the primary electrons, X would be constant but larger than predicted by FACT $\cdot \sigma[N_2]I$. As Figure 2 shows, the cross-sections σ_s for excitation of the 0,2 N_2 Second Positive band by secondary electrons with energy >11 eV (the C state's threshold) are a few x 10^{-18} cm^2, which is a factor 10^4 higher than those we quoted above for the ~hundredtimes more energetic primary beam electrons. Moreover, the cross-sections of N_2, O, and O_2 for emission of secondary electrons with energy >11 eV under impact of the 2-8 keV primaries are ~10^5 those for direct excitation of 0,2 band radiation (Ref's 15,18). Thus these secondary electrons could be expected to contribute to the 3805Å signal,as we discuss further here.

The volume rate of direct, single-step excitation of the 0,2 band is

$$\phi\sigma[N_2],$$

where ϕ is the beam current density or flux (I per unit beam area). This direct excitation of course takes place only in those air volumes traversed by the beam, which is a small fraction of the total photometer field of view. (It is somewhat larger than Fig 3 shows, as the injected beam has a small, albeit not quantitatively measured, angular divergence).

In the two-step process secondaries are first produced (in this restricted volume) at a rate

$$\phi\ \Sigma[M_i]\sigma_i,$$

where $[M_i]$ is the concentration of the ith atmosphere species (including N_2) and σ_i the species cross-section for impact ionizations leading to secondary electrons with energy >11 eV. These secondaries are ejected largely at angles about 60° from the primary beam direction (Ref 19), with most having energies below 50 eV (Ref 19). (Refer also to the plots in Appendix II.) They spiral within a gyroradius of their initial magnetic field line, which is $<\sim 1/2$ m, between momentum transfer collisions with neutral and charged species that scatter them onto new field lines about one gyroradius away. Because of their their initial transverse velocity these secondaries excite N_2 Second Positive band (and other triplet state) radiation outside the magnetically-confined beam volume (as was seen, for example, in the EXCEDE: Spectral color photographs, Ref 20). It should be pointed out that secondaries (and tertiaries,..., which we have neglected here) originating at reasonably large fractions of the primaries' end-point range may contribute to the excitation of air near the accelerator, as is shown by detailed calculations of electron transport and energy dissipation (for example Ref 21). We point out also that the number of ions produced in the initial impact of these secondaries on N_2, O,

and O_2 increases extremely rapidly above 13 eV, and for impacting electrons with kinetic energy 16 eV exceeds the rate of excitation of 3805Å radiation by an order of magnitude.

The omnidirectional flux of secondaries through individual volumes, unlike that of the primary (directed) beam electrons, can not be readily calculated because it depends on contributions from neighboring volumes. We can approximate the average flux of these secondaries by defining a characteristic length L of the volume in which most of the irradiance originates. (Were it filled by the primary beam, L would be closely (this volume)/(surface area through which the electrons escape).) L would appear to be of the order of 1 meter (refer to Fig 3) if only secondaries produced within a few times the separation between the photometer and accelerator anode contribute to the irradiance signal. In describing the secondary excitation-ionization it becomes necessary to refer to this total "effective" photometer field rather than the volume within the primary beam's trajectory, as the secondaries occupy a large number of ~1 m-diameter tubes tubes extending along the geomagnetic field with their axes on points along the initial beam.

This omnidirectional flux is then

$$L \cdot \phi \, \Sigma[M_i]\sigma_i,$$

and the mean-value 3805 Å excitation rate by the secondaries is

$$L \, \phi \, \Sigma[M_i]\sigma_i \cdot \sigma_s[N_2].$$

Here σ_s is the excitation cross-section averaged over the secondaries' energy distribution, which from Figure 2 and the distribution measured in Ref 19 (shown in Appendix II) is about 3×10^{-18} cm^2/N_2 molecule. Rearranging terms and for convenience expressing the sum as an average $[M]\sigma_i'$ (justified in view of the fact that the ionization cross-sections of the principal ambient species differ only by about a factor two, and a mean

σ_i' can be readily calculated for each altitude from the concentrations on Table 3), we find that the secondary excitation rate is

$$\phi[M]\sigma_i' \cdot \sigma_s[N_2]L \ .$$

The two terms of this expression will be recognized as the rate of production of secondary electrons and their probability (<1) of colliding with an N_2 molecule to excite 0,2 band emission.

Unlike calculation of the excitation by the primary beam (when it is assumed not to be substantially broadened by Coulomb scattering), calculation of the secondary ionization rates involves solving radiation transport equations with a summation over the secondary electrons' energy and angular distributions. The ratio of the two excitation rates is

$$(\sigma_s/\sigma) \cdot \sigma'_i[M]L \approx 10^4 \ \sigma'_i[M]L.$$

For example at 180 km altitude where [M] = 1-1/2 x $10^{10}/cm^3$, and 4 keV injection at which the species-averaged ionization cross-section $\sigma_i' \approx 2 \times 10^{-17}$ cm^2, this secondary/primary ratio is about $3 \times 10^{-3} \cdot L$ in cm. Thus if secondary electrons are to contribute significantly to the optical signals the characteristic length parameter that we have defined must be a few meters (more above 180 km because [M] is decreasing).

It is instructive to calculate the absolute magnitude of PHOT due to the primary electrons only (as it is defined). We select as typical experiment conditions I = 10 ma, V = 4 keV ($\sigma = 2 \times 10^{-22}$ cm^2/N_2 molecule), altitude = 180 km ($[N_2] = 6 \times 10^9/cm^3$). We adopt also an average figure for FACT, (200 cm beam path)/4π(300 cm range to photometer)$^2 \approx 3 \times 10^{-4}$/cm (refer again to Fig 3 to verify these dimensions). Applying the radiance/irradiance ratio of 0.10 that we referred to earlier, these inputs result in a radiance of 1/500 rayleigh

averaged over the photometer field. This figure is much smaller than the tens of rayleighs that was actually measured under these conditions. Thus (at least for these sample conditions) the photometer signal cannot be due principally to direct excitation by the primary beam electrons. Rather than continue with such episodic calculations, we have prepared the data for systematic computer analysis to determine the dependence of PHOT on the input variables I, V,[M] and [N_2], the others mentioned above, and still others that may be identified in the course of the data analysis.

PHOTOMETER LEAKAGE

In view of this finding that the direct excitation of 3805Å radiation by the primary beam is extremely small, we investigated the possibility that contamination by a permitted transition from a Coulomb collision-excited state of some atmospheric species is responsible for the high irradiance. Several emission features partially overlapping the photometer's 31Å FWHM bandpass were identified, but all had either low excitation cross-sections at 2-8 keV incident electron energy, long radiative lifetime (so that few photons would be emitted during the ~millisecs traverse of the rocketborne photometer's field), and/or low transmission by the filter.

Among the molecular bands that we found and rejected as contributing less than an estimated 10% of the directly-excited N_2 C→B 0,2 band signal (in most cases, substantially less) were, in crude order of perceived importance,

N_2^+ First Negative 2,2 with head at 3858Å and shaded to the UV --: intensity 2×10^{-4} that of the 0,0 3914Å band, and mean filter transmission 1%; thus its contribution

is 10^{-2} that from the 3805 Å band. The still weaker 3,3 and 4,4 N_2^+ bands with heads at 3835 and 3818Å, for which the filter's transmission is ~10% and 2%, result in comparable low-level contaminant signal.

O_2^+ Second Negative 0,7 band at 3830Å --: weak excitation, low atmospheric O_2/N_2 ratio (see Table 2), 5% filter transmission.

O_2 afterglow 2,7 band at 3829Å --: weak excitation, forbidden transition with long radiative lifetime.

N_2 Vegard-Kaplan 3,13 band at 3854Å --: intercombination transition with low excitation cross-section, long lifetime, low filter transmission.

(No OI, OII, NI, or NII lines were identified). We conclude that barring some pinhole or severe off-axis, off-passband leakage of the photometer (which were not found in its calibration and testing) negligible photocurrent from air fluorescence other than the N_2 Second Positive 0,2 band would result directly from impacts of the primary beam electrons.

Reference is again made to previous observations with a similarly programmed electron accelerator of the same design (Ref 5), which were interpreted as showing collective interactions for all 100 ma injections and for 10 ma at 1.9 and 4 kV (not at 8 kV, and not for 1 ma at any voltage). The large return fluxes of electrons with energy between 100 eV (the detector's limit in that experiment) and the beam-ejection energy that were measured may be the source of the excess 3805Å radiation that is observed in SCEX. Since the volume in which these energetic electrons was confined was found to depend on

the angle between the injected beam's axis and the geomagnetic field, the column intensity of radiation would also be expected to depend on pitch angle [under discharge conditions].

DATA INTERPRETATION, CURRENT PROGRAM STATUS

The reduced data file and procedures in SCEXC permit direct systematic determination of the dependence of the normalized 3805Å-band irradiance factor X on individual experiment factors over selected ranges (for example, altitude above 130 km), as well as its joint dependence on two or more parameters (for example, V and I as in Ref 5; a threshold for beam-plasma discharge varying with $V^{3/2}/I$ was found in Ref 1's JSC Chamber A measurements). As noted above the absolute magnitudes of X as well as its relative values provide information about the nature of interactions of the injected beam with the atmosphere. Some of the critical ideas in interpretation of the single-parameter dependences are as follows.

If X varies with

-- I: Nonlinear beam interaction. Note, however, that when I is several times the threshold current for exciting a beam-plasma discharge PHOT again becomes about proportional to I, and thus under this condition X would appear to be constant.

We note also that the solid angle into which the electron beam is injected -- or more strictly speaking, its angular distribution of brightness per unit current -- may depend on the total current I from the accelerator. (This experiment issue was apparently not

considered in detail in the preflight testing). A variable beam-spread would introduce some error into FACT and so make X appear to change slowly with I (The onset of discharges depends on the beam current density rather than the total current I only.)

-- V: Nonlinear beam interaction, if a large relative change in X takes place over one of the two intervals in which V decreases by a factor 2.

The beamwidth might also be a function of the accelerator's anode potential V, which again would impact FACT. More importantly, the rate of excitation of secondary electrons changes with V because the number of secondaries ejected from the atmosphere's atoms relative to the number of direct impact excitations of 3805Å photons is a function of the primary electrons' energy. This ratio of secondaries to 3805Å photons increases by a factor 2.7 between 2 and 8 keV, while the average cross-section for C-state excitation by these secondaries decreases somewhat over this energy range because of the secondaries' increased mean energy. The result is an about doubled ratio of C-state excitations by secondaries relative to primaries over these injection voltages. Thus if the photometer signal is due principally to secondaries, X would increase

about as $V^{1/2}$ between 2 and 8 keV. Further, the initial angular distributions of secondary electrons could be varying with primary energy in a way that impacts measurably the total 3805Å irradiance. These two impact-ionization effects would be evidenced by continuous rather than abrupt change in X with V, and further would indicate that the signal is due principally to linear (with current and voltage) secondary processes.

--$[N_2]$: X inversely proportional to ambient $[N_2]$ means that either the number density of N_2 molecules within the effective measurement volume is being maintained constant by outgassing, or some discharge process that produces essentially-constant irradiance is taking place.

--[M]: X inversely proportional to [M] is further evidence that single-step impact excitation does not explain the 3805Å irradiances. Such a finding becomes consistent with the signal being due principally to secondary electron excitations if the magnitude of L needed to explain the magnitude of X/[M] is physically reasonable (refer to our earlier discussion); otherwise either outgassing that leads to enhanced C-state excitation by greater-than-expected fluxes of secondaries, or collective processes, is the controlling process. Noise in the data in part obscures the difference between $X \cdot [N]$ and $X \cdot [M]$, as $[M]/[N_2]$ increases by less than a factor

2 over the altitude range of the upleg data. ($\Sigma[M_i]\sigma_i/[N_2]$ x (crossection for impact ionization of N_2) changes even less because the crosssection of O is less than that of N_2.)

-- Time after launch: A monotonic decrease of X with time after apogee suggests that outgassing results in the enhanced production of secondary electrons by the beam that leads to domination of the total excitation by these secondaries' impacts on ambient N_2 molecules. Before apogee, the effect could be masked by the increase in X with decreasing $[N_2]$, which is discussed below. If the time constant for outgassing from the vehicle is large compared to the experiment time, the released gas might still be playing a role in initiating nonlinear interactions and enhancing the optical signal through secondary impact excitations despite the lack of any measurable time dependence. (Current-voltage thresholds for initiation of beam-plasma discharges are known to decrease with increasing neutral density at densities somewhat greater than those at ~130 km altitude (Ref 1).)

X can of course be determined for narrow ranges of the individual input parameters, with the disadvantage of increased data noise because of the smaller number of samples (an example is in Figure 6). Arguments similar to those above can also be developed for the the beam's pitch angle to the geomagnetic

field and to the vertical (as noted beam energy absorption differs between injection into the nadir and zenith hemispheres).

We have investigated the dependence of X averaged over upleg altitude intervals on $[N_2]$, [M], V, and I, with the results for the first three variables shown in Figures 4,5, and 6. The so far unaddressed downleg data extend to greatly increased values of $[N_2]$ and [M], where nonlinear beam interactions are known not to take place, and thus will provide an improved perspective on these preliminary results from the upleg data.

As Fig's 4 and 5 show, X clearly decreases with decreasing air density or increasing altitude. The product $X \cdot [N_2]$ or $X \cdot [M]$ appears to be essentially constant -- although noisy -- when $[N_2] < 5 \times 10^9/cm^3$ (180 km altitude), with $X \cdot [M]$ showing less variability. This result is similar to that reported in Ref 3 (the Polar V experiment), where the N_2^+ First Negative 3914Å photometer signal remained essentially constant, although also very noisy, above 140 km rocket altitude. It has also been observed (for 3914Å radiation) in laboratory tank tank experiments in which beam-plasma interaction has been unequivocally identified (Ref 22).

As Fig 6 shows, X averaged over 10 km altitude intervals increases with V, and is proportional to V^2 -- or $V^{3/2}$ within experimental error -- at each range of $[N_2]$. This is a stronger dependence than the $V^{1/2}$ that we showed would be expected from the change in relative number density (and possibly angular distribution) of secondary electrons. Although this observed behavior is suggestive of the familiar Child's-law limiting of current flow by space charge, its physical significance in the electron-injection experiment is not immediately clear. We note also that the 8 kV, 10 ma data points lie above and fair smoothly into the 4 kV, 10 ma points; this

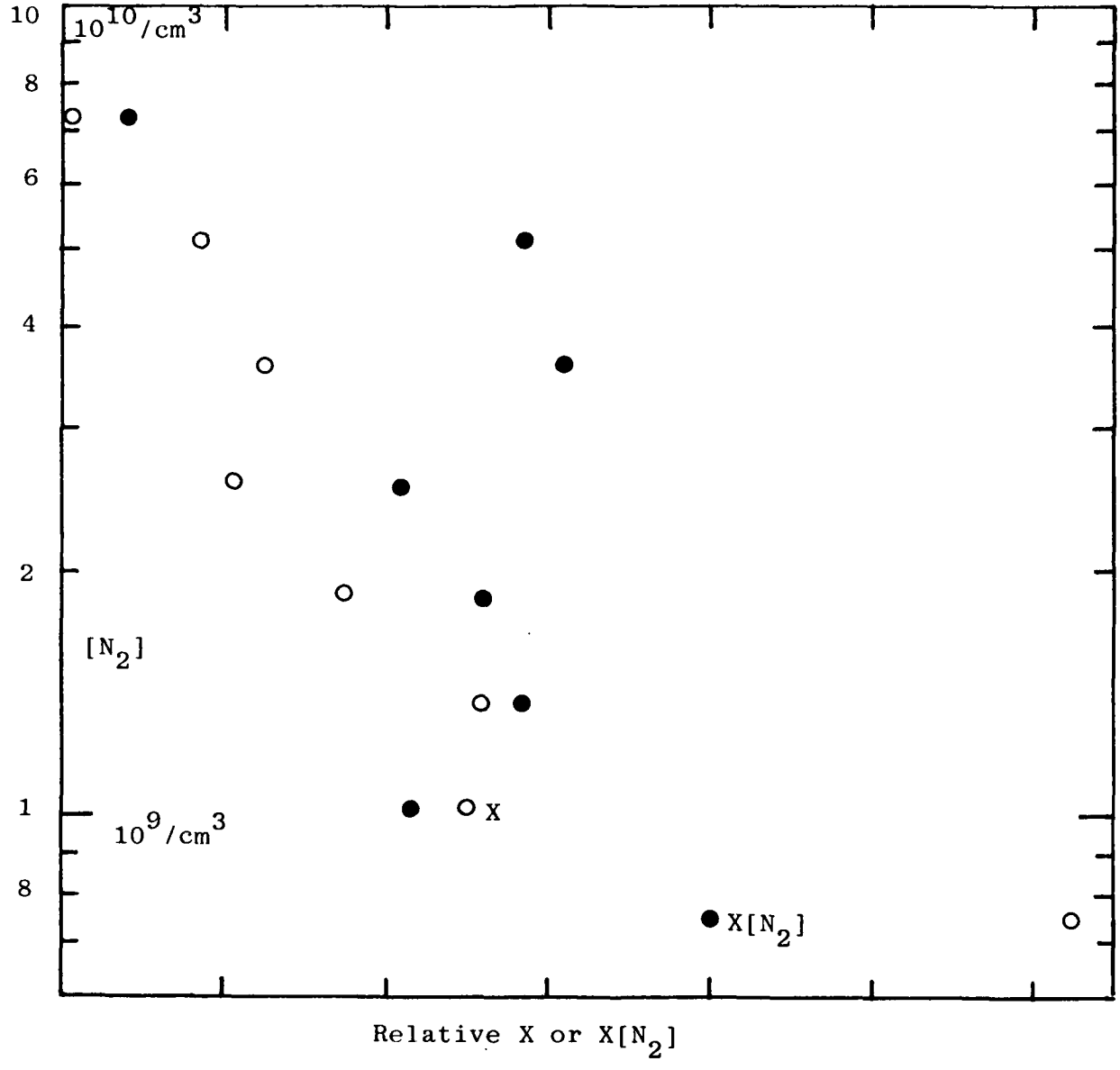

Figure 4. Dependence of X and X · $[N_2]$ on $[N_2]$ at upleg altitudes.

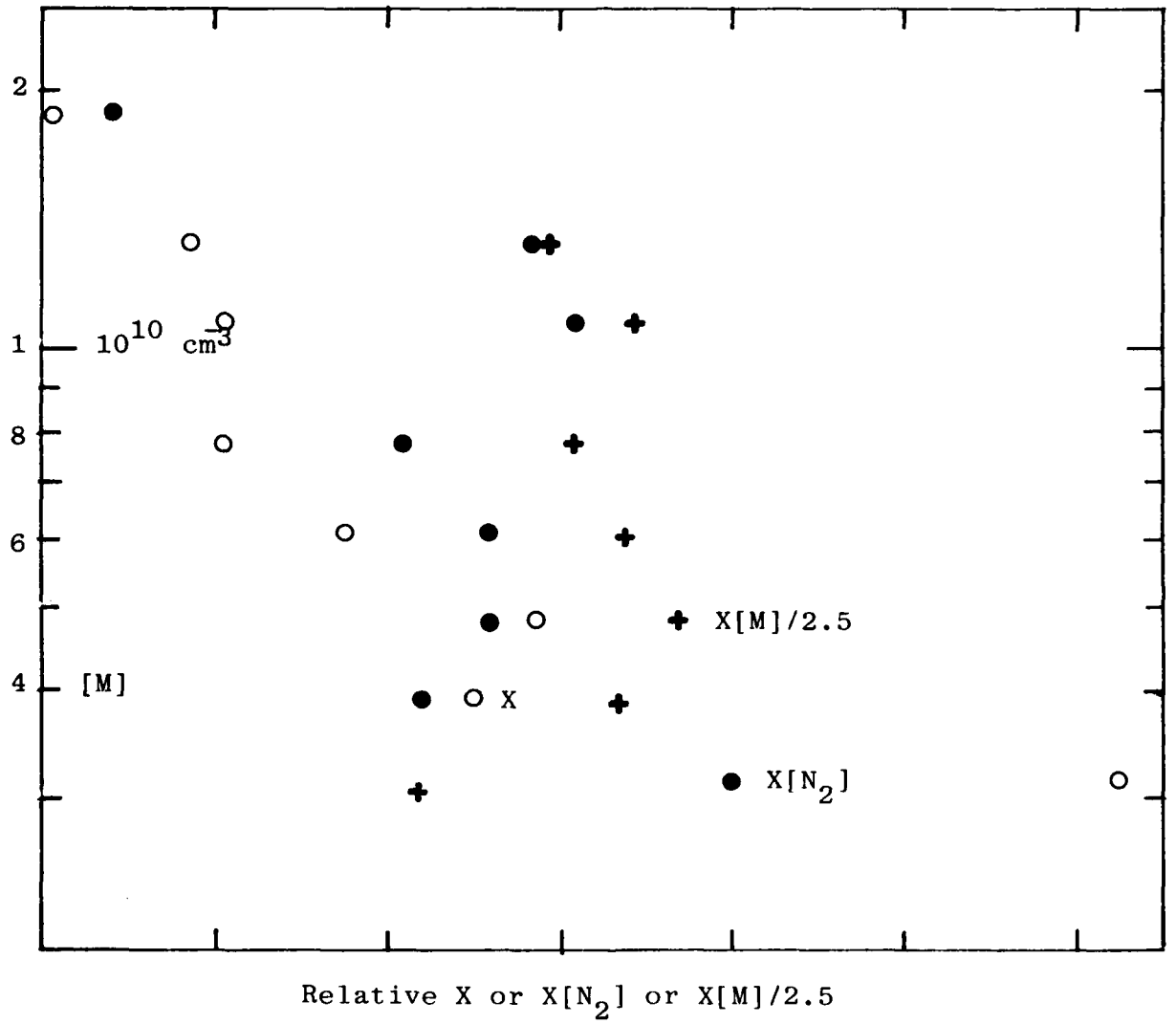

Figure 5. Dependence of X and X[M] on [M] at upleg altitudes.

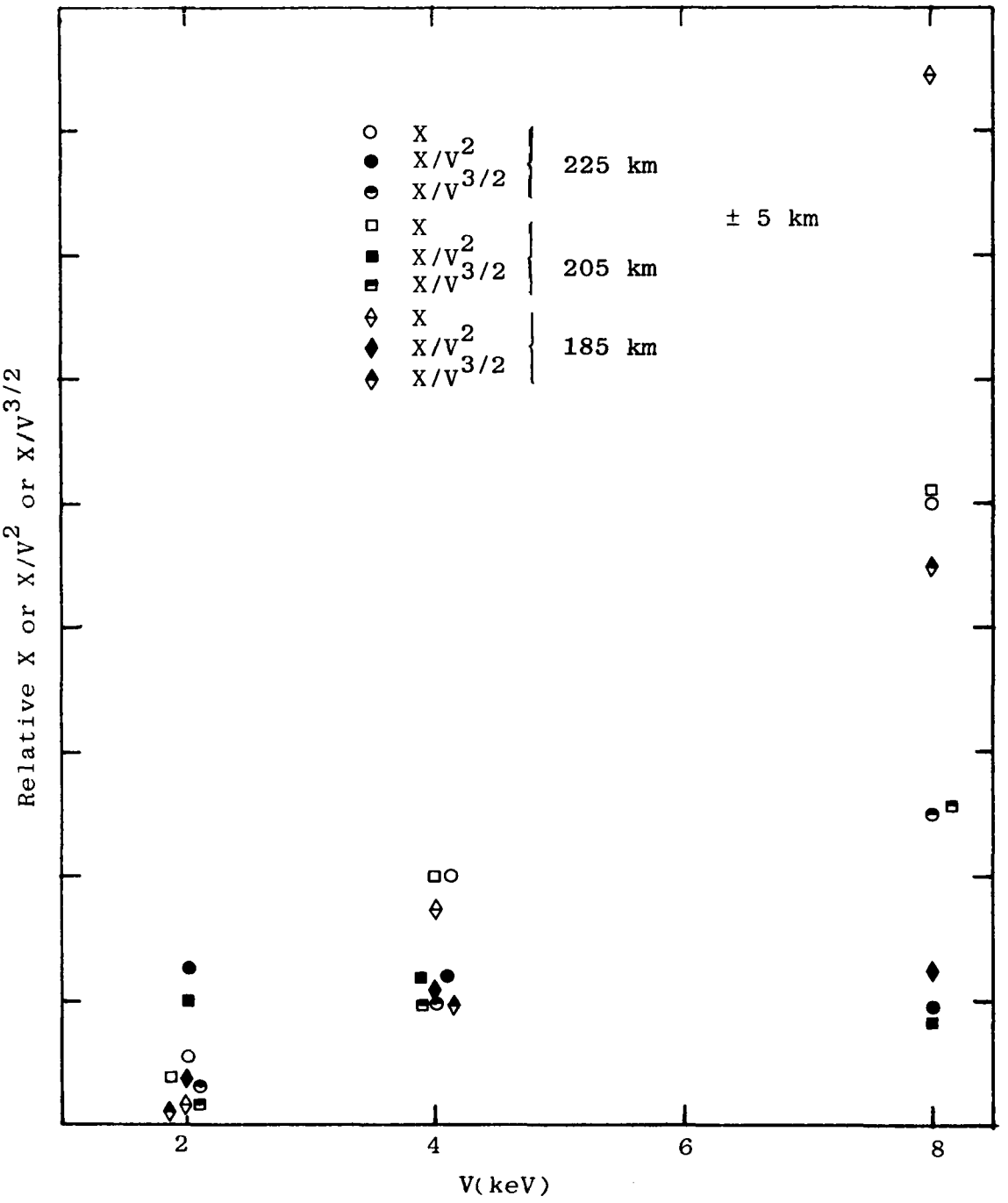

Figure 6. Dependence of X on V at upleg altitudes.

appears to be in disagreement with Ref 5's finding of qualitatively different interaction modes at the two injection voltages.

Since $\sigma(V)$ in our expression for X varies as $V^{\sim -3/2}$, PHOT at fixed altitude turns out to be virtually independent of V. (The ionization cross-section σ_i', on the other hand, varies with $V^{\sim -3/4}$.) The threshold for initiation of beam-plasma discharge increases with increasing V; this leads to the preliminary conclusion that over the experiment's range of injection voltages there is no evidence of turnon or turnoff of such discharges at the three altitudes so far considered. (We have not investigated the effect of noise in PHOT when I = 1 ma, where the results of Ref 5 indicate that discharge may not be occurring.) Laboratory experiments to date have not explicitly addressed the issue of how the volume excitation rates depend on particle energy while a beam-plasma discharge avalanche is sustained. Theory (Ref 23) predicts a weak dependence on V, as we observe; the change can be in either direction, depending on experiment conditions. Theory also predicts an increasingly noisy photometer signal near threshold where the discharge is not fully stable (Ref 23); this phenomenon can be readily investigated by analysis of PHOT's variability within individual 50-msec data pulses and between averages over pulses.

The dependence of X on I is not yet determined, as the photometer data have not been treated to minimize the effects of noise introduced by subtraction of auroral background (particularly troublesome at 1 ma) or the loss in statistical precision due to the spread of points where the accelerator was operated at its maximum achievable current. At the present stage of data analysis X appears to decrease between 1 and 10 ma and then increase to the 40-90 ma data set. Under beam-

plasma discharge conditions PHOT would increase with I (as shown by Ref 1 and other laboratory experiments), and become about proportional to I when I is several times threshold; thus if X is found to be constant over the range of maximum injected currents its magnitude becomes the measure of whether a discharge is taking place.

CONCLUSIONS, RECOMMENDATIONS

This preliminary analysis of the SCEX 3805Å photometer data indicates that the ejected electron beam is interacting nonlinearly with the atmosphere (at least at currents >1 ma); it has not, however, been carried to the point of providing quantitative information about the dependence of this interaction on the several experiment variables. The major finding is that the irradiance is virtually independent of both ambient density above about 180 km (as has been observed in other experiments) and energy of the injected electrons (not hitherto observed, albeit consistent with beam-plasma interaction models). The important issue of dependence of normalized irradiance on electron beam current has not yet been adequately addressed. The calculational machinery (SCEXC, Table 4) is fully in place, and precise interpretation of the experiment will become possible when the improved statistics and -- particularly -- wider dynamic range of [M] and [N_2] in the trajectory's downleg data segment are included in the analysis.

The work to date leads to ideas for improving the effectiveness of optical and in situ diagnostics in future particle beam injection experiments (including of course BERT-1). Primarily, it underscores the importance of imaging instruments -- cameras -for measuring the spatial distribution of the primary and secondary (and discharge-induced) radiations.

Further recommendations are

1) The injected current should be varied in arithmetically rather than geometrically increasing steps, better to identify nonlinear changes in radiant intensity. Additionally, the dependence of optical emissions on current would be more precisely quantified by use of more than the present three values.
2) Beam voltage should also be varied in at least four arithmetic increments to establish its effect on the plasma conditions.
3) The photometer's throughput should be increased to improve signal/noise at low injected currents (<10 ma), and the beam-on time lengthened.
4) If continuous rocket spin is not needed to measure the pitch angle distribution of the secondary electrons, the electron beam should be injected at a) a limited number of discrete angles to the geomagnetic field (parallel, perpendicular,...) and b) at 0° and 180° zenith angle only (that is, along the atmosphere's density gradient). Additionally, the detailed analysis of the SCEX data may suggest more frequent sampling and even higher photometer throughput better to characterize noise in the irradiance (i.e., instability in the plasma conditions), and higher rocket apogee to increase the dynamic range of $[M]/[N_2]$.

5) Concentrations in the viewed beam volume of the principal outgassed species, water vapor, should be measured optically as described in Appendix I (or alternatively by the return flux to the rocket measured by mass spectroscopy).

SECTION III

BERT-1 INSTRUMENTATION

BACKGROUND

BERT-1 (Beam Emission Rocket Test-1) is an AFGL rocket investigation of the interaction of low-energy electron and positive ion beams with the atmosphere, and of the effects of vehicle charging on beam ejection and propagation. (The behavior of higher-energy particle beams is to be investigated by BERT-2 and from space shuttle, according to current plans.) PhotoMetrics was responsible for design and construction of the experiment's in-flight optical diagnostics system.

The planned program of injected currents-voltages, the angle the beam makes with the rocket axis (and its divergence), the rocket's spin rate and angle to the geomagnetic field, the measurement altitudes, and other parameters in Table 5 were considered in setting the sensitivity thresholds, dynamic range and sampling time of the optical sensors. The electron injection sequence extends over 2.0 sec, in the following program:

0.5 kV:	4 current pulses logarithmically increasing from 0.02 to 20 ma in 50 msec and decreasing back to 0.02 ma in 17 msec;
1.0 kV:	50 msec rise time from 0.5 kV at 0.02 ma, then the above current pulses are repeated;
2.0 kV:	50 msec rise time from 1 kV at 0.02 ma, then the above current pulses are repeated; then 0.25 sec pulses of 0.02, 0.2, 2, and 20 ma;

repeat above sequence.

Table 5. BERT-1 Experiment Parameters

Item	Parameter	Value	Comments
1	Rocket Spin Rate	Despun to 1/2 s^{-1}	Determines rate of change of optical radiances; rocket has attitude control
2	Directions of injections from rocket	90° from long axis, from station 62	Determines instrument pointing directions, fields of view
3	Instruments turnon Apogee	120 km 250 km	$[N_2] = 4 \times 10^{11}$ cm^{-3} $[N_2] = 6 \times 10^{8}$ cm^{-3}
4	Velocity at turnon Horizontal velocity	~2 km s^{-1} ~1/4 km s^{-1}	With spin, determines instrument dwell time
5a	Angle of trajectory plane to magnetic meridian plane	0°	Launch N along magnetic field direction
5b	Magnetic field intensity	0.49 gauss	White Sands Missile Range at ~150 km altitude; gyroradii ~ same as at SCEX
5c	Dip angle	62°	
6	Range of injection pitch angles	0° - 85°	Depends on ACS program
7	Ejected Electrons: Energy Current Half-angle	 0.5 - 2 kV 0.02 - 20 mA 2-1/2°	 Concentration on 2 kV with four 1/4 sec pulses
8	Ejected Ions: Energy Current Half-angle	 4-1/2 kV max 0.01 - 20 mA 7° (nominal)	 He^+ and Ar^+. Little magnetic deflection
9	Electron gun pulse sequence	Refer to text	Requires response time <10 ms and telemetry rates >100 Hz, puts constraints on video

Currents (up to 20 ma is planned) and timing of the 0.1-5 keV positive ion injections have not yet been established. The particle beams will be ejected normal to the rocket's long axis from near its forward end; the optical sensors are located toward its tail end to achieve the desired projections to the excited air volumes. As with the SCEX rocket, apogee is 250 km, but with the data period starting at a substantially lower altitude. The factor-500 range in ambient air density, -1000 in injected current, and -4 in primary electron impact cross-section (between 1/2 and 2 keV) results in a dynamic range of primary excitation rates of about 2×10^6 over the experiment.

PROGRAM TIMETABLE

Planning for BERT-1's optical sensors began in February 1981 (before the results from SCEX became available). We prepared and submitted on 15 July a 48-page Design Evaluation Report "Design of an Optical Measurement System for Diagnosis of Beam and Plasma Conditions Near a Charge-Ejection Rocket," AFGL-TR-81-0000, which was approved by AFGL on 23 July 1981. The actual instrument buildup began in June 1982, when funding for purchase of the low light level video camera's components and construction of the photometers was received.

The video camera body, delivery of which had been promised by its vendor (Edo Western, Salt Lake City, UT) for 16 Feb 83, was not received until 29 April. PhotoMetrics completed construction and calibration, and delivered the completed camera system, two wide-field ("total light") photometers, and a plasma sheath photometer on 05 Aug 1983.

Numerous conferences with AFGL staff and other BERT-1 program contractors were held in the period May 1982-July 1983 on the mechanical and electrical interfacing of these instru-

ments, and on their ruggedization for the rocket environment. In June 1983 AFGL specified a major change in the mounting of the video camera, which as delivered by PhotoMetrics is designed to view a relatively narrow angular field from inside the rocket body envelope rather than the initially-planned "all-sky" field from a platform erected to extend 30 cm outboard from the skin. (The latter arrangement would have permitted viewing the beam at the accelerator anode as well as the back-scattered-electron component; the spatial distribution of air fluorescence in these close-in regions is an indicator of discharge processes.)

DESIGN EVALUATION REPORT

The rationale and performance specifications for the optical instruments system is presented in detail in the Design Evaluation Report. For reference we have reproduced in Table 6 its Table of Contents, List of Illustrations, and List of Tables.

The report in particular considers the impact of the experiment parameters in Table 5 on design of the optical instruments. It reviews corona (Ref 24) and beam-plasma discharges (Ref's 25, 26) excited by electron beams, optical emission by/from ion beams, and performance specifications for the instruments selected to diagnose these phenomena. The Design Evaluation Report serves as background for the engineering documention in this Section.

OVERVIEW

The optical sensor system consists of a low light level (Intensified Silicon Intensifier Target, ISIT) video camera; two wide-field photometers for viewing the beam and back-scattered-secondaries volumes; and a narrow-field photometer for investigating the plasma sheaths ("corona") surrounding

Table 6. Table of Contents and Lists of Illustrations and Tables in PhotoMetrics' Design Evaluation Report "Design of an Optical Measurement System for Diagnosis of Beam and Plasma Conditions Near a Charge-Ejection Rocket" (15 Jul 81).

TABLE OF CONTENTS

Table 6. Continued

Table 6. Concluded

LIST OF ILLUSTRATIONS

LIST OF TABLES

the vehicle. The beam temperature photometer described in Section 4.4 of the Design Evaluation Report, which applies the spectroscopic features ratios principle that we used in SCEX (refer to Section II), was eliminated from the final instrument package due to lack of funds.

The Design Evaluation Report originally specified the video camera to have an extremely wide field from an outboard viewing platform, so as to achieve a better projection of the beam and glows enveloping the rocket body than had been available in previous experiments. As a result of the above-mentioned mandated engineering change the camera as realized is fixed within the rocket, and views a relatively limited longitudinal segment of the ejected beams from station 160 (inches from the nose, 2-1/2 m from the accelerator). Its S-20 photocathode is sensitive principally to the N_2 First and Second Positive and N_2^+ First Negative fluorescence bands excited by the electron and (with substantially less efficiency) ion beams. A principal function of the camera is identifying onset of nonlinear electron beam interactions, whose spatial distribution signatures include a "halo" of radiation excited by laterally-scattered secondaries surrounding and within the spiral made by the primary beam along with increased backward scattering (Ref's 1-5, 25, 26). A further function is monitoring the angular spread and current of BERT-1's ion beams.

The wide-angle photometers provide substantially lower threshold sensitivity and higher frequency response than the video cameras (at the expense, of course, of imaging capability). Since this sensitivity is limited by the background of airglow, stellar, and zodiacal light rather than photon noise in the signal, the photometers use Si diode photodetectors rather than electron multiplier tubes. These are filtered to respond

to blue N_2 Second Positive and N_2^+ First Negative band radiation. With Lambertian angular response, they integrate the radiance distributions from the beam and secondaries over much of the forward and backward hemispheres. This irradiance signal increases by about an order of magnitude when the beam's propagation mode changes from individual electron-transport to collective-interaction mode (Ref 1). These fast-responding photometers are sensitive to up to 215 Hz noise components in the optical radiation (this noise is discussed in Section II) and to the optical flicker that is expected to occur at the 25 Hz (N_2^+) ion cyclotron frequency (Ref's 23,26) under beam-plasma but not corona discharge conditions.

The plasma-sheath photometer has a narrow (4° x 8°) field pointed along the rocket skin, at 90° from the beam ejection direction (rearward) from a point 180° in azimuth from the accelerator anode (that is, on the opposite side of the rocket). Its principal function is to measure radiation from the plasma sheath associated with corona discharge thought to surround the vehicle (Ref 24). To achieve this view parallel to the rocket's long axis requires in-flight deployment of a mirror, which folds the photometer's optic axis while translating it some 15 cm outboard from the skin.

Figure 7 shows the three instruments with their electronic controls and power supplies (internal in the plasma sheath photometer, see below). Their characteristics and telemetry are summarized in Table 7. The optical-diagnostics system is powered by a separate 28 volt battery (supplied by the payload integration group), and draws 18 watts.

WIDE FIELD PHOTOMETERS

These photometers are designed to measure the irradiance from the beam and backscattered electrons, at a sampling rate

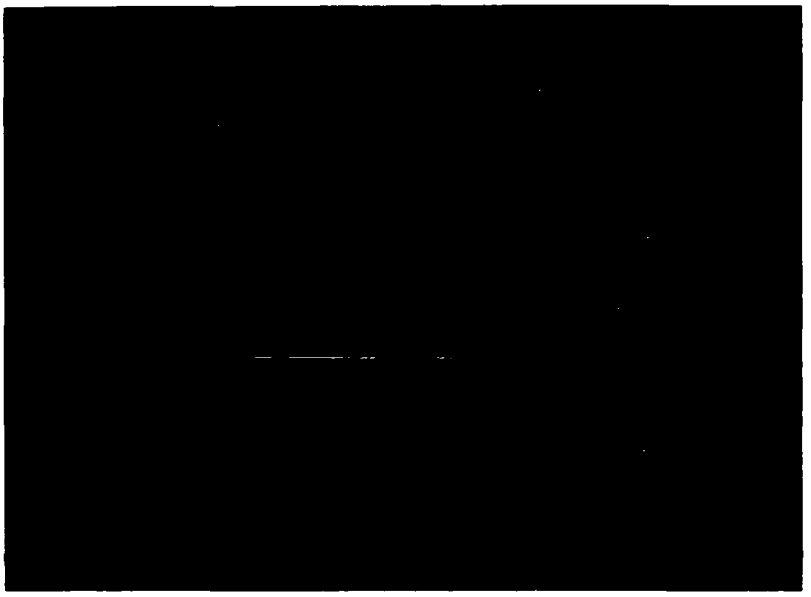

Figure 7. BERT-1 optical instruments and mechanical mounts. The plasma sheath photometer (black anodized) is at left. The low light level video camera (white) with its control electronics and connecting cable is in the center. At right front is the electronics box, cables, and sensor heads of the two wide-field photometers. Dimensions may be estimated from the 171 mm (6-3/4 in) width of the black video electronics box.

Table 7. BERT-1 Camera and Photometers

		Video Camera	Wide Field Photometers (2)	Plasma Sheath Photometer
Optical System		5.7 mm f.ℓ., f/1.8 on axis (T = 2.2 at 4000Å) lens, 3/8 x 1/2 in photocathode	Flat circular photodiode with 2 mm Schott BG-12 filter	Koehler illumination, 60 mm f.ℓ. objective and 31.7 mm relay lens, 4.8 x 9.5 mm field stop, 2 mm BG-12 filter (Figure 14)
Photo-detector		RCA 4849/AH	EG&G HUV 4000B	Hamamatsu 1288, 3/4 in Bialkali
Clear aperture		N/A	1.0 cm^2	15.2 cm^2
Angular field		40° x 80° Vignetted by skin opening	Lambertian (120° circular half-response)	4° x 8° Rectangular (0.099 steradians)
Spectral Sensitivity, photon units	PEAK	4400Å	4075Å	3900Å
	FWHM	3850-6000Å	3400-4720Å	3400-4600Å
	FW1/10M	3750-7660Å	3200-4950Å	3250-4900Å
Response		Video 60 Hz Half frame	Linear, 3 gain channels	Logarithmic, 4 decades
Sampling rate of telemetry		Gain ckt 215/sec FM video	430/sec low gain 215/sec others (~10/sec ± 15V monitor)	215/sec (~10/sec HVPS and 28V DC monitors)
Location and C/L pointing on rocket		Station 160 Az 0° El 34°	Station 140 Az 0°, 180° El 55°	Station 110 Az 180° El 180° with mirror

several times the 25 Hz ion cyclotron frequency. Because of their wide, essentially-Lambertian, angular field their response is limited by the sky background (airglow -- and also ground light sources -- when they look into downward hemisphere, stars and zodiacal light in the upper hemisphere); thus these instruments have no need for the noise free amplification of photomultipliers, and can operate with photodiode detectors. This greatly simplifies both the mechanical and electrical design of the units (for example no high voltage power supply is required).

Figure 8 shows one photometer head and the amplifier-controller for the two units. Their total weight is 1-5/8 lbs. Dimensions are as follows:

Head: 2-1/4 x 1-1/8 x 7/8 inches

Head mounting plate (upper right in top photograph): 3 x 1-1/8 x 1/8 inches, aluminum

Control box: 5 x 3 x 1-5/8 inches

Box mounting plate: 6 x 3 x 1/8 inches, aluminum.

Cable connecting heads to controller (shown in Fig 7): 4-1/2 ft, 1/4 inch diameter, 8 wires in each section (refer to Figure 10).

(As the mechanical design of these rectangular boxes is so simple we have omitted outline drawings; copies of these were submitted to AFGL to facilitate mechanical interfacing of the photometer units.) The electrical interface to the rocket's 28V primary power input and telemetry output is diagrammed in Figure 9, and the electrical interconnection between the two heads and the controller is documented in Figure 10.

Figure 11 is a schematic of the circuit that feeds the photometer outputs to the rocket's telemetry. Three gain

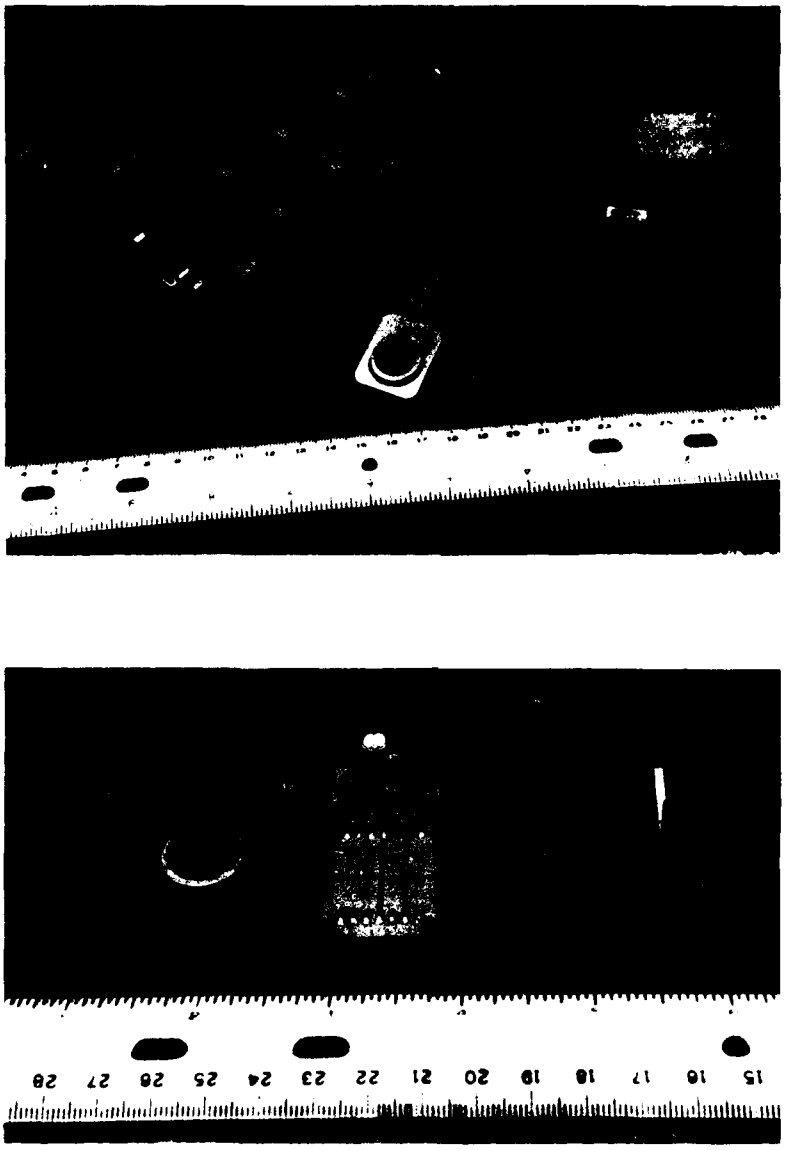

Figure 8. Wide field photometer head with voltage conditioner, and six channel amplifier-controller box.

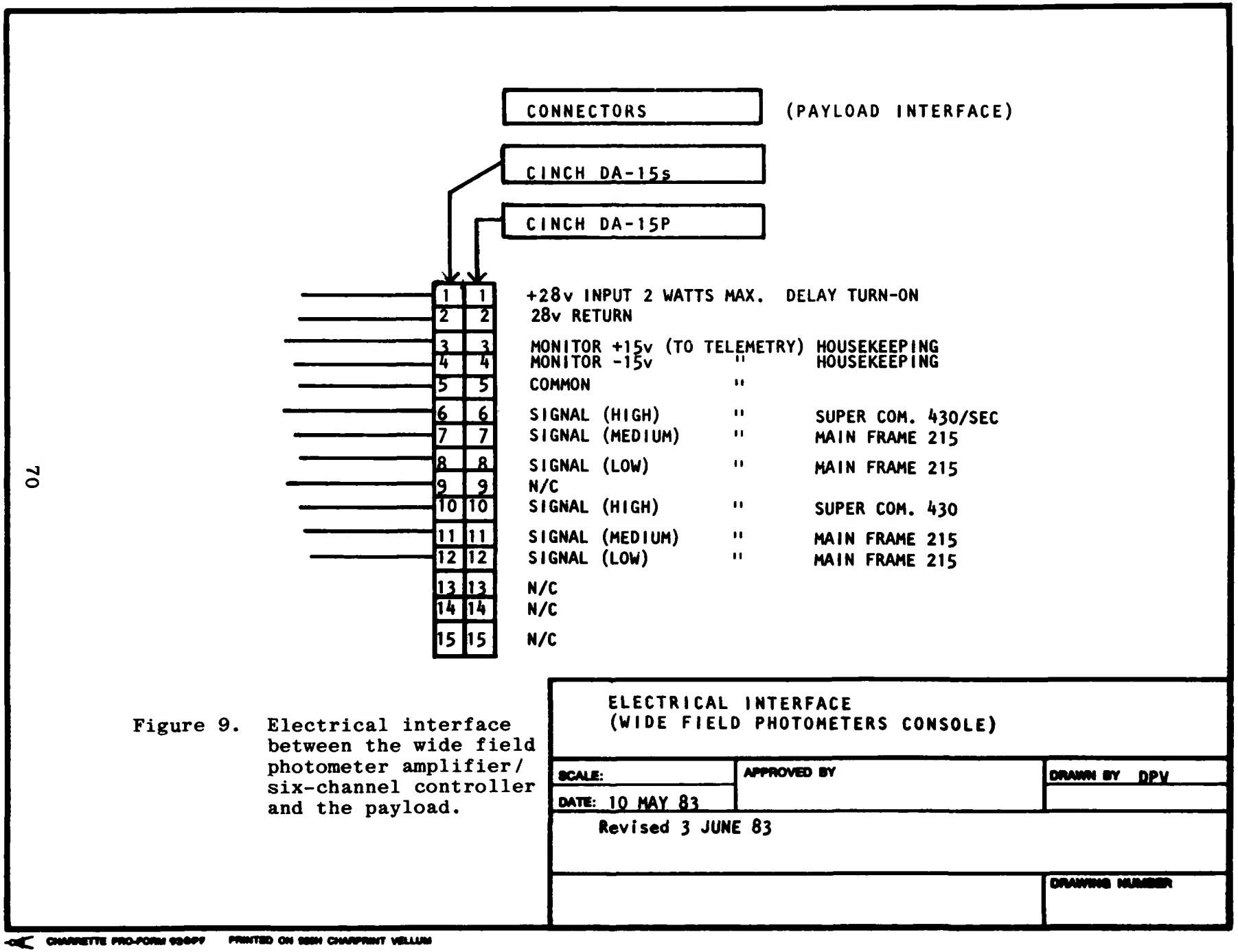

Figure 9. Electrical interface between the wide field photometer amplifier/ six-channel controller and the payload.

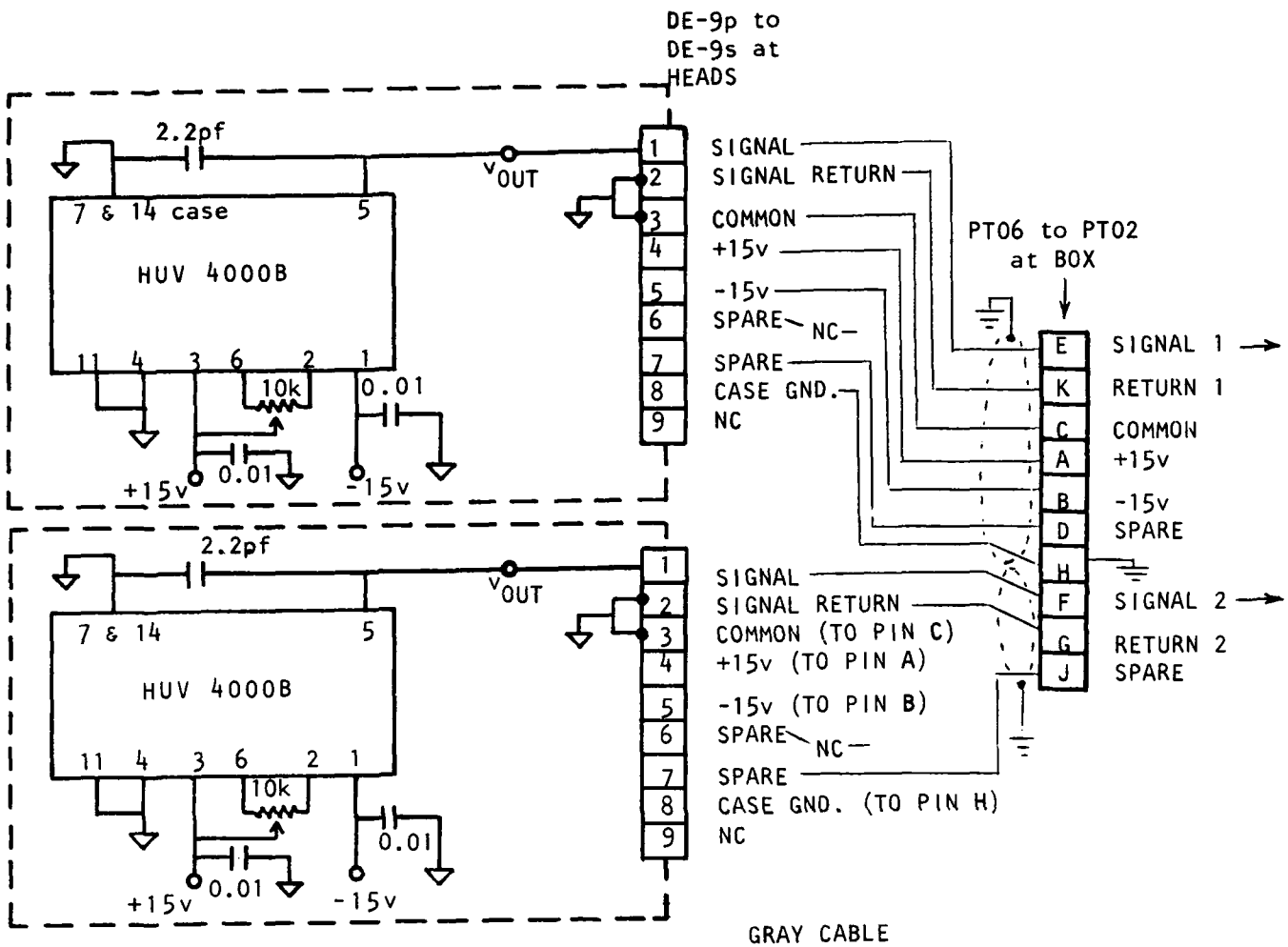

Figure 10. Electrical connections between the wide field photometers and their control console. Each photodiode case is isolated from chassis ground.

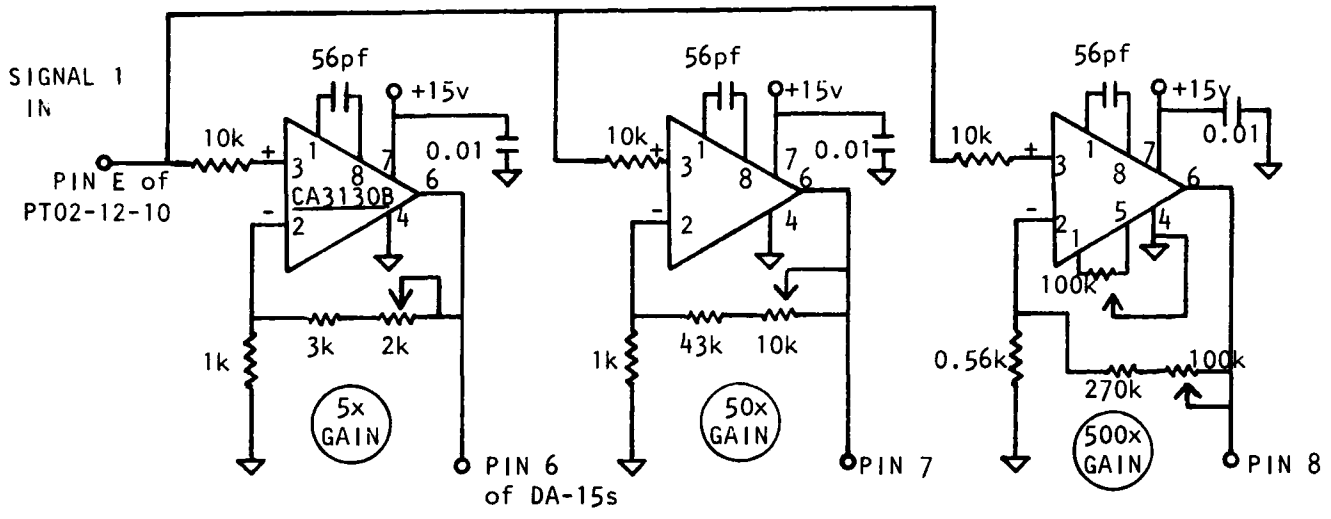

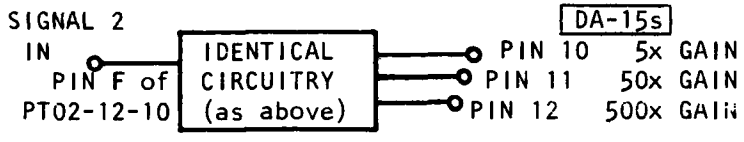

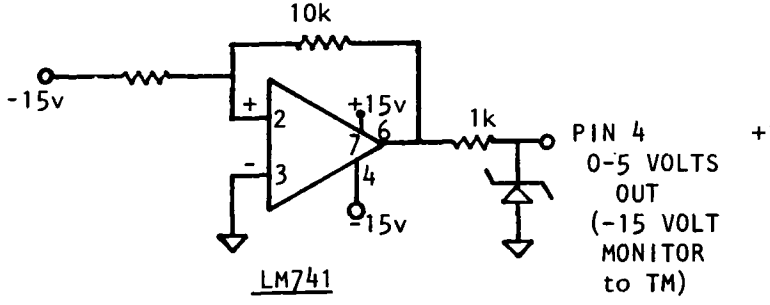

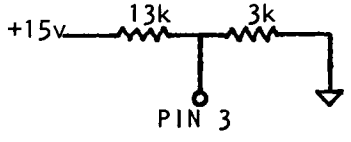

Figure 11.

Circuit diagram of the wide-field photometer amplifiers. Power is supplied by one ±15V Technetics 1-watt unit.

channels, 5x, 50x, and 500x, are used to increase the dynamic range of each photometer, with the sampling rates listed in Table 7. The ±15 V power supply's terminal voltages are also monitored during flight.

The silicon diodes are standard commercial units made by EG&G, Inc. (Salem, MA; data sheet D30002-D), with their Suprasil front window replaced by 2 mm of Schott BG-12 (blue) filter. Sensitive area of the diodes is designed to be 100 mm^2. The small electronic circuit in the bottom of Fig 8 serves to null out the dark current of the photodiodes; its schematic diagram is shown in Fig 11.

The photometers were calibrated against the uniform continuum (tungsten) low-brightness source that will be used by AFGL to check their stability and performance after vibration and other environmental testing (Unit D3), with the results shown in Figures 12a and b. Attention is directed to this transfer unit's anomalously large (factor-9) brightness step between apertures with nominal relative area 32 and 64, which although distorting the data presentation in no way damages the calibration. The absolute-irradiance point refers to radiation at the 4075A peak of the wavelength sensitivity characteristic summarized in Table 7. We note that the actual absolute irradiance response depends on the actual spectral intensity within the scene; with the model emission spectrum of the electron-irradiated thermosphere, an absolute calibration accurate to ±50% could be derived (as we did for the EXCEDE wide-band photometry; refer to the discussion in Ref's 2 and 20).

PLASMA SHEATH PHOTOMETER

This instrument, shown in Figures 13 and 14, has its two power converters (HV for the photomultiplier and ±15 V for the electronics and signal conditioning electronics) mounted

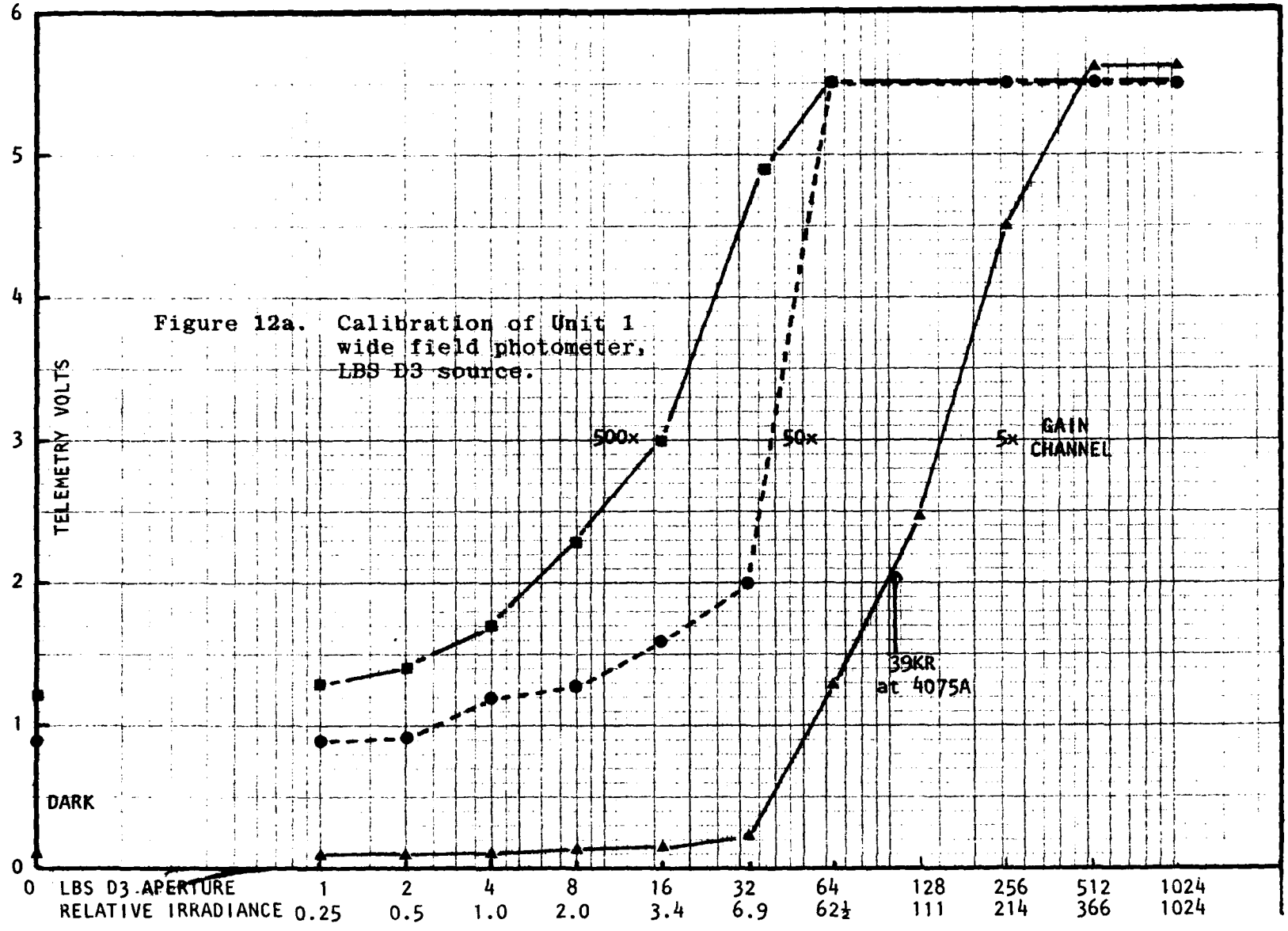

Figure 12a. Calibration of Unit 1 wide field photometer, LBS D3 source.

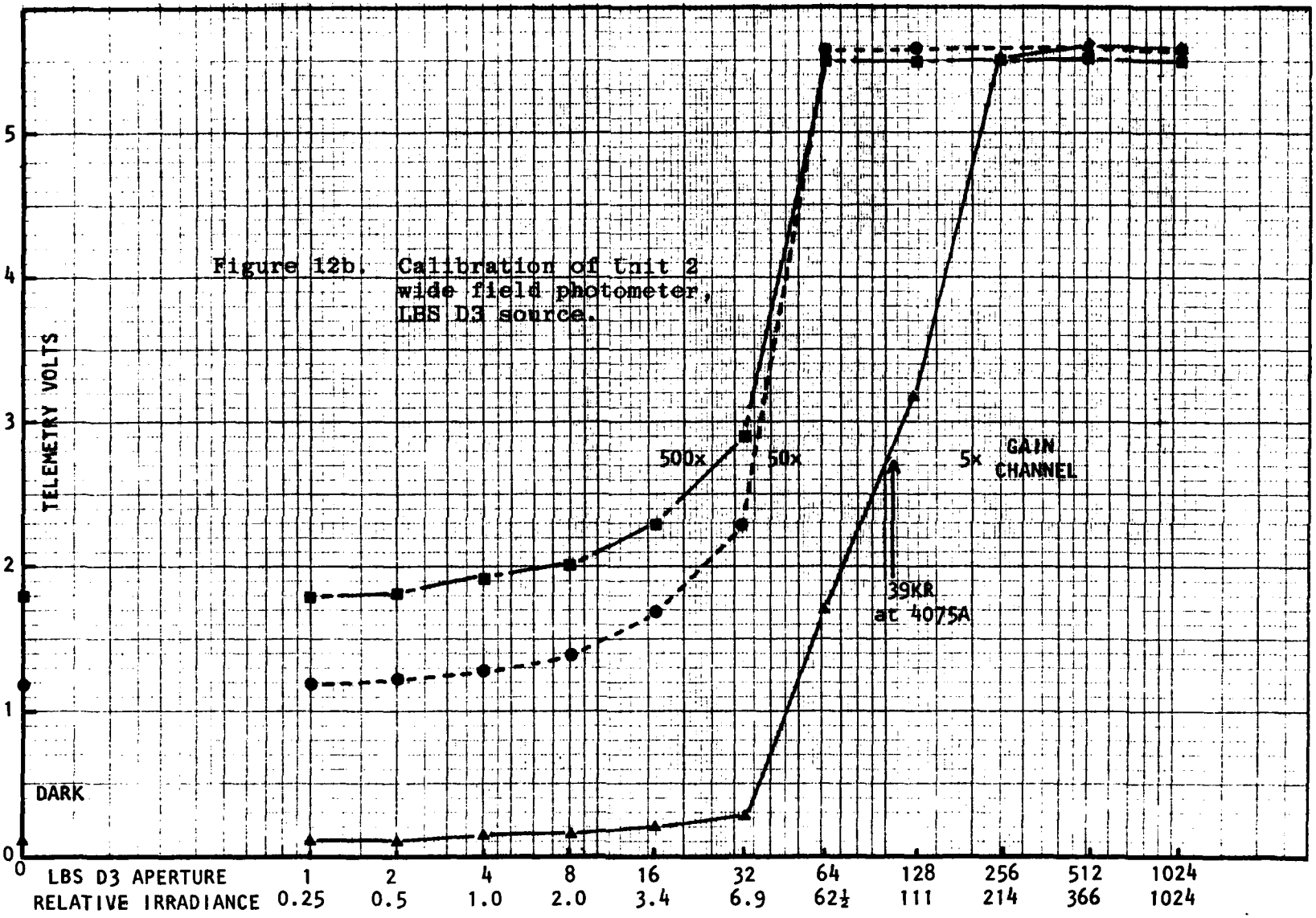

Figure 12b. Calibration of Unit 2 wide field photometer, LBS D3 source.

internally. The caption of Fig 13 provides a further description of its mechanical construction. Total weight with mounting hardware is 5-3/4 lbs. 28V primary power is brought in and the 0-5V telemetry signal is taken out by a single 9-pin cable. Figure 15 is an outline (mechanical interface-mounting) drawing, and Figure 16 shows the photometer body's mounting relative to its field-folding mirror.

The plasma sheath photometer's circuitry with its logarithmic amplifier are shown in Figure 17, and the electrical interface to the payload is documented in Figure 18. Voltage applied to the photomultiplier is regulated to <1/10% per 1 volt change in the input battery voltage. Both those voltages are monitored and telemetered as shown in Fig 17. Any changes in the high voltage due to photocurrent drain are compensated in the radiance-to-output TM voltage calibration. The resistors directly connected to the logarithmic amplifier (Burr Brown 4127, hybrid) adjust its scale factor and condition the output to 0-5 volts for the telemetry.

The photometer's location on the rocket and angular field are designed to make it view the space within a few cm of the skin, while rejecting radiation that might be excited at the material surface. Its optical system (Fig's 13,14) is a Koehler illuminator that provides virtually uniform angular response while spreading the image over the photocathode to eliminate error due to its local variation of photoelectron conversion efficiency. Out-of-field radiation is further rejected by an internal baffle, and the angular field is defined by a machined slit at the field stop. A large-area objective lens is used to partially compensate for this necessarily narrow field, resulting in an etendue of 1.5 cm^2 sterad. The photometer is mounted with its axis perpendicular to the rocket's long axis, and views the sheath on the side of the rocket away

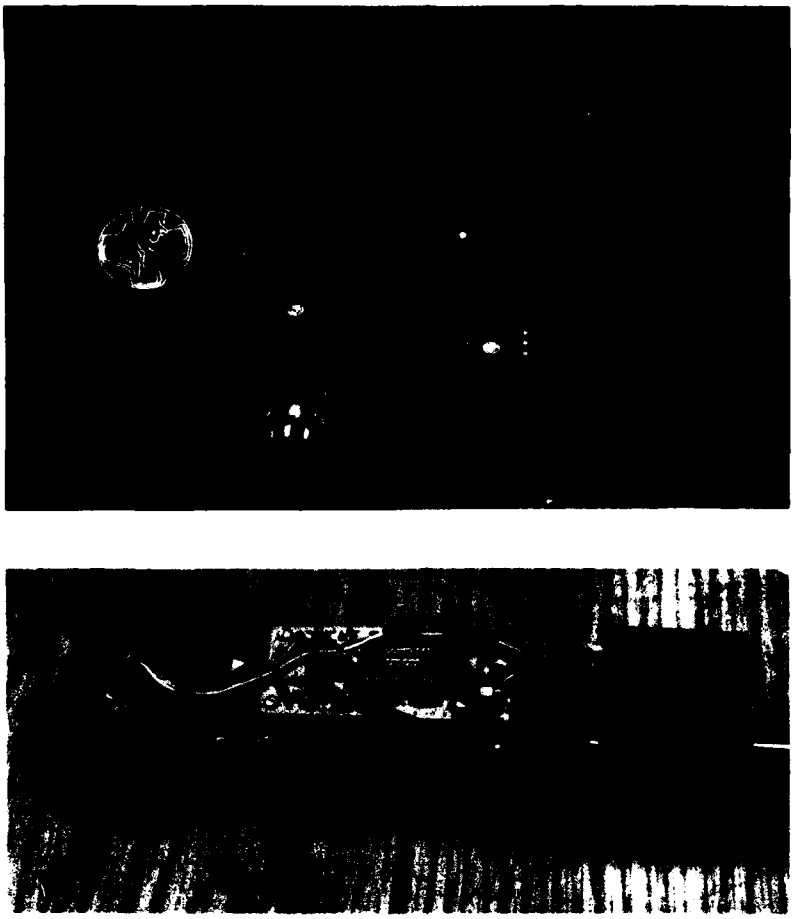

Figure 13. Plasma sheath photometer, disassembled and partially-assembled (before potting of the electronics board). Figure 7 includes an assembled view looking toward the lens. The unit with its high voltage (left rectangular package) and low voltage (center, with three output pins) power supplies and logarithmic amplifier (top of assembled view) is completely self-contained. The primary power and signal output cable, provided by AFGL, mates to the DE9P connector of the back plate. Elements of the optical system are, from left to right: threaded retainer ring, BG-12 filter, objective lens, spacer, baffle, spacer, and assembly of field stop (slit) with relay lens (out of view behind stop). At right of the bottom figure is the photomultiplier tube housing, with dynode chain attached (back view is shown in top figure). The thin silver alignment rod at right in the lower figure fixes the orientation of the field stop.

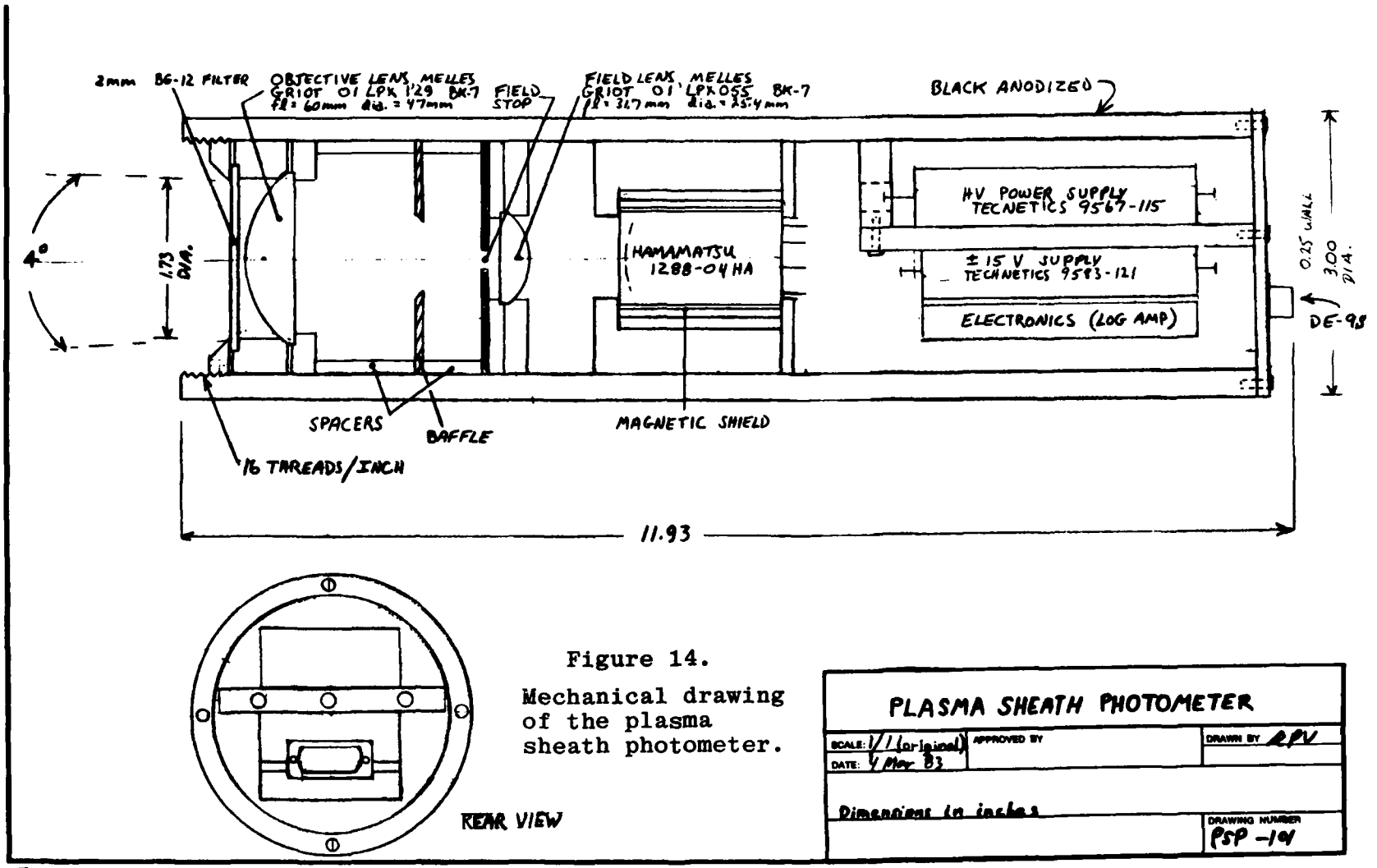

Figure 14.

Mechanical drawing of the plasma sheath photometer.

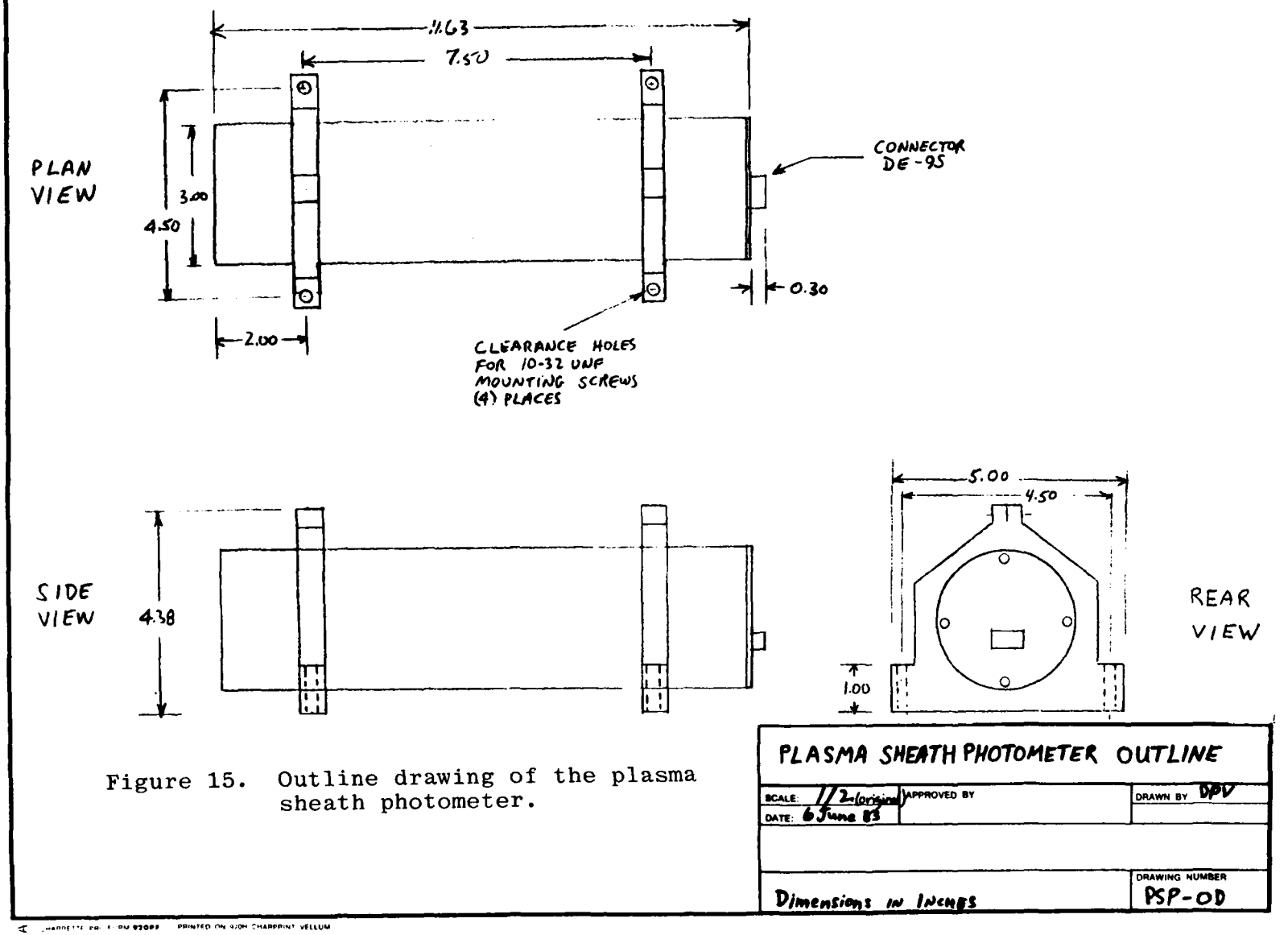

Figure 15. Outline drawing of the plasma sheath photometer.

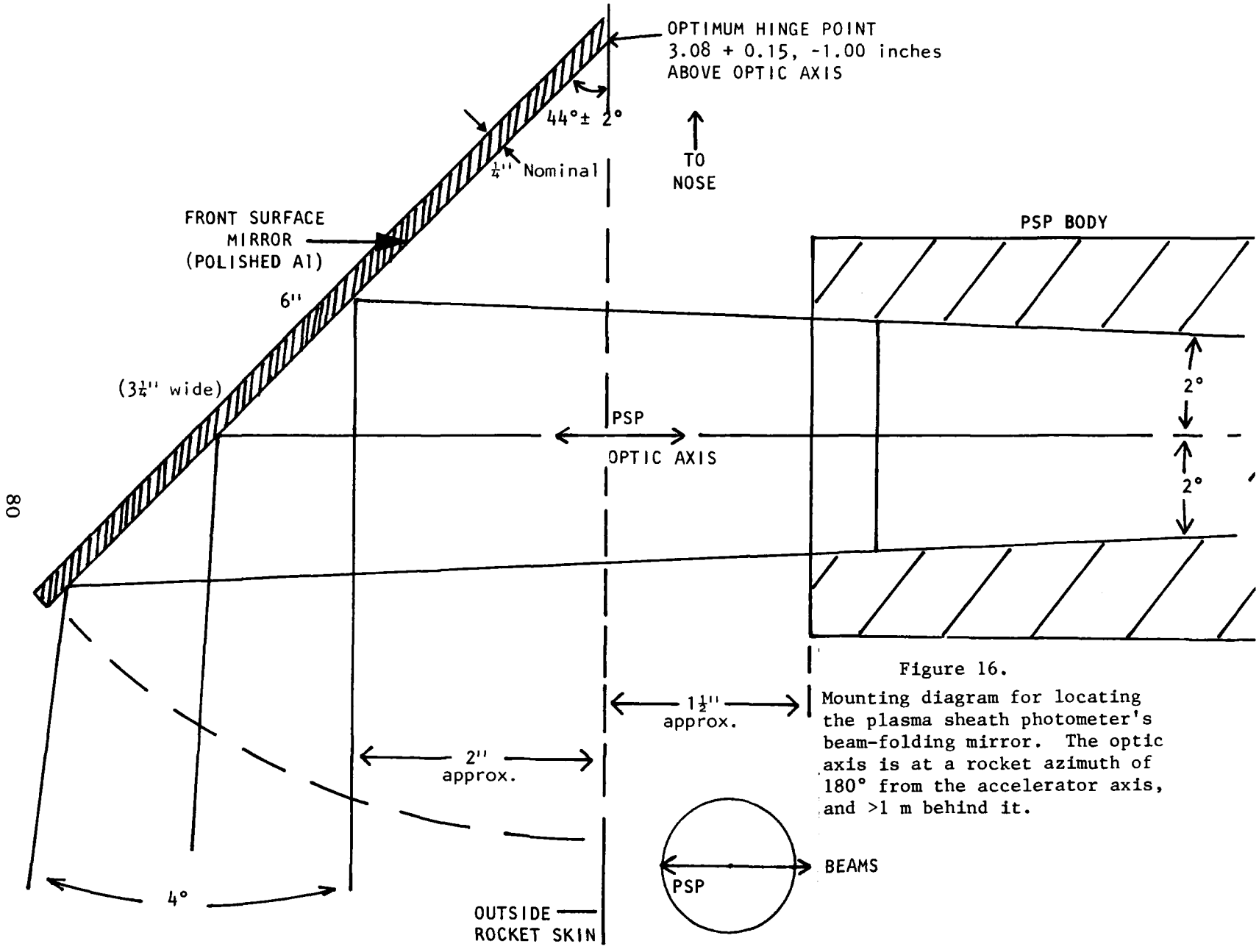

Figure 16.
Mounting diagram for locating the plasma sheath photometer's beam-folding mirror. The optic axis is at a rocket azimuth of 180° from the accelerator axis, and >1 m behind it.

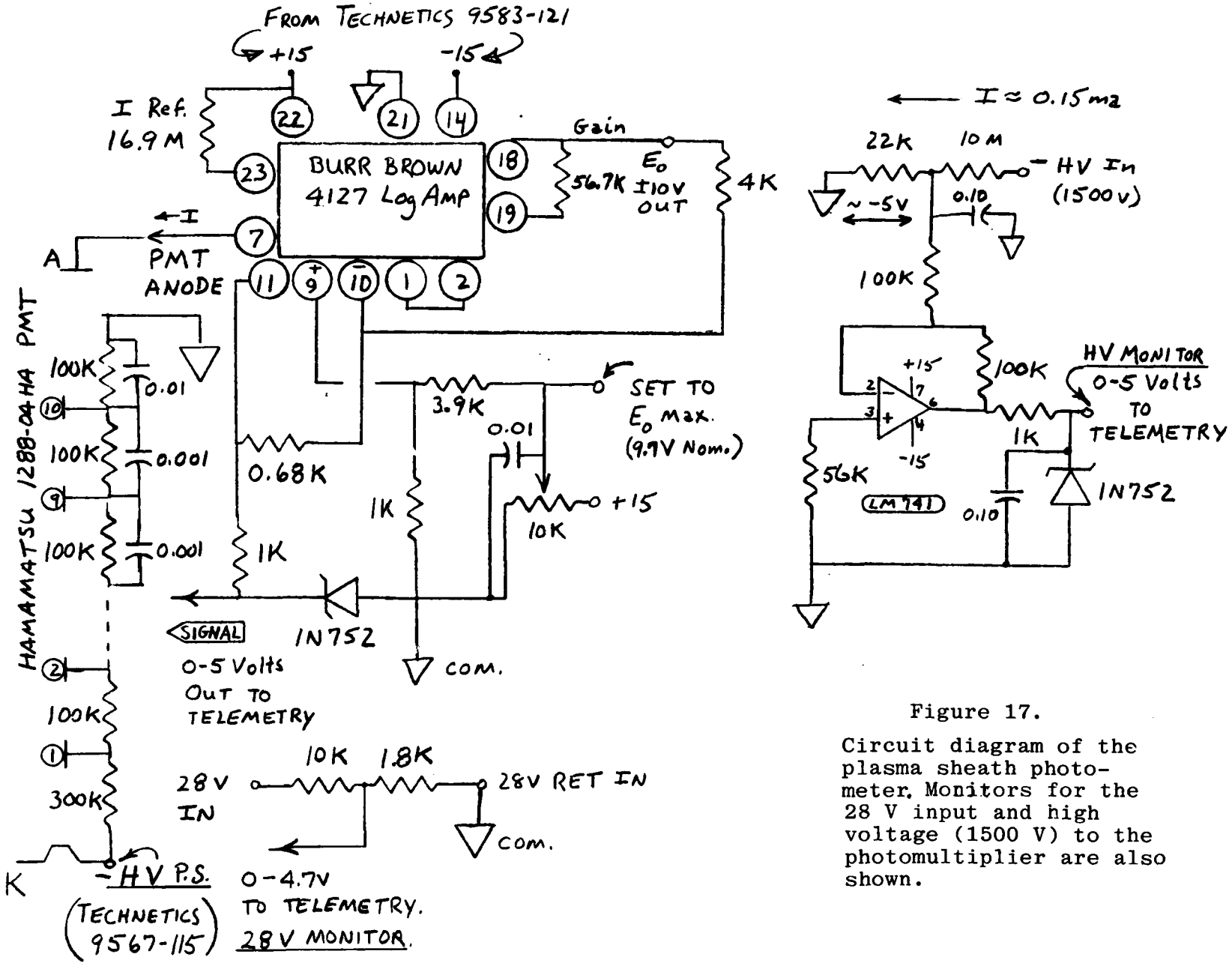

Figure 17.

Circuit diagram of the plasma sheath photometer. Monitors for the 28 V input and high voltage (1500 V) to the photomultiplier are also shown.

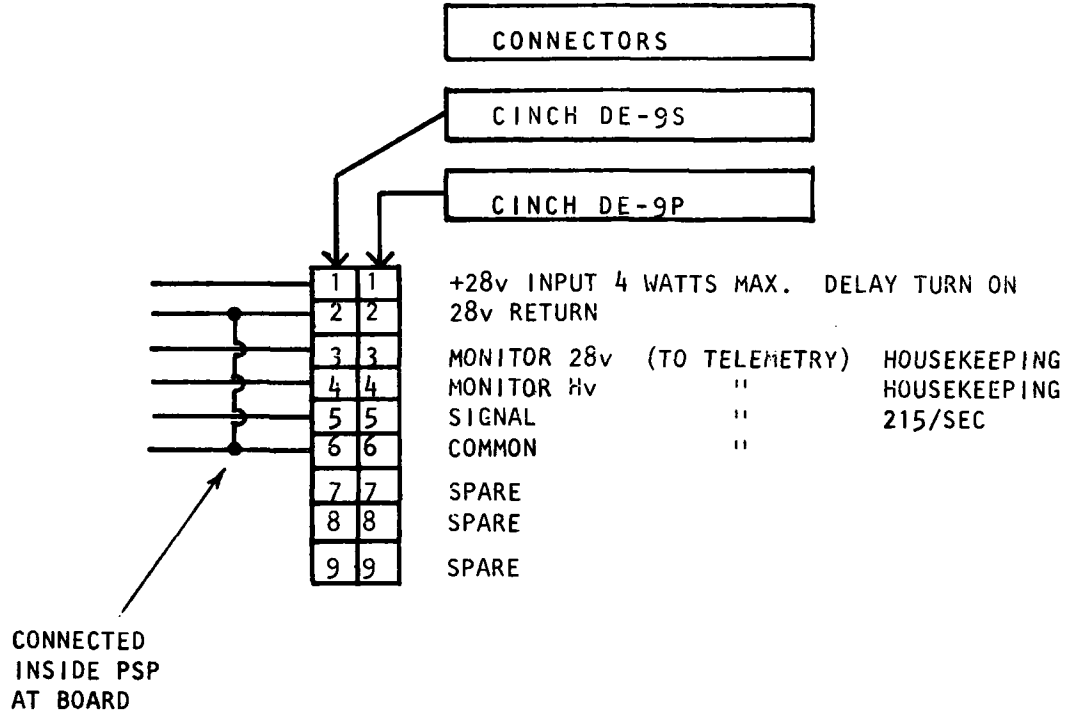

ELECTRICAL INTERFACE (PLASMA SHEATH PHOTOMETER)		
SCALE:	APPROVED BY	DRAWN BY DPV
DATE: 10 MAY 83		
		DRAWING NUMBER

Figure 18. Interface drawing for the plasma sheath photometer.

from the particle ejection direction by means of the flat 45° mirror shown in Fig 16 (provided by the payload integration group). It is positioned as far as practical from the electron and ion accelerators (>1 electron gyroradius) to minimize the contamination from radiation excited by backscattered (rather than plasma sheath) electrons.

Figure 19 shows the sensitivity calibration of the photometer against PhotoMetrics' uniform-radiance continuum light source. Also shown is the response to the similar source available to AFGL (LBS D3), for checking the unit's performance after environmental testing and in the field. Note that a 4-decade dynamic range of scene radiance is achieved.

A blue broadband filter (Schott BG-12) restricts the photometer's wavelength sensitivity to the N_2 Second Positive and N_2^+ First Negative fluorescence bands, and discriminates against background radiations and metastable radiators; a blue-sensitive (bialkali) photocathode minimizes dark current. The absolute sensitivity point in Fig 19 again refers to monochromatic spectral radiance, at the 3900Å peak of the photometer's wavelength response. As with the comparably wavelength-sensitive wide field photometer, this absolute calibration can be improved by calculating the instrument's response to a model emission spectrum of the plasma sheath glow; this spectral distribution can be estimated from the energy spectrum of the electrons in the sheath, using the procedure outlined in Section II (refer especially to Fig 2).

VIDEO CAMERA SPECIFICATION AND PROCUREMENT

The specification and procurement of an ultrasensitive rocket flight-survivable video camera (eventual purchase price $26K less lens) represented a major element of the program.

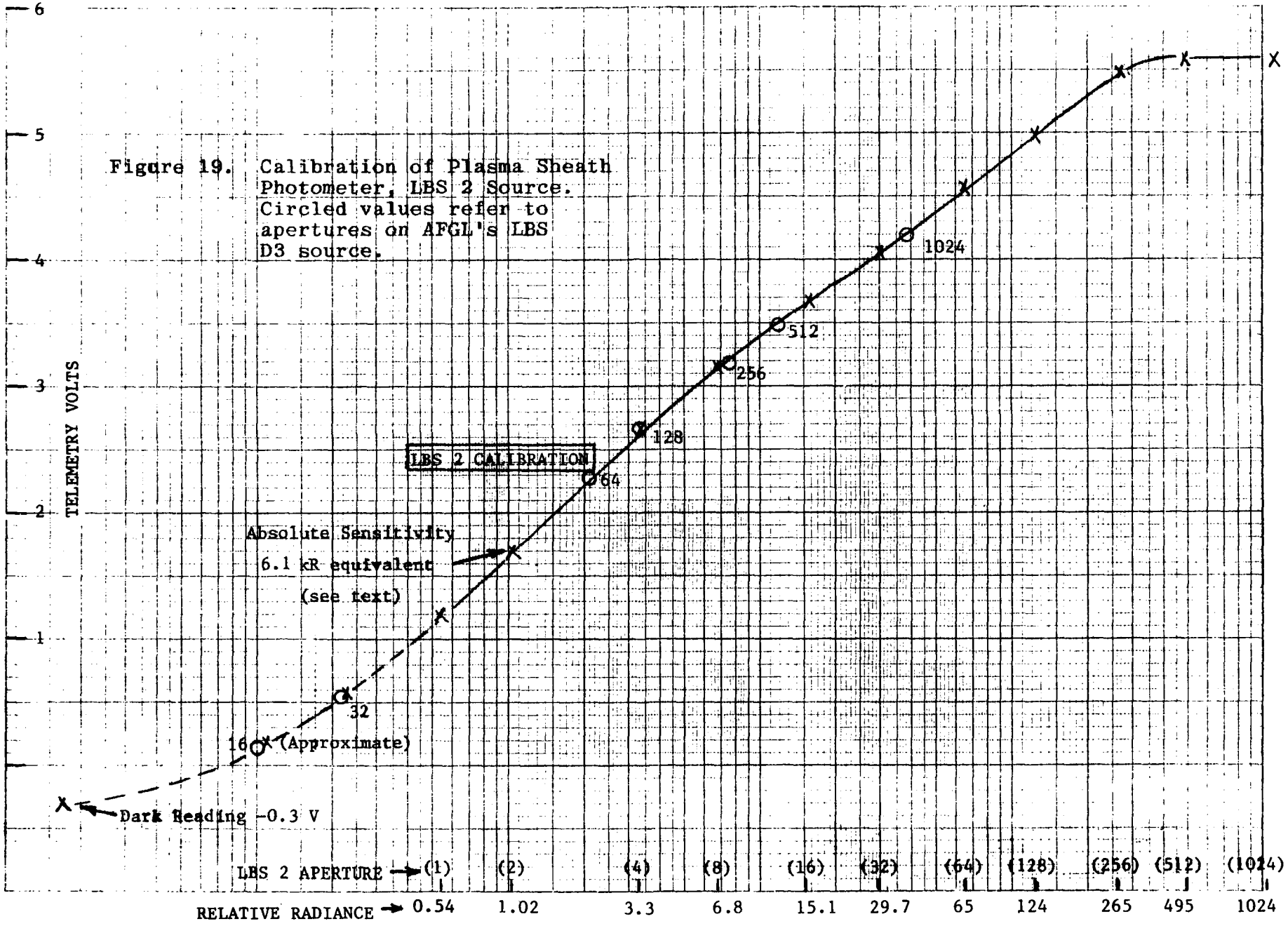

Figure 19. Calibration of Plasma Sheath Photometer, LBS 2 Source. Circled values refer to apertures on AFGL's LBS D3 source.

Initially the basically-unruggedized ITT 4546 camera flown on SCEX was considered. In view of the risk of mechnical failure of this camera, it was decided to fly a system that had been specially designed to withstand the environment of rockets, balloons, and research aircraft, with state-of-the-art threshold sensitivity to record the low radiances expected on the basis of SCEX results. An investigation showed one such video camera to be commercially available, ten units of which had been flown successfully. Negotiations with the manufacturer (Edo Western, Salt Lake City, UT) were initiated just after funds became available in July 1982, and the purchase order was placed on 03 August.

The camera as purchased (Figure 20) consists of a hermetically sealed cylindrical head containing a premium-grade (selected for low blemish count and high sensitivity) RCA 4849/AH Intensified Silicon Intensifier Target [vidicon] tube (Item CH-1434/36369-2); a vacuum-tight electronic control box containing 5 circuit boards (Item CCU-1430/24133); and a 6 ft x 5/8 inch diameter cable interconnecting the two elements (Item 3Q576). The order as accepted by the vendor called for him to reduce the weight of the control units from 11 to 6 lbs by milling out mechanical strengthening material; the actual final weight, however, was 7-1/4 lbs. The head weighs 4-1/2 lbs, and with its mechanical mount to the payload, lens, and lens strengthening cylinder (shown in Figure 21) the total weight of this instrument is 10 lbs.

Delivery of the camera was promised for 16 February 1983, 6-1/2 months after receipt and acceptance of PhotoMetrics' order. Our staff maintained contact with the vendor, and as late as 28 January 1983 we were assured it would be shipped on-time. Actual delivery, however, was delayed until 29 April, which left only three months for PhotoMetrics to complete the

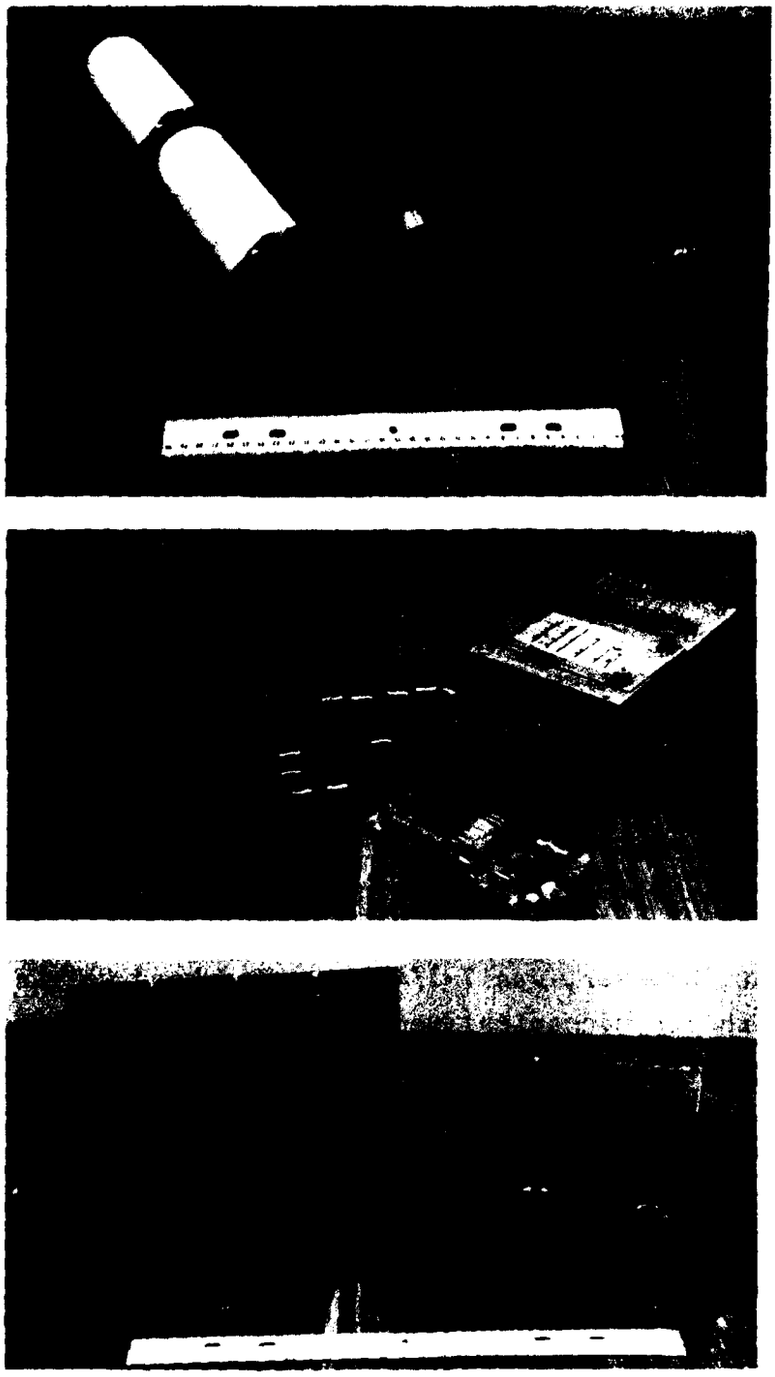

Figure 20. Three views of the video camera and controller systems.

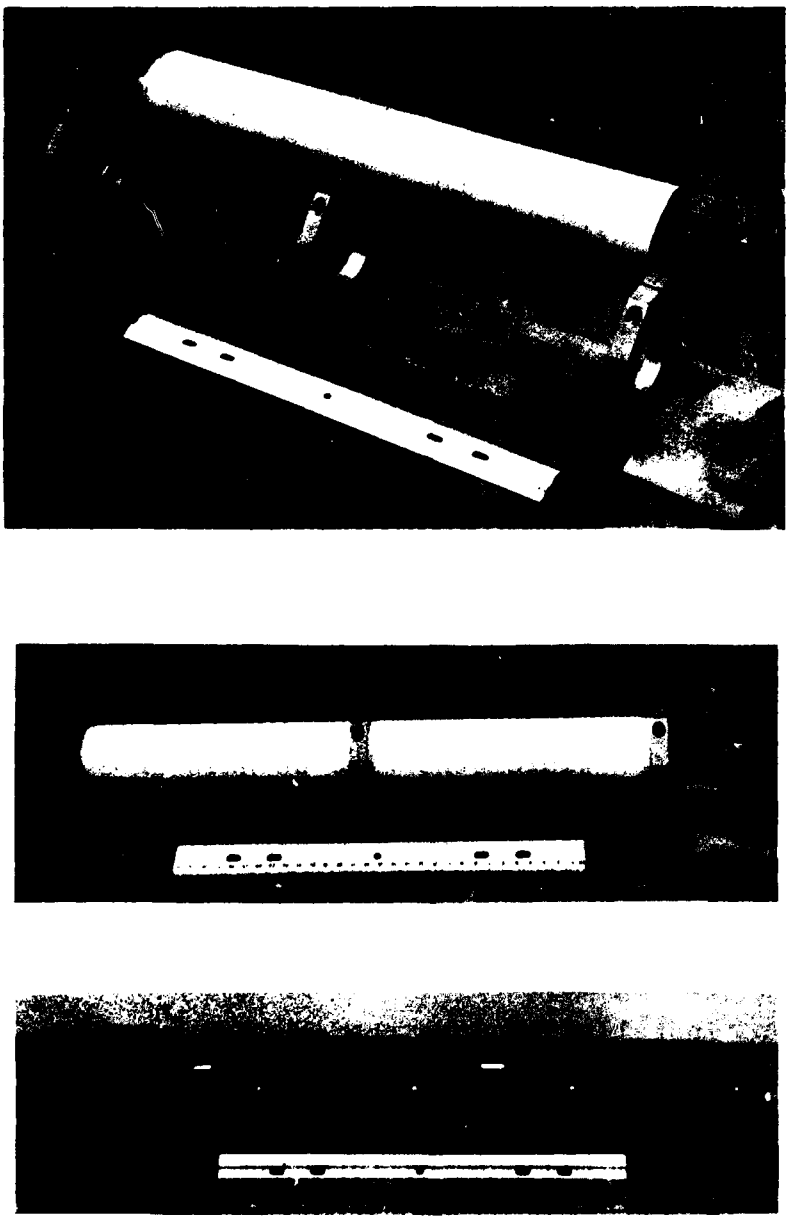

Figure 21. Three views of the video camera head and mechanical mount. The cylindrical black anodized object fits over the lens to add mechanical strength; see Figure 7.

mechanical and electrical interfaces to the rocket, make the necessary performance tests, and radiometrically calibrate the unit with the lens selected. The camera manufacturer claimed that his 2-1/2 month delay was due to "need to test the instrument to meet specifications."

These specifications and other pertinent performance data are summarized in Table 8. Of principal concern are vibration and shock resistance, and stability of the electronics (principally the high-voltage circuitry) under the near-vacuum conditions at rocket altitude. PhotoMetrics' modifications to the camera, which were designed to maintain these performance standards while completing the video system, were as follows.

1. Installation of a short-focus lens for wide-angle imaging (refer to Table 7);
2. Construction of mechanical mounts for the camera head and for this lens (which would otherwise be held in by only 3 threads of a standard 16 mm C-mount);
3. Construction of a mounting plate for the control box (shown at the bottom of Fig 20);
4. Installation into the control box of a monitor for the camera's automatic gain control voltage, to allow end-to-end radiometric calibration (input radiance to output signal voltages).

Insofar as the camera system is highly complex, PhotoMetrics has provided AFGL with a copy of its 200-page instruction and operating manual and of the 25-page factory acceptance

Table 8. Camera Specifications (Manufacturer's Data)

Environmental	
Temperature:	-20°C to +55°C
Altitude (external pressure):	Unlimited
Humidity:	MIL-Std-810C, Curve C
Vibration:	Head: 15g, 11 ms, 3 axes Controller: 5g, 11 ms, 3 axes
Explosion:	Controller: Per MIL-E-5272C Procedure IV

Structural	**Controller**	**Head**
Material:	Aℓ	Aℓ
Dimensions:	7.92 x 6-3/4 x 4.39 in	2-5/8 in diameter, 18 in long including rear connector

Video Performance	
Horizontal resolution:	600 lines across field
Sensitivity, nominal	2×10^{-7} foot candles at the faceplate, 10 shades
Sweep rate:	60 fields, 30 frames/sec
Sync generator:	EIA RS-170 (USA)
Dynamic range of automatic light control:	10^4:1

test procedures (of temperature and vibration sensitivity, resolution, low light level response, and other parameters in Table 8) performed by its manufacturer. This manual contains schematics and theory of all the electrical circuits with detailed instructions for their maintenance and trouble-shooting, as well as mechanical and optical documentation of the head and controller. The material in the following sub-section, which documents PhotoMetrics' completion and integration (and calibration) of the video camera system, is intended to complete the information needed by AFGL to install and operate the system in the BERT-1 experiment.

VIDEO CAMERA SYSTEM

Figures 22 and 23 are outline drawings of the video camera head with its mounting hardware and control box (for mechanical interfacing), and Figure 24 documents the system's electrical interface to the rocket payload. The schematic diagram of the gain control monitor is shown in Figure 25.

To expand the dynamic range of scene brightnesses that it can record the camera automatically adjusts the high voltage (3-20 kV) applied to its intensifier segment, under control of circuitry that senses the mean amplitude of the vidicon's output signal. We tapped into this circuit at a point in the feedback amplifier at which the voltage (0-10V, which we convert to 0-5V for telemetry) is a quantitative measure of the voltage applied to the intensifier. The combination of this system gain-measuring voltage and the video output voltage (Standard RS-170 1.4V peak-to-peak range) establishes a series of calibration curves that allow scene radiance levels in the field to be directly related to scene radiances applied in the laboratory. We return to this issue in our description of the calibration procedure.

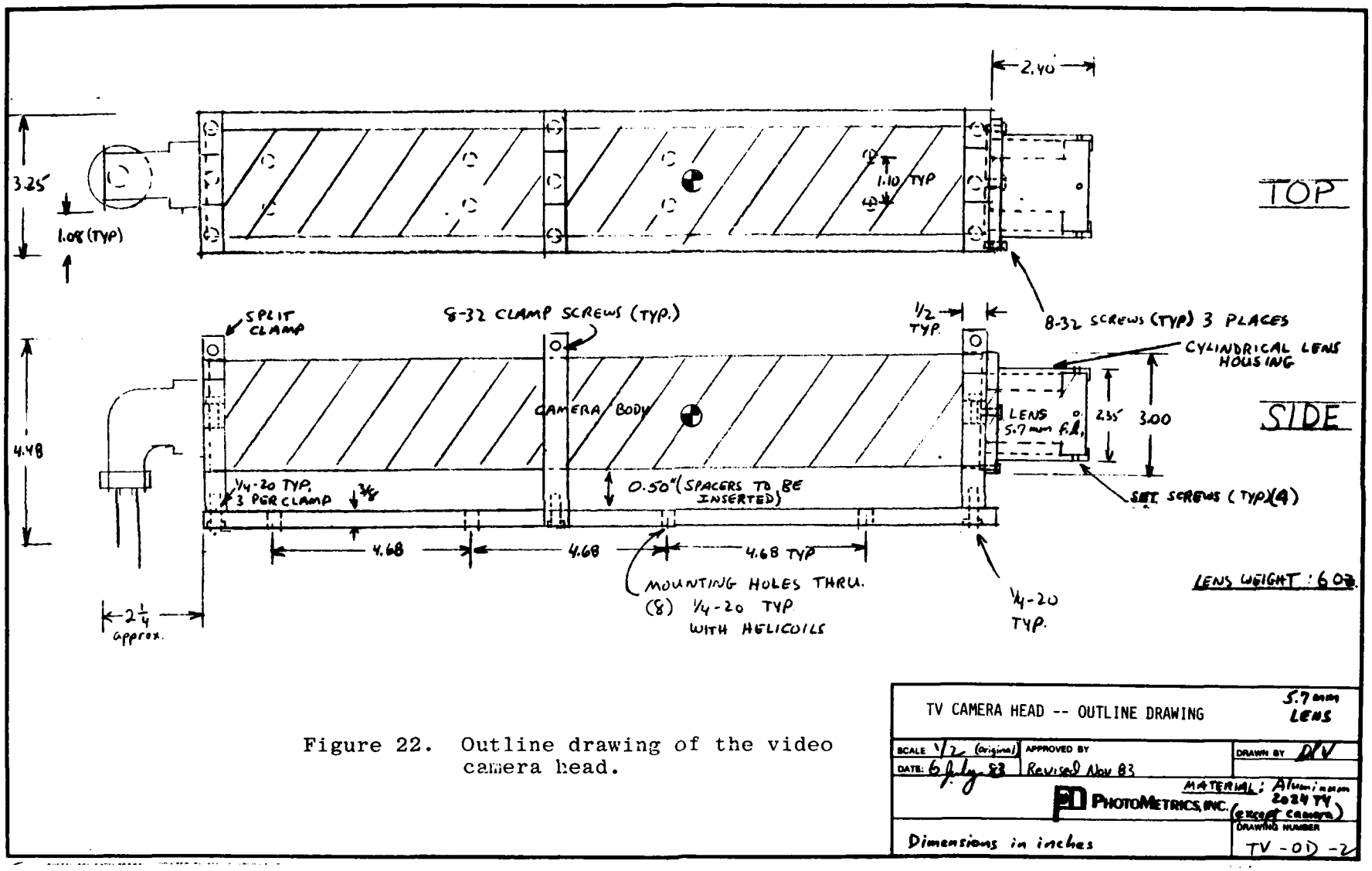

Figure 22. Outline drawing of the video camera head.

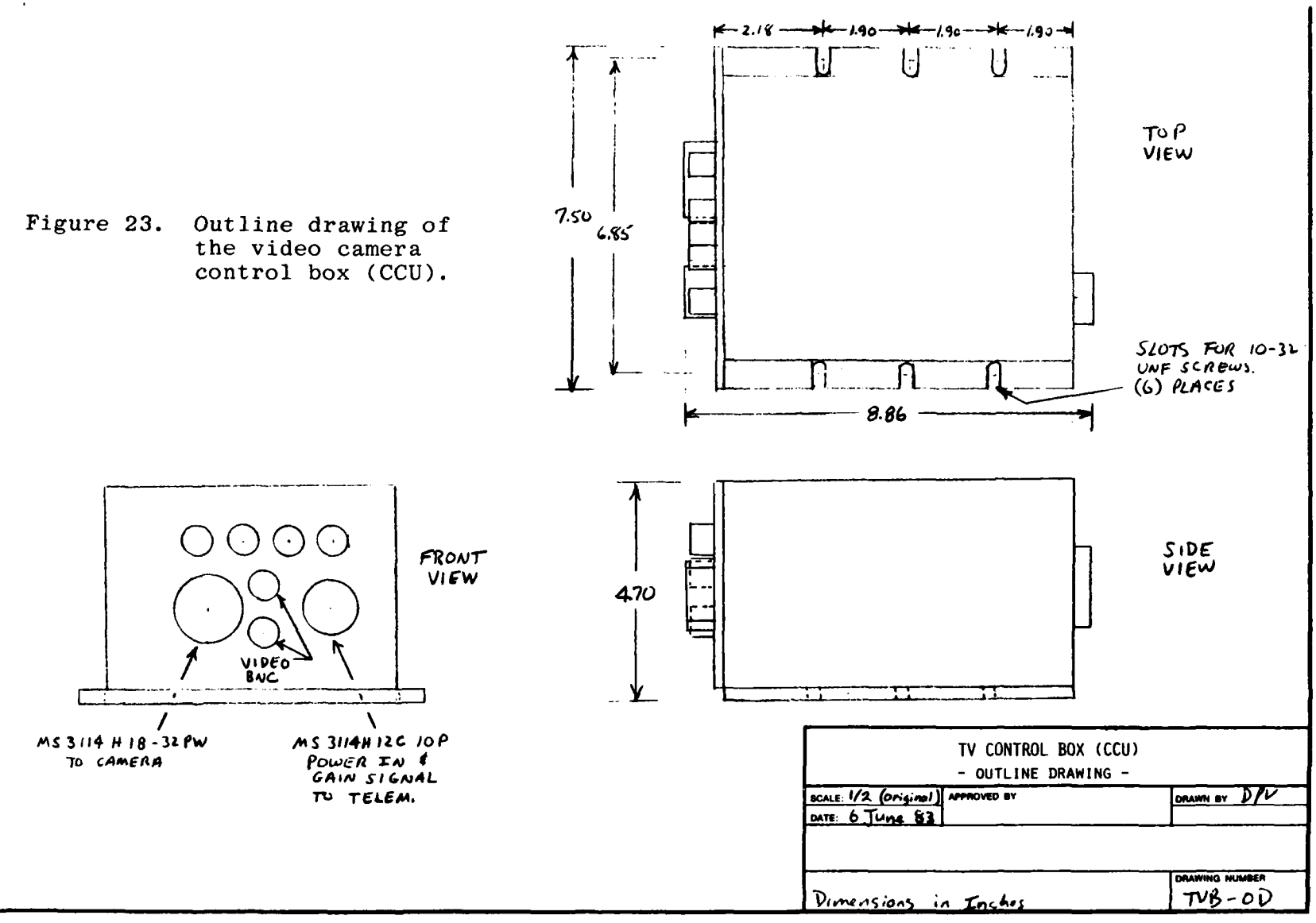

Figure 23. Outline drawing of the video camera control box (CCU).

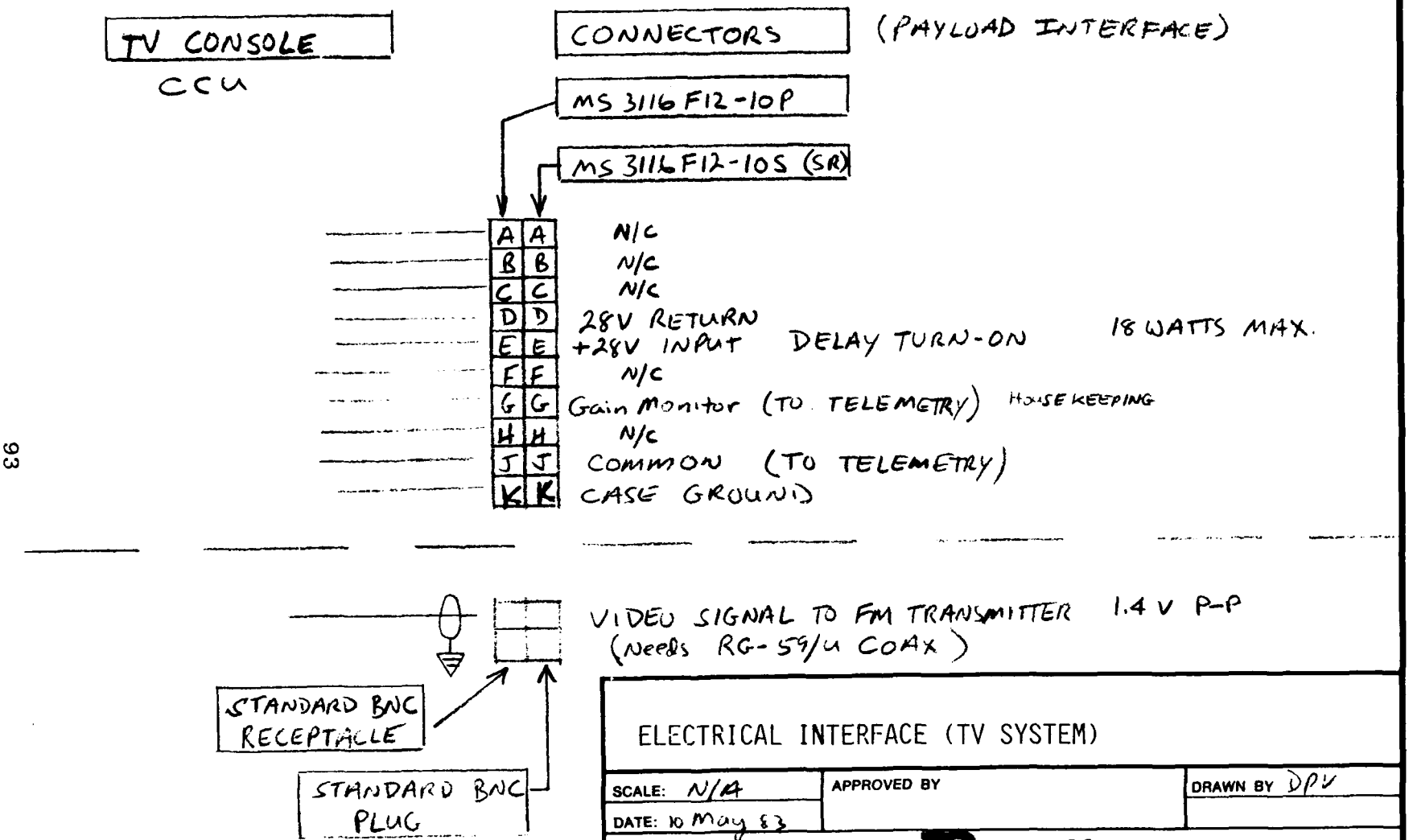

Figure 24. Electrical interface of the video camera system.

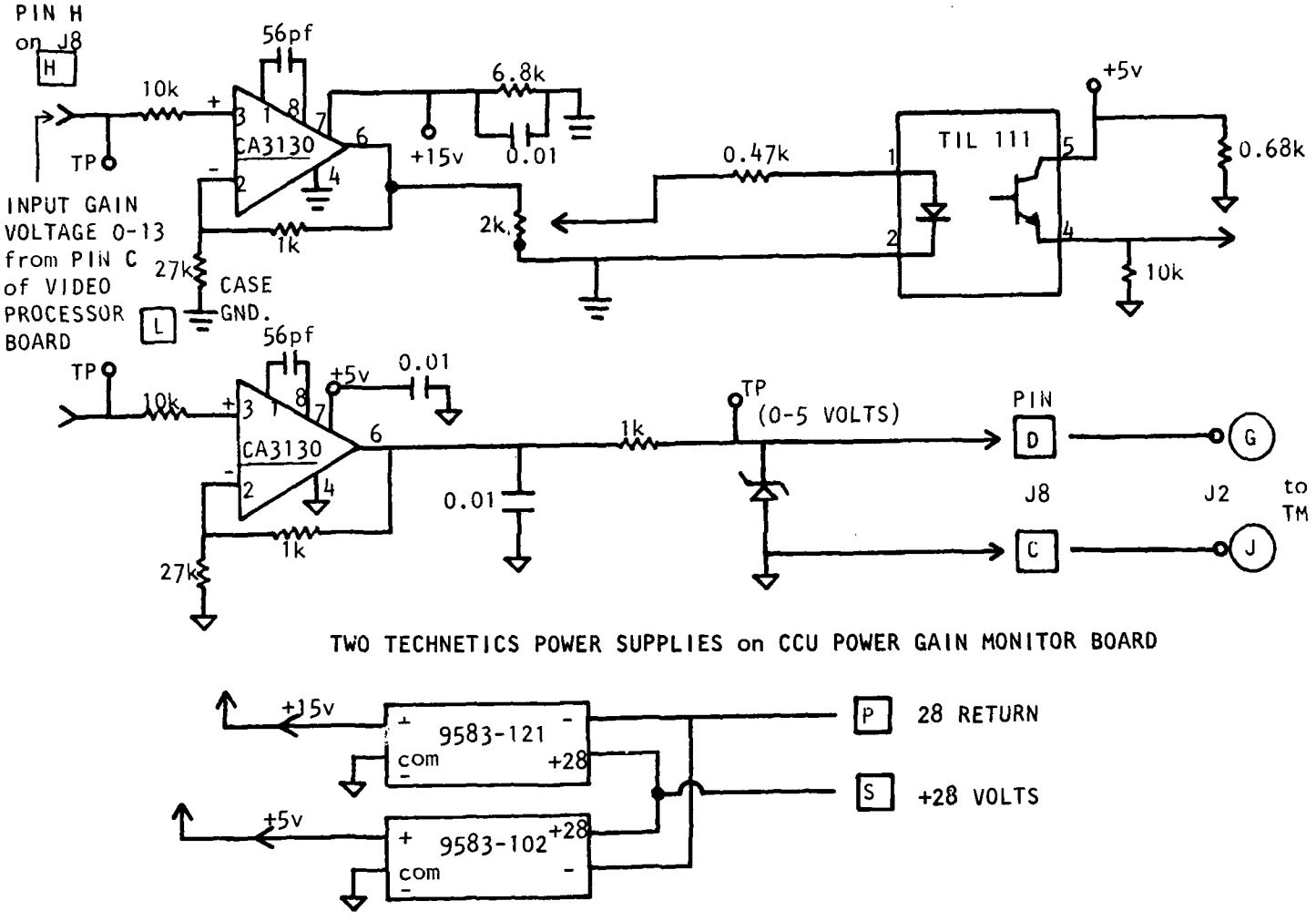

Figure 25. Schematic of circuitry for monitoring the video amplifier gain levels. The printed circuit board with two power supplies is mounted in the camera control unit at the "accessory" position. Letters in boxes refer to pins on edge connector J8 inside the CCU. Circled letters refer to pins on connector NS 3114H12C-10P for telemetry input.

AD-A143 277 EXPERIMENTS ON INTERACTION OF KEV PARTICLE BEAMS WITH 2/2
THE IONOSPHERE(U) PHOTOMETRICS INC WOBURN MA
I L KOFSKY ET AL. 31 AUG 83 PHM-TR-83-01
UNCLASSIFIED AFGL-TR-83-0316 F19628-80-C-0133 F/G 4/1 NL

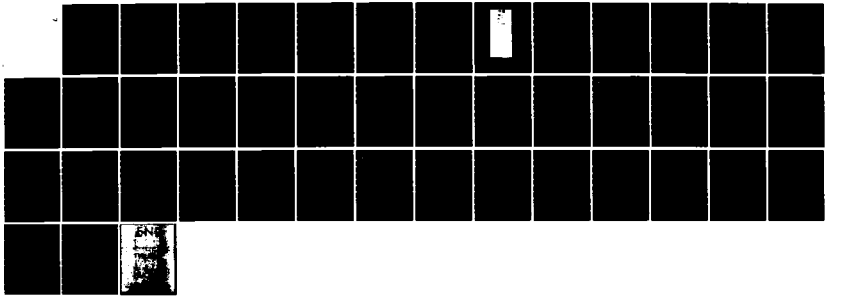

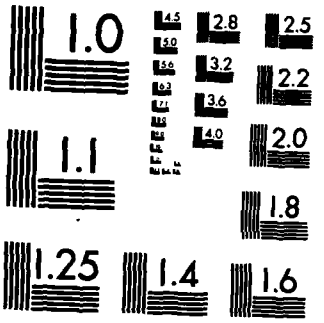

Mounting of the already-ruggedized control box represented no problem, a simple flat plate bolted to its rear (Fig 23) being all that was needed. The circuit boards were conformal-coated with Dow Corning 3140 RTV for vibration damping and to prevent any components that might fall off from short-circuiting critical elements. The boards not secured by dual rails are bolted in place, following standard practice for harsh environments.

The camera head and lens, however required construction of the mechanical clamping system shown in Fig 22. (The simple pair of straps provided by the camera manufacturer was judged inadequate, and in any case does not provide strengthening for the lens.) Its cylindrical body is held by three 1/2-inch thick split rings, and in addition pressed against the bottom mounting plate as shown in Fig 21. This clamping is firm enough to meet the rocket's vibration and acceleration specifications, without exerting sufficient force to damage the thin-walled cylinder. Both the front and rear rings are ridged to overlap the ends of the housing, effectively preventing it from moving along its long axis. Particular care was needed to fit the rear clamp to the bead of a weld holding on the camera head's back plate. The lens also required mechanical strengthening, by the black-anodized holder shown, which is screwed into the front split ring. The bottom plate is the mechanical interface to the payload, with eight 1/4-20 Helicoil inserts spaced as shown in Fig 22.

As noted, the initial concept had been to mount an all-sky lens on an outbound camera so as to view a large area of the beam and backscattering volume. As little or no spatial radiance structure is expected (Ref 20), there is little impetus to increase angular resolution by decreasing the field of view. We performed extensive measurements of the limiting

useful fields of three very wide-angle lenses, to make optimum use of the camera's image plane area and to determine whether the electron beam's first refocusing node could be included in the field. (Distances of the node from the accelerator are given in the Design Evaluation Report.) In practice the acute angle of view to the beam even at the 1/2 keV electrons' close-in node (about 13°), coupled with the low image resolution near the edge of the camera field, results in low quality information about refocusing of the primary electron beam.

After the decision was made that the camera head itself would not be erected outward, we considered various mechanical arrangements to achieve a projection to a lens outside the rocket body (so that the rocket itself would not obscure the camera's field). We investigated the practicality of extending outboard only a lens, connected to the camera with a coherent (imaging) fiber-optic cable. The drawbacks were the cost of the necessary cable ($6,700 for the 6-ft length available), its at least one stop loss of optical throughput, and its reduction of spatial resolution; further, the mechanical difficulty of erecting the all-sky lens and cable (which weighs 15 lbs and has a minimum bend radius of 6 inches) was judged not much less than that of moving the complete camera head.

The idea of swinging outward one end of the camera (like the mirror in Fig 16) with the lens mounted perpendicular to the cylinder axis was also abandoned when it was recognized that two further relay lenses would be needed in an optical system to turn the extremely short-focus all-sky lens's optic axis through ~90°. (The clearance between the rear of this lens and the front glass plate of the sealed camera is only about 1 mm.) It will be noted that the area of a flat mirror

that would accommodate the all-sky field would be impractically large, and the cost of designing a special curved outboard mirror to achieve wide angular coverage was judged well beyond the budget of the program (particularly since less than two months of the performance period remained when PhotoMetrics was informed that the camera head would not be translated outward when the rocket had reached experiment altitude).

The restrictions that the 22-1/2 inch long cylindrical head (with lens and rear electrical connector) must fit within a rocket body of inner diameter 16-3/4 inches with 1/2-inch buffer clearance at each end, and view through an opening that could be no larger than 12 inches in the direction of the rocket axis and 6 inches (chord) azimuthally, sharply reduced the achievable angular field. They led to selection of a lens that with an unobstructed view would provide a 80° x 60° field (100° diagonal), and a maximum angle between the cylinder and rocket long axis of only 34°. The camera is mounted at this angle with its optic axis intercepting the outer surface of the rocket at 3.6 inches from the rear edge of the opening cut into the skin (8.4 inches from the front edge), and with the 80° field direction aligned with the rocket's long axis so as to maximize the length of beam in the image. Its objective lens is unobscured in a 40° x 60°-wide field, and partially obscured by the rocket at the front edge of the opening over an adjoining about 23° x 40°-wide field. The camera can "see" the ejected beams, with reduced effective aperture ratio due to this vignetting by the viewing port, to within 1/3 m of the accelerator anode; when the electron beam is injected along the geomagnetic field direction, 7 m of its length is in the camera field. (Note: under the beam-plasma discharge conditions of EXCEDE: Spectral the volume emission rate increased extremely sharply toward the accelerator within the first few meters (Ref 20).)

In summary: the camera's optic axis points at an elevation angle of 34° from the rocket's long axis in the plane defined by this axis and the centerline of the ejected beam. Its principal point is 2-1/2 m behind the accelerator, 1-7/8 inches inside rocket's outside skin, and 5/8 inch in front of the rear edge of the 12 inch long (by 6 inch wide) opening in the skin. The optic axis intercepts the axis of the magnetically-undeflected beam at 3 m from the camera's objective lens.

VIDEO CAMERA CALIBRATION

The full S-20 wavelength response of the camera's photocathode is used, both to increase response to air fluorescence excited by the electron beams and to provide sensitivity to the various radiations from/by the ejected ion beams. This standard spectral response is given in the Manual (and of course elsewhere), and is summarized in Table 7.

The photometric and photogrammetric calibration of the 5.7mm lens (which we performed in connection with the work reported in Ref 2) are shown in Figure 26. The data below refer to the region within ~ 25° of the camera axis; radiometric calibrations for points further off-axis can be directly determined from the irradiance-transfer curve in Fig 26, which also gives the scene angle-to-video image (geometric) factor.

The video camera's contrast sensitivity and photometric response characteristic were determined using the uniform low-brightness (LBS-2) standard source transilluminating a bar target and a step tablet. Reference is made to the fact that the spectral radiance of this tungsten source increases by a factor 100 between the 3750Å and 7660Å tenth-power photon sensitivity points of the camera (the short-wavelength limit is set by the transmission of its objective lens);

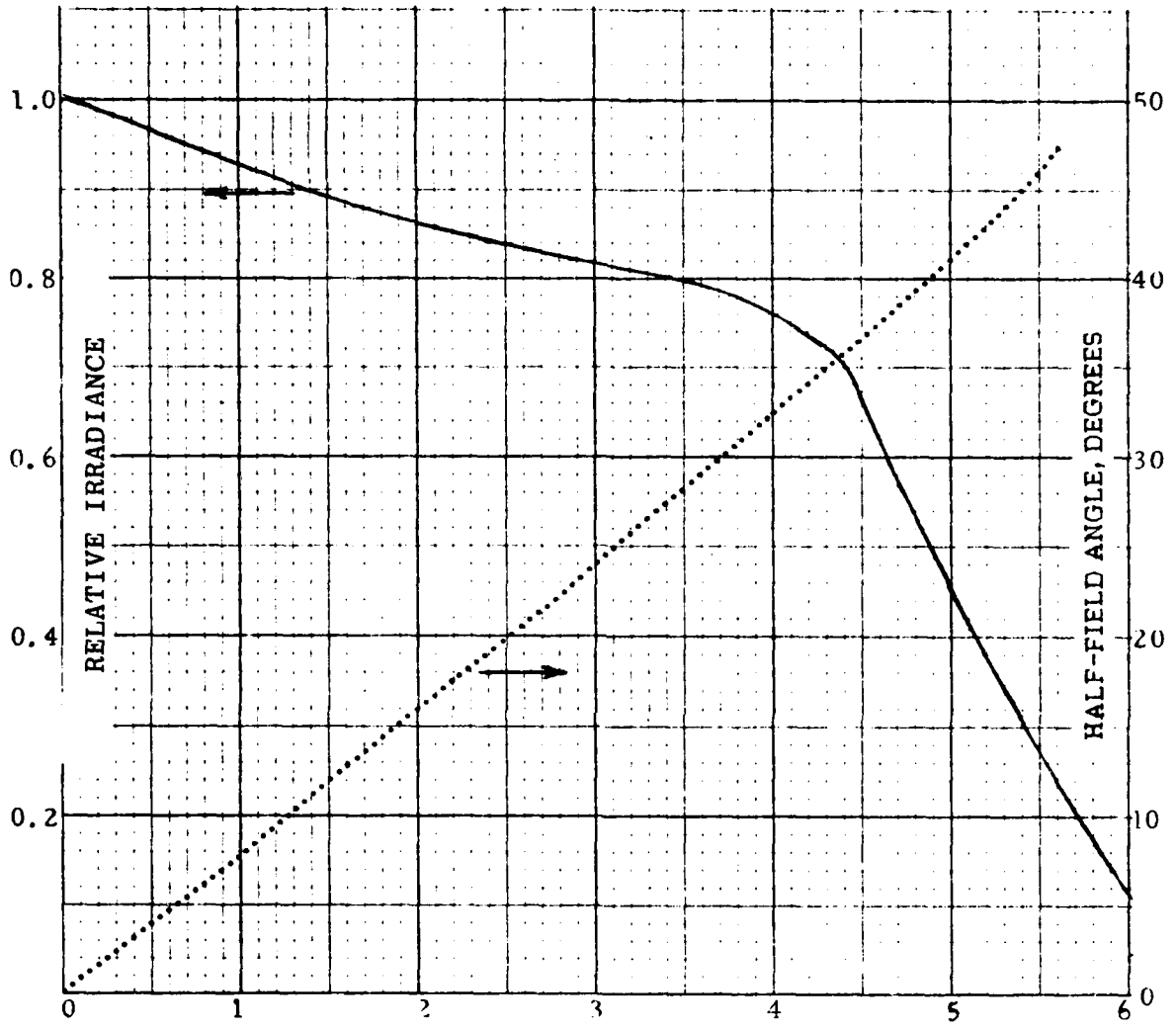

Figure 26. Relative irradiance in the image plane (solid line) and angle in the field of view (dotted line) as a function of displacement of the image point from the center of the video camera field. These calibrations of the vignetting and distortion of the camera lens are taken from Ref 2.

where the illumination levels were adequate we narrowed the bandpass to increase the accuracy of calibration. The camera as usual serves as a transfer standard, with the telemetered gain-setting and signal voltages relating scene brightnesses in the BERT-1 experiment to those on the source's faceplate.

Contrast sensitivity was measured by photographing a USAF 1951 three-bar test target, with the standard source filtered to a 10Å bandpass centered at 5630Å. A 4 inch focal length relay lens was placed directly in front of the camera's 5.7 mm objective lens to achieve appropriate focus with this target filling the image field. Images at these illuminations are shown in Figure 27, and Figure 28 gives the camera's limiting line-pair spatial resolution (in the sense of the three-bar test target, and corrected for the magnification and small reflection losses of this lens) as a function of brightness in the clear areas of the target. Since the S-20 photocathode's photon response at 5630Å is 0.68 that of its very flat peak centered at 4400Å -- the standard specified response varies by <5% between 4000Å and 4800Å -- the abscissa in Fig 27 would be multiplied by 0.7 if the illumination were at these shorter wavelengths. Even more so than for the two types of photometer, the very broad range of wavelengths to which the photocathode responds (refer to Table 7) makes the absolute radiometric calibration depend on the spectral distribution of the imaged patch of scene, radiance at 4400Å producing more output voltage than radiances at longer and shorter wavelengths; again, the emission spectrum allows the calibration to be more accurately quantified.

We measured the dependence of intensifier gain monitor voltage (conditioned for telemetry by circuit shown in Fig 25) on mean scene brightness by overfilling the camera field, specifically, placing the lens in virtual contact with the

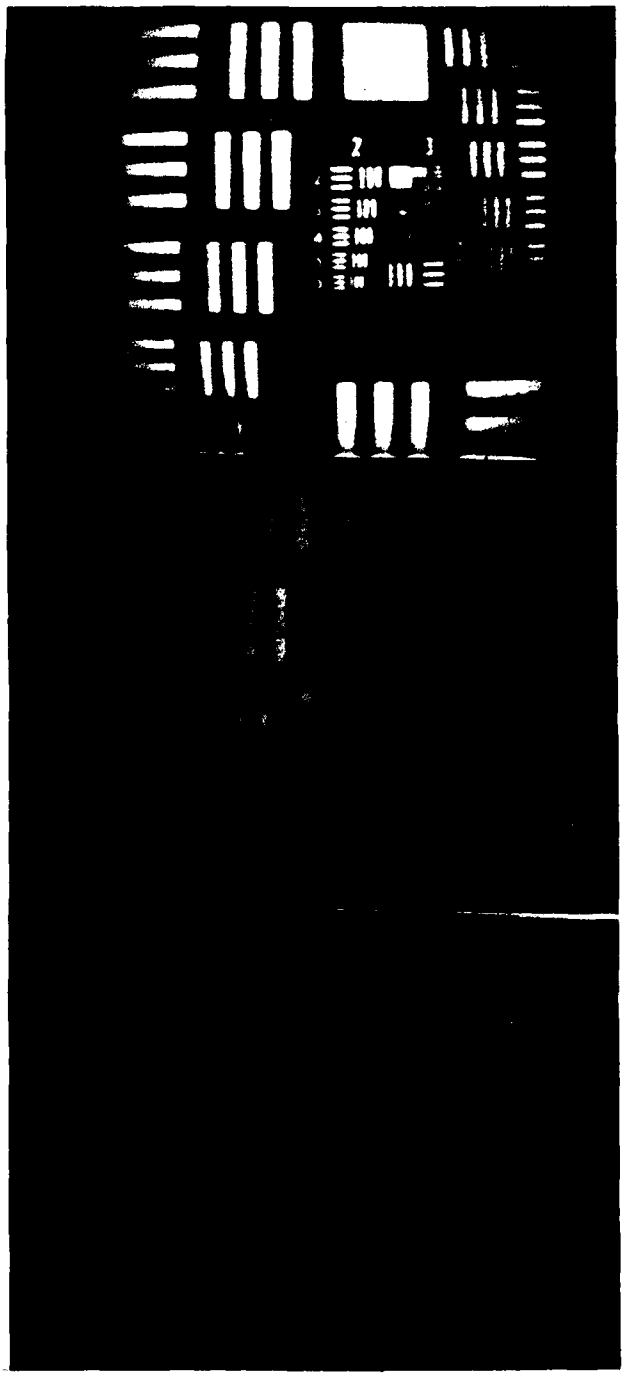

Figure 27. Resolution of the video camera at relative mean illuminations 16.7:4.2:1, in 5630 ± 5Å light. In the original 1/10 sec photographs of the video monitor the line pairs in Group 2, Element 4 can be resolved at the lowest illumination in this series. Note the decrease of video contrast with average scene brightness.

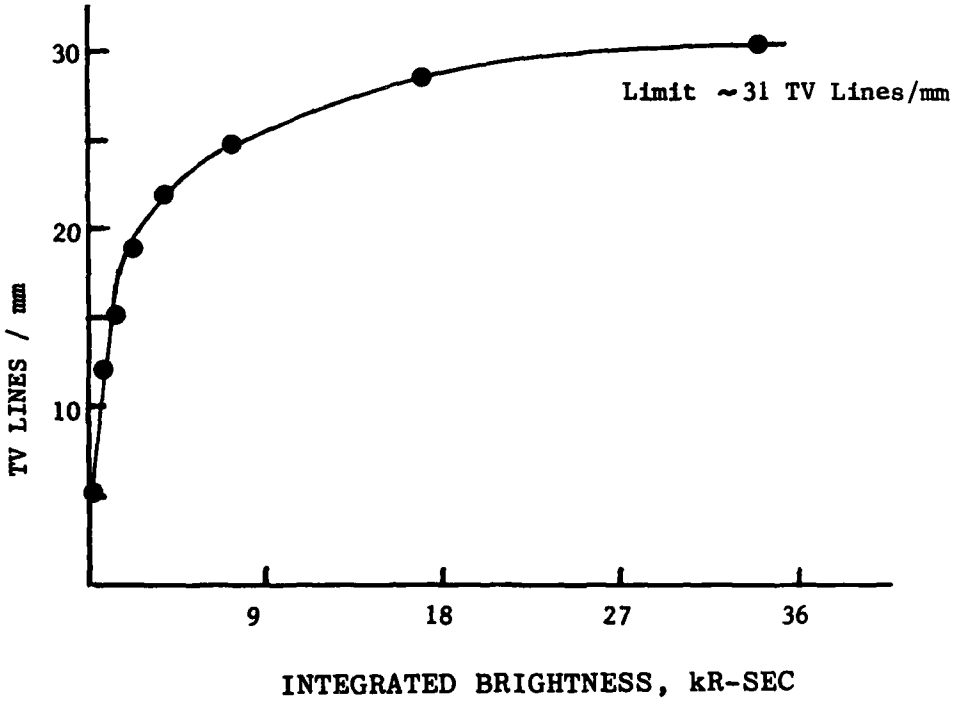

Figure 28. Visual resolution of the video camera determined from 1/10 sec exposures of the USAF bar chart (from Figure 27), 5630Å illumination.

uniform source's surface. To achieve sufficient brightness it was necessary to maintain the source unfiltered; we calculated the equivalent monochromatic radiance at 4400Å from its spectral radiance and the S-20 photocathode's response (the effect of decreasing lens transmission below 3900Å is negligible in this calibration). The results, graphed in Figure 29, show that the automatic control circuitry adjusts the video system to full gain when the mean scene radiance is less than about 100 kilorayleighs. Thus the intensifier video gain would be expected to be fixed at its maximum over much if not most of the BERT-1 experiment. We also found that the camera system produced video output signal readily detectable over noise, ~0.05 volts, at a mean scene illumination of 2/3 kilorayleigh (4400Å; near the center of the field).

The response time of the video feedback loop was 0.1 to 0.2 sec for factor-2 changes in scene brightness at most mean brightnesses. However the complex circuitry was found to operate nonlinearly near the onset of maximum intensifier gain, with the hysteresis effect shown in Fig 29. For example in that range a factor-10 step increase in brightness resulted in a 3-sec gain undershoot followed by damped noise, while a similar decrease also required 3 sec to stabilize.

We calibrated the video output voltage signal by trans-illuminating a 21-step Eastman Kodak photographic tablet. With the standard source filtered to 5630 ± 5Å (to maximize photometric accuracy) and the remainder of the field masked off, the video control circuitry provided maximum gain; other gain voltages were produced by uncovering this source area and/or operating the source with the wider-band Wratten 55 and BG-18 (green) filters. The 4-inch lens was again placed in front of the operational 5.7-mm focal length lens to produce acceptable-size video images of the individual steps, and

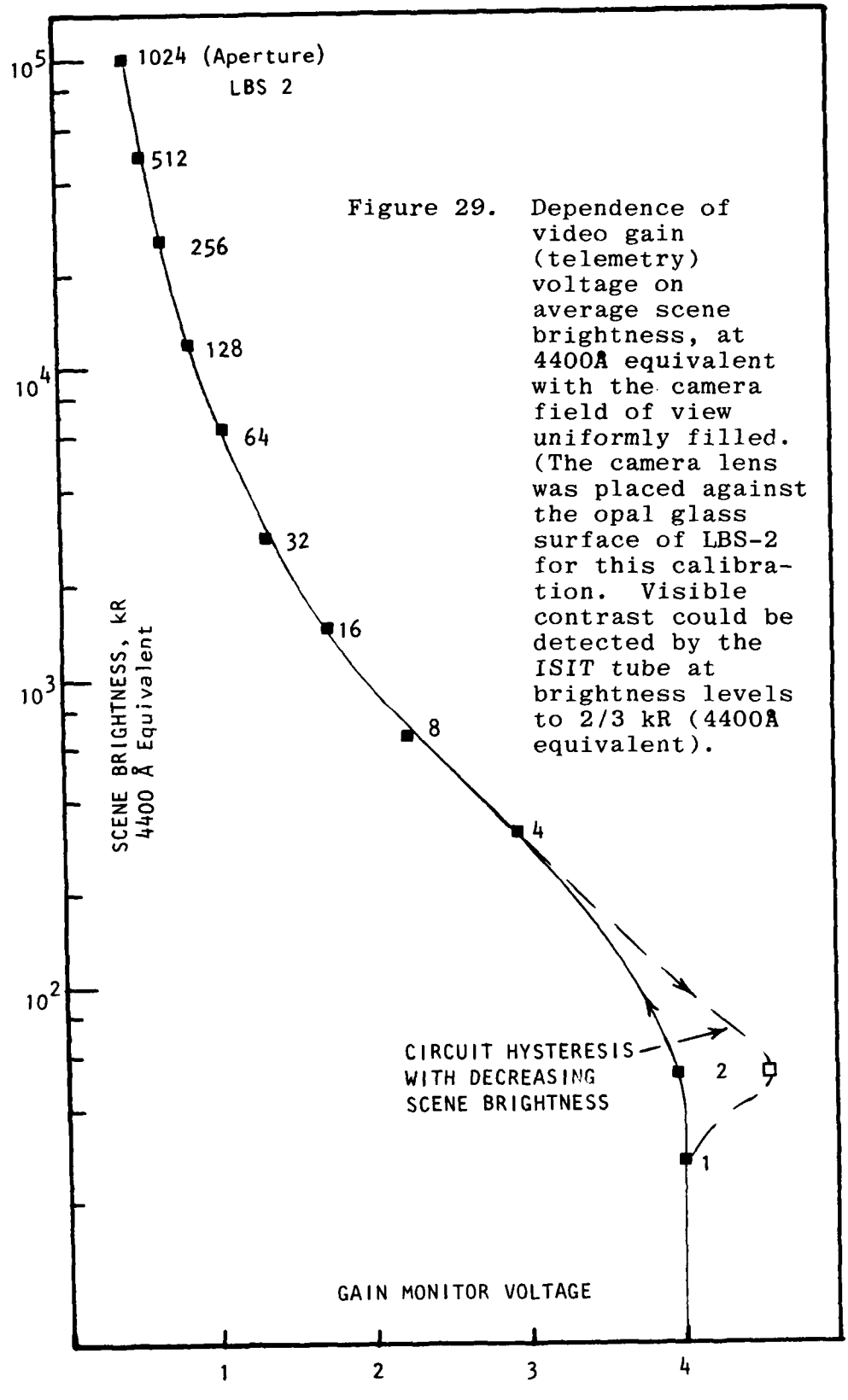

Figure 29. Dependence of video gain (telemetry) voltage on average scene brightness, at 4400Å equivalent with the camera field of view uniformly filled. (The camera lens was placed against the opal glass surface of LBS-2 for this calibration. Visible contrast could be detected by the ISIT tube at brightness levels to 2/3 kR (4400Å equivalent).

its small transmission loss was considered in the calibration. With appropriate triggering of an oscilloscope trace the video output voltages as a function of position on the tablet -- a ledge each time the radiance changes, by factors ∂2 -- were displayed on the screen and photographed.

Absolute paraxial calibration for the camera at full gain is shown in Figure 30, and relative calibration for other gain monitor voltages in Figure 31. The absolute calibration at these latter gain settings follows from normalizing to the data in Fig 30. For points in the scene at angles >25° to the optic axis, the response is reduced by the factor graphed in Fig 26. It was necessary to use the BG18-W55 combination to realize sufficient source radiance to reach the higher output voltage in the full-gain calibration; with the radiance normalized to the narrow-band measurement, this introduces only a small error in the resulting scene brightness-to-output voltage transfer function.

SUMMARY

This Section documents the optical, mechanical, and electrical design of the sensors built by PhotoMetrics for BERT-1, and the information needed for installing and maintaining the instruments in the rocket. It provides the appropriate radiometric calibrations with descriptions of methods for checking calibration and other performance parameters with equipment available to AFGL's payload integration staff. A background on the selection and design of the optical sensors is in the Design Evaluation Report (see Table 6); particulars of the purchased parts of the video camera system are in its operating manual and report of factory acceptance tests; and further details of the instruments and their calibration are maintained in PhotoMetrics' laboratory notebooks.

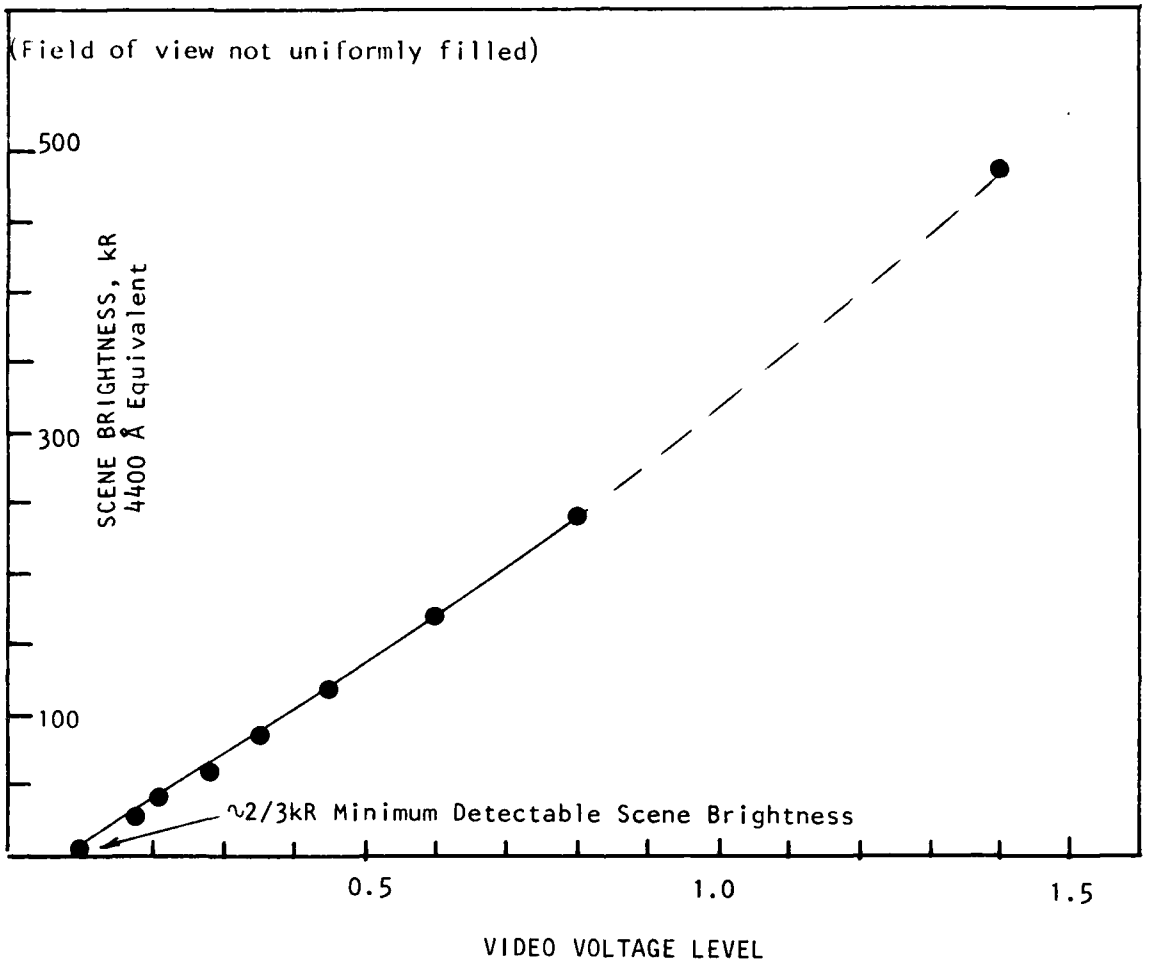

Figure 30. Dependence of video output voltage level (at maximum amplifier gain) on average scene brightness at 4400Å. A set of brightnesses was generated by trans-illuminating a standard step tablet pressed against the opal glass of LBS-2. This source was imaged onto the ISIT faceplate using the camera's 5.7 mm lens and an intermediate (relay) 102 mm lens.

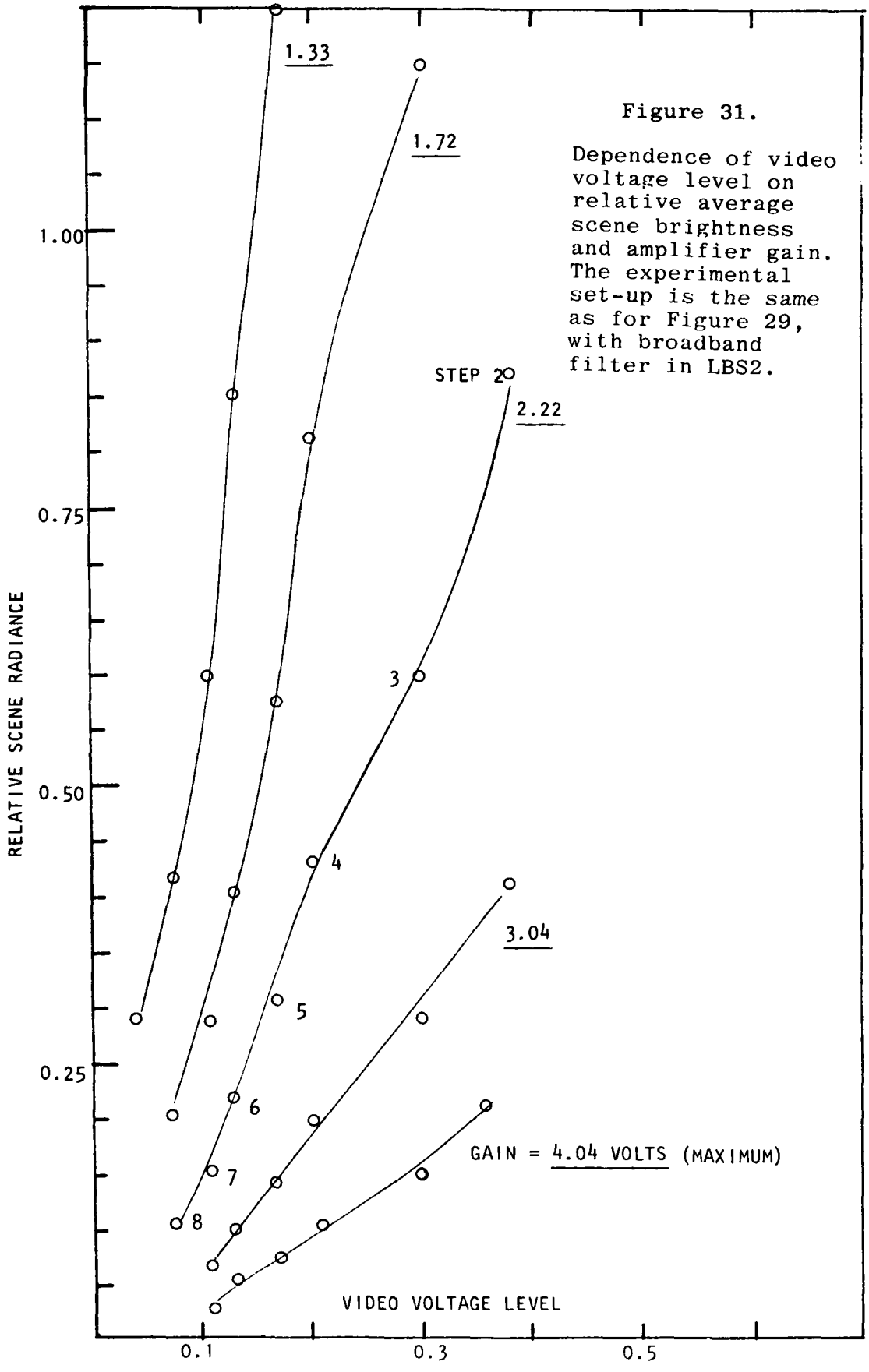

Figure 31.

Dependence of video voltage level on relative average scene brightness and amplifier gain. The experimental set-up is the same as for Figure 29, with broadband filter in LBS2.

REFERENCES

1. W. Bernstein, H. Leinbach, P.J. Kellogg, S.J. Monson, and T. Hallinan, Further laboratory measurements of the beam-plasma discharge, J. Geophy Res 84, 7271 (1979).

2. I.L. Kofsky, D.P. Villanucci, and R.B. Sluder, Evaluation of Infrared Simulation Data, DNA 5521F (26 Nov 80).

3. B.N. Maehlum, K. Maseide, K. Aarsnes, A. Egeland, B. Grandal, J. Holtet, T.A. Jacobsen, N.C. Maynard, F. Soeraas, J. Stadsnes, E.V. Thrane, and J. Troeim, Polar 5 -- An electron accelerator experiment within an aurora, Papers 1-4, Planet. Space. Sci. 28, 259-319 (1979).

4. R.J. Jost, H.R. Anderson, and J.O. McGarity, Electron energy distributions measured during electron beam-plasma interactions, Geophys. Res. Lett. 7, 509 (1980).

5. G.R.J. Duprat, B.A. Whalen, A.G. McNamara, and W. Bernstein, Measurements of the stability of energetic electron beams in the ionosphere, J. Geophys. Res 88, 3095 (1983).

6. S.T. Lai and H.A. Cohen, Electron Beam Trajectory in a Photometer Field of View, AFGL-TR-83-0045, 1983, AD A131949.

7. Instruction Manual for Photometer Model VI-06, Visidyne (Burlington, MA) Report VI-572, November 1980.

8. R. H. Eather and D.J. Reasoner, Spectrophotometry of faint light sources with a tilting filter photometer, Appl. Opt. 8, 227 (1969).

9. J.R. Winckler, Electron beams for magnetospheric research, Rev's Geophys. Space Phys. 18, 659 (1980).

10. P.M. Banks, C.R. Chappell, and A.F. Nagy, A new model for interaction of auroral electrons with the atmosphere: Spectral degradation, backscatter, optical emission, and ionization, J. Geophys. Res. 79, 1459 (1974).

11. A. Vallance Jones, Auroral spectroscopy, Space Sci. Rev's 11, 776 (1971).

12. T.L. Stephens and A.L. Klein, Electron Energy Deposition in the Atmosphere, (General Electric TEMPO, Santa Barbara, CA) GE-75-TMP-7, 1975.

13. D.C. Cartwright, S. Trajmar, A. C. Chutjian, and W. Williams, Electron impact excitation of N_2, Phys. Rev A16, 1041 (1977).

14. W.L. Borst and C. Zipf, Cross-sections for electron impact excitation of the 0,0 First Negative band of N_2^+ from threshold to 3 keV, Phys. Rev. A1, 834 (1970).

15. J.W. McConkey and I.D. Latimer, Absolute cross-sections for simultaneous ionization and excitation of N_2 by electron impact, Proc. Phys. Soc. 86, 463 (1965).

16. A.E. Hedin, C.A. Reber, N.W. Spencer, H.C. Brinton, and D.C. Kayser, Global model of longitude/UT variations in thermospheric composition and temperature based on mass spectrometer data, J. Geophys. Res. 84, 1 (1979).

17. H.E. Coffey, Geomagnetic and solar data, J. Geophys. Res. 87, 3628 (1982).

18. M. Imami and W.L. Borst, Electron excitation of the 0,0 Second Positive band of nitrogen from threshold to 1000 eV, J. Chem. Phys. 61, 1115 (1974).

19. C.B. Opal, W.K. Peterson, and E.C. Beaty, Measurements of secondary-electron spectra produced by electron impact ionization of a number of simple gases, J. Chem. Phys. 55, 4100 (1971).

20. I.L. Kofsky, R.B. Sluder, and D.P. Villanucci, Onboard radiometric photography of Excede Spectral's ejected electron beam, in Artificial Particle Beams in Space Plasma Studies (ed. B. Grandal), Plenum, New York, 1982, pp217-228.

21. P.W. Tarr, Arctic Code Electron Deposition Theory with Application to Project Excede, DNA 3636T, 18 Jun 75.

22. A. Konradi, W. Bernstein, D. Bulgher, J.L. Winkler, Jr., and J.O. McGarity, Laboratory studies of the beam-plasma discharge, abstract of paper at the (ESA) International Symposium on Active Experiments in Space, Alpbach, 24-28 May 1983.

23. K. Papadopoulos, private communication (1983).

24. R.E. Leadon, A.J. Woods, E.P. Wenaas, and H.H. Klein, An Analytical Investigation of Emitting Probes in an Ionized Plasma, Jaycor (San Diego, CA) Report J200-250A/2172, 1981.

25. J.R. Winckler, The application of artificial electron beams to magnetospheric research, Rev's Geophys. Space Phys. 18, 659 (1980).

26. L.M. Linson and K. Papadopoulos, Review of the Status of Theory and Experiment for Injection of Energetic Electron Beams in Space, Science Applications, Inc. (La Jolla, CA) Report LAPS 65, 1980.

APPENDIXES

BACKGROUND

In the course of the program PhotoMetrics participated in formal and informal conferences at AFGL on issues related to those addressed in the the SCEX and BERT-1 experiments, in connection with which we prepared and submitted the technical memorandums reproduced here. Some of this effort was in support of concepts for validating the performance of future spaceborne particle-beam weapons systems under the real conditions of low altitude orbits, which are being advanced in view of the expectation that the effects of vehicle charging, beam neutralization and return currents, outgassing, and collective interactions with the atmosphere will degrade alignment and integrity of ejected neutral and charged particle beams. (Reference is made to the fact that neutral-particle beams are accompanied by comparably intense fluxes of charged particles.)

Not reproduced here are reports on brightness and transport of MeV neutral beams, atmospheric beam applications, suggested laboratory measurements of arcing along surfaces of injection structures, and on a site visit to Johnson Space Center's Chamber A and Rice University's Department of Space Physics and Astronomy's electron beam interactions group (Houston, TX; air fare for these conferences was paid by PhotoMetrics). In support of the program's particle beam validation aspect, a PhotoMetrics staff member attended the DARPA Technical Interchange Meeting on Exoatmospheric Neutral Particle Beam Technology (17-18 Nov 1981, at Huntsville, AL), all expenses for which were paid by the company rather than contract funds. PhotoMetrics also participated in various beam-injection program planning and review exercises held by AFGL, in

particular those of 28-30 Oct 1981, 23 Jun 81 (at which we made a presentation reviewing optical diagnostics and monitoring in megavolt particle beam ejection experiments), and 10 Mar 82 (AFGL's Definition Study of High Energy Accelerators for Space Applications).

TOPICS

The specific topics covered in the attached Appendixes I-IX are as follows.

I. Optical sensing of water vapor outgassed from charge-ejection rockets. It is shown that the concentration of water vapor within the beam interaction volume can be measured from the radiance in spectroscopic emission features of H and OH excited by impact of electrons on H_2O molecules. This outgassing, which is almost invariably observed from sounding rockets, is expected to play an important part in ignition of discharges by injected particle beams and (through its serving as a source of secondary electrons, as described in Section II) in excitation of nitrogen molecule features.

II. Optical measurement of ambient N_2 densities, shown to be insensitive to the ratio of intensities of molecular bands.

III. Heating of the atmosphere by neutral particle beams from space vehicles, reviewed and shown to be small under all realistically-achievable injection conditions. (The concept had been suggested by an AFGL staff member.)

IV. Potential damage to spacecraft components from the charging-up of vehicle surfaces by impact of neutral particles.

VII. Status and application of the GEODSS satellite-tracking cameras (White Sands Missile Range, NM) in diagnostics of electron and ion beams injected into the atmosphere.

VIII. Review of interactions of charged-particle beams with the earth's atmosphere.

IX. Calculation of the magnitude of artificial enhancement of the ionosphere's electron density. The increase is shown to be small under achievable particle-beam conditions, with no clearly identifiable application to defensive systems.

APPENDIX I

NOTES ON OPTICAL EXCITATION OF WATER VAPOR BY ENERGETIC-ELECTRON IMPACT

Laboratory

Most of the emissions below 1 μm are from dissociation of H_2O into OH (3064Å, 2810Å A-X electronic bands), H (Lyman VUV-EUV and Balmer visible series), and O (8446 and 7774Å permitted multiplets, 1304Å resonance and 1356Å lines). The H_2O molecule itself does not have strong bands in this region, but does radiate in the infrared as discussed below. A general reference is J.J. Olivero, R.W. Stagat, and A.E.S. Green, J. Geophys. Res. 77, 4997 (1972). The cross-sections for exciting the ν_1, ν_2, and ν_3 bands of H_2O at 2.74, 6.27, and 2.66 μm in Fig 3 of that reference are incorrect and have been superseded in work reported by F. Linder and G. Seng, J. Phys. B9, 2539 (1976).

Electron impact on H_2O results in excitation of only the first, second and perhaps third vibrational state of the ground state of OH (Fujita et al., J. Phys. Chem. 86, 1427 (1982)). (Some of the H atom's Brackett and Paschen series lines are also seen in the NIR spectrum.) Thus only the Meinel bands originating from these low-lying vibrational states, rather than those from states up to 9 present in the chemiluminous airglow, appear in the electron-excited emission spectrum.

Atmosphere

Polar 5's photometer measured a $H\beta/N_2^+$ 4278Å ratio of about 1/10 (K. Maseide, abstract of 1981 NATO Advanced Research Institute on Artificial Particle Beams in Space Plasma Physics, (Geilo); this paper did not appear in the published Proceedings). This translates to a local relative concentration of about 1 H_2O per 4 N_2 molecules.

At EXCEDE: Spectral (7A, 3 kV; maximum altitude 128 km) the following features were seen/not seen:

Lyman series (<1216Å): No spectral coverage

OH 1,0 2810Å: Yes; OH 0,0 3064Å: No coverage

Balmer α, β, γ: Yes

OI 8446, 7774Å: No coverage (these lines are also directly excited from O_2 and O)

2.7 μm ν_1, ν_3: Yes; 6.3 μm ν_2: Yes

> ~17 μm rotational: Yes.

Profiles of altitude intensities in these features have not been quantified because the data are not yet adequately reduced. The Hβ/4278Å ratio from a spectrum in the visible at 118 km upleg also indicates 1 H_2O/4 N_2 molecules.

No other spectroscopic measurements have been made on electron beam excited water vapor in the upper atmosphere. The presence of substantial vapor pressures near rockets and satellites is well substantiated by mass spectrometer measurements on Shuttle Orbiter (G. Carignan, R. Narcisi) and other vehicles such as EXCEDE SWIR (Narcisi).

Selection of a Feature for Measurement

Most Lyman series lines of H are at wavelengths that cannot be isolated from O and N_2 fluorescence features by filter photometry. Spectrometers, whose lower throughput is not matched to the rapid changes in injected current and voltage planned for BERT-1, would not provide adequate signal/noise.

OH 3064Å is at least a factor 20 more intense than any of the other OH electronic bands. The feature lies between the N_2 Second Positive's $\Delta v = -2$ and $\Delta v = -1$ sequences, where the fluorescence background from other band systems is fortunately also extremely low. Plate 3 of Gaydon and Pearse's The Identification of Molecular Spectra (Chapman and Hall, London, 1965) shows this band as a contaminant in a laboratory discharge through N_2. Only modest effort is needed to make focusing optical systems at this wavelength. 3064Å is the prime candidate for onboard optical measurement of H_2 concentrations near sounding rockets.

Hα at 6563Å is overlaid by $\Delta v = 3$ N_2 First Positive bands, and Hγ at 4340Å by the 0,4 N_2 Second Positive band at 4344Å. Hβ at 4861Å is reasonably clear and is in fact used by ground-based photometers to assess the proton aurora. Its intensity is most likely 1/6 that of OH 3064Å. In fact, the Hβ/3064Å ratio is an excellent measure of the flux of soft (~<40 eV) electrons -- that is, of discharge phenomena --, perhaps even better than the 3914Å/3805Å measurement that we attempted at SCEX.

The O lines are also excited by electron impact on O_2 and O, and thus do not serve well to measure H_2O concentrations.

OH fundamental bands near 2.7μm are weak and require cooled radiometers, as do H_2O's 6.3μm and longer wavelength features. All these infrared vibrational bands have radiative lifetimes ~>20 millisec, which weakens the emission within the fast-moving fields of rocketborne spectroradiometers.

In sum: OH 3064Å is the most effective choice for onboard optical remote sensing of H_2O, and Hβ at 4861Å second choice.

PHOTOMETRICS, INC.

APPENDIX II

MEMORANDUM

DATE: 4 March 1983

TO: H.A. Cohen, PHG/AFGL FROM: I.L. Kofsky

SUBJECT: Determining Atmospheric N_2 Densities from Intensity Ratios of Electron Impact-Excited N_2/N_2^+ Band Intensities

This concept is appealing in principle, but in my judgment impractical to apply.

The figure on the left below (from Opal et al., J. Chem. Phys. 55, 4100 (1971)) shows the spectrum of secondary electrons from primary electrons impacting on N_2 molecules (essentially the same as on He atoms), on which I have overlaid the total cross-sections for excitation of the N_2^+ First Negative ($B \rightarrow X$) and N_2 Second Positive ($C \rightarrow B$) bands and the cross-sections for elastic scattering of electrons. Virtually all the Second Positive radiation is excited by secondaries of the ~1000 eV primaries.

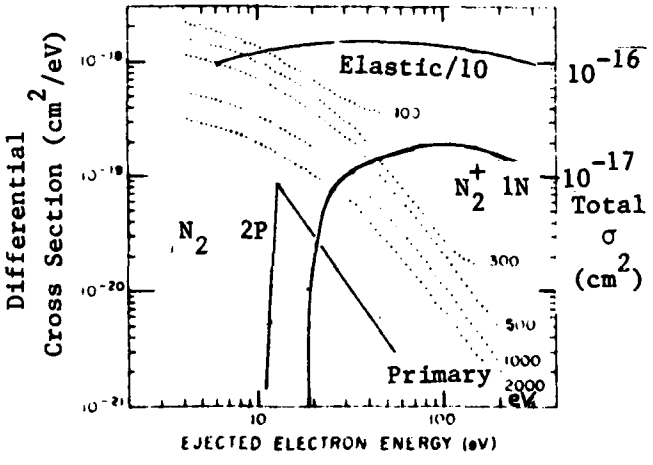

Fig 1. Helium spectra, integrated over angle, at several energies (in electron volts). Spectra are similar in shape ... ies considerably less than half the primary energy. The ... ctions have been normalized to an assumed 90° 100 eV ... attering cross section of 2.0×10^{-18} cm² sr

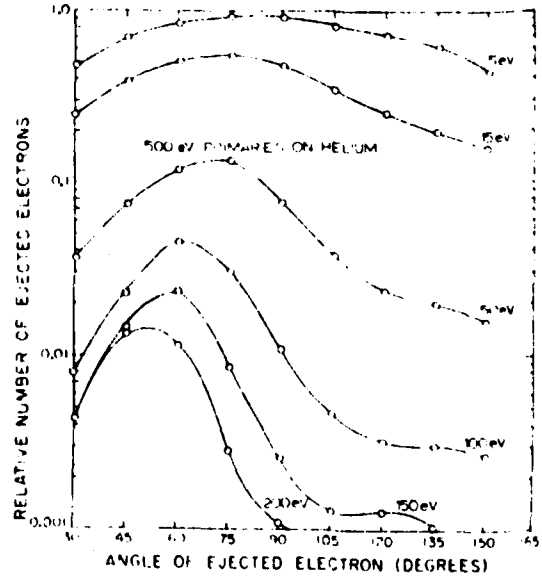

Fig 2. Angular distributions of electrons ejected from helium for several secondary electron energies (relative number of ejected electrons per steradian-electron volt). The angular resolution was about 15°. The peaks between 45° and 90° are due to conservation of momentum

Secondaries with kinetic energy >19 eV can also excite N_2^+ First Negative radiation, and since there are substantial numbers of the latter (as the graph shows, the probability of exciting a secondary with energy E_S decreases only with E_S^{-2}) in practice between one-third and one-half of the total First Negative radiation is due to impact on N_2 of secondary electrons.

The rate of production of all secondary electrons is proportional to [M], the local concentration of all atmospheric species. (More strictly speaking, it is about proportional to the total number of orbital electrons per unit volume, which in turn is about proportional to [M]). Consider only the excitation within a restricted volume, whose characteristic dimension is small compared to the collisional mean free path of either primaries or secondaries. This is the physical situation that applies to onboard-rocket measurements of irradiance from the glow, in which the effective viewed volume is a few meters on a side and the particle mean free paths are of the order of kilometers (molecular cross-sections $\sim 10^{-15}$ cm^2 x molecular densities $\sim 10^{10}$/cm^3).

The optical "signals" from the two band systems for a fixed primary current i are then

$$\text{Signal } (N_2\ 2P) \approx ai[M] \times [N_2] \quad \text{(all secondaries)}$$
$$\text{Signal } (N_2^+\ 1N) \approx bi[M] \times [N_2] + ci\ [N_2] \quad \text{(two sources)},$$

where a, b, and c are constants. Were it possible to keep all the First Negative emission within an instrument's filled field of view, $b[M]\ [N_2]/c[N_2]$ would turn out to be between 1/2 and 1; the uncertainties in cross-sections of competing collision processes (e + O for example) preclude improving the accuracy of this ratio of relative excitations.

Next let's look more closely at the actual trajectories of the secondary electrons and the excitation that lies within the fields of real photometers. The right-hand figure (also from the above reference) shows the angular distribution of the secondary electrons as they are ejected from air atoms. Note that the low-energy secondaries are ejected more or less isotropically from the track of the initial electron beam, and the higher-energy secondaries go more toward the beam direction. Clearly, the two band systems are not being excited in the same volumes of space: the First Negative clusters principally near the initial beam, while the Second Positive (and also the First Positive, B → A N_2 bands) comes from a wider volume. This effect shows clearly in color photographs of electron beams in air or N_2: a blue core is surrounded by a purple (blue 2P + red 1P) halo.

How can the irradiances produced at the photometer by this diffuse spray of poly-energetic electrons be calculated? Recall that the secondaries spiral around the magnetic field, with these in the 10 - 70 eV energy range that excites Second Positive having maximum radius of curvature of a few 10's of cm; they also elastically scatter off all molecules and atoms before exciting N_2 (see figure), and excite O and O_2 as well. (At the typically 200 km altitude at which the electron beam is ejected, $[N_2]/[M]$ is about 1/2.)

Clearly the problem calls for computer solution, most likely by a Monte Carlo procedure. Even with a detailed and careful calculation, however, errors in cross-sections (which lead to errors in the parameters b[M] and c above) and imprecision of the geometry and $[N_2]/[M]$ ratio would be likely to result in substantial uncertainty in the calculated relative irradiances from the two band systems. As a result, the $[N_2]$ profile information extracted from the ratios of in-band irradiances (or of radiances, if small field, imaging-detectors (cameras) are employed) is unlikely to be more accurate than extrapolations aided by theoretical modeling.

In summary, while the ratio of irradiances in Second Positive and First Negative bands is useful for assessing departures of the secondary-electron spectrum from the impact-excited distribution shown in the left-hand figure, quantitative $[N_2]$ profiles cannot be effectively extracted because of the inherent imprecision of the necessary supporting calculations.

PHOTOMETRICS, INC.

APPENDIX III

MEMORANDUM

DATE: 18 January 1982

TO: Lt. R. Davis, AFGL/PHG

FROM: I.L. Kofsky, PhotoMetrics, Inc.

SUBJECT: Heating of the Atmosphere by Neutral Beams ("Snowball")

I have made some simple and approximate calculations of the amount of atmospheric plasma production and heating that could be expected from neutral particle beams of the intensities currently planned from spaceborne accelerators. The conclusion is, that the irradiated air's fractional ionization and temperature rise are insufficient to produce any collective "snowball" effect such as mentioned in your memo of 04 Jan 82.

The detailed calculation is reasonably complex and looks to be an interesting exercise -- you may want to try it, to develop scaling rules. In any case, I'd appreciate some check on my method.

I started with the canonical threat, as follows.

- -- 1 ampere of H, 100 MeV/particle
- -- 4000 cm^2 area natural spread after propagating ~1000 km (this area turns out to be uncritical)
- -- 1 sec pulse length (6×10^{18} particles/pulse, 2.5×10^{-5} kilotons total energy).

In addition I neglected any effect of lateral movement of the beam due to the spacecraft's motion in its 1 sec duration, which of course would have the effect of lowering the dose deposited in a unit volume and thus reducing the plasma density.

I considered two segments of the particle trajectories, when they make their first atmospheric ionizations and near the end of their range. Near their first ionizations horizontal diffusion of the target air during the 1-sec pulse spreads out the energy input, and near the end of the particles' range their lateral spreading due to multiple Coulomb scattering lowers the flux densities. Curiously in each case the spread is about 200 meters laterally. The rate of ionizing-exciting energy loss by 100 MeV H atoms is 6 MeV per gm/cm^2 (3×10^{-16} ev cm^2/target particle) and a peak rate of 1000 MeV per gm/cm^2 is reached at 0.32 MeV (at which energy a nadir-directed beam has penetrated to 40 km altitude in the atmosphere).

100 MeV atoms. The aforementioned rate of energy loss indicates that the first ionizations take place near 100 km. At this altitude the diffusion coefficient D in the undisturbed atmosphere is about 10^8 cm^2/sec; thus the rms lateral transport of molecules $(4Dt)^{1/2}$ is 20000 cm in 1 sec. The effective area in which the beam deposits energy is therefore 4×10^8 cm^2, so the specific energy deposit is

$$(3 \times 10^{-16} \text{ eV cm}^2\text{/target particle}) \times (6 \times 10^{18} \text{ H atoms}/4 \times 10^8 \text{ cm}^2) = 4 \times 10^{-6} \text{ eV/target particle.}$$

This is very small indeed, resulting in a temperature rise of less than 1/10 degree K and a fractional ionization $\sim 10^{-7}$.

1 MeV protons. The incoming beam then 1) multiply Coulomb scatters to spread over a much larger area and 2) having become charged, is bent in the earth's magnetic field. For the record, the Larmor radius of a 100 MeV proton directed perpendicular to the field is 16,700 meters, and when the energy falls to 1 Mev it is 1670 meters. The beam is thus bent many km from its initial path before stopping.

The mean spreading of protons in the atmosphere during slowdown is undoubtedly calculated somewhere, but I couldn't find any reference. I made an approximate calculation with Moliere's formula

$$\Theta_{rad}^2 = 0.157 \times Z^2/A \times t_{gm/cm}^2/E_{MeV}^2,$$

where Z^2/A (= 7/2 for N_2) are the atomic number and weight of the scattering species and t the thickness traversed. The result is again a spread of some 200 meters. (This is much larger than the diffusion length at 40 km altitude.) Since specific ionization increases by a factor 160 between 100 MeV and $\sim$ 1/2 MeV, the energy deposit is $\sim 10^{-4}$ eV/target particle. I would expect this small figure would be further reduced somewhat by range straggling of the protons.

Wrapup: The spread of either 1) the irradiated air or 2) the initial now-ionized hydrogen atom beam reduces the energy deposited per molecule of atmosphere to well below that required for collective stopping effects, for 6×10^{18} -particle 100 MeV beams. Note that the result doesn't depend on the area of the beam from the accelerator before it strikes the atmosphere, provided that area is less than about $(100)^2$ $meter^2$.

PHOTOMETRICS, INC.

APPENDIX IV

Memo to: H. A. Cohen, AFGL/PHG 17 December 1981

From: I. L. Kofsky, PhotoMetrics

Subject: a) Chargeup of Spacecraft Irradiated by Neutral Particle Beams
b) Implications for Future Research of the "Charging" Damage or Kill Mechanism

It doesn't seem to be generally appreciated that irradiation by neutral particle beams produces a net surface charge on target spacecraft, and that the magnitude of this chargeup depends on the energy of the incident beam. If chargeup can be qualified as a mechanism for kill or damage of complex military targets, it will probably turn out possible to use much lower energy neutral particle beams -- 1 MeV or even less -- than presently in DARPA's current concept for weaponization. Thus the whole direction of the NPB thrust would be changed.

However, until we have some firm ideas about how the chargeup phenomena affect spacecraft systems we won't have much credibility with the missile/satellite defense community. While charge ejection may have done serious damage at Scatha, you don't have any reliable scaling to what will happen to hardened electronics. I would suggest some tests in space chambers to get some further ideas about the mechanisms by which surface charging can impair performance of military circuitry.

Here are the principal mechanisms by which an initially neutral energetic particle beam charges surfaces.

1) Sputtering. Both positive and negative ions are sputtered off (as well as neutral atoms). Absolute yields depend in a non-simple way on the ionization potential and electron affinity of the target atom, and at keV incident energies of the incident atom; this means that differential chargeup (with potential lateral sparking) can result when adjacent different materials are irradiated.

Since H atoms mass-mismatch most atoms present in the first few atom layers of spacecraft surfaces, the sputter yields of atoms are low at 10's keV incident energy -- of the order of 10^{-3}. For Li the mean yields would be an order of magnitude higher, with negative ions where electron affinities are positive because alkalis are good electron donors. I made a brief search for sputter yields at multi-Mev incidence, but so far I haven't turned up anything on the energy scaling; you may want to assign Davis to sort out this issue.

2) Secondary electron emission. The yield depends on material properties, so again some differential chargeup would result. This topic also merits investigation/quantitation by your staff.

3) Forward knock-ons. This looks to be rather difficult to calculate, and I doubt that there exists much experimental data about it. In any case, the target will have protuberances of thickness less than the range of the incident particle, and as the particle passes out not only will it be (perhaps multiply) charged but it will be accompanied by a spray of ions and atoms and "secondary" electrons. All this is over and above the meson and electron-positron and proton shower that Prof. Olbert reminded us of, which sets in at about 200 MeV. Stating this somewhat differently, those particles that pass through the target are likely to produce rather unpredictable surface-spacecraft charging effects. The secondaries come out with generally high energies, so they aren't likely to return to discharge the vehicle.

I should point out that these knock-on phenomena take place at surfaces in the interior of the vehicle also, for example on electronic chips, when the incoming beam particles penetrate that far. This might be a more effective damage mechanism than the bulk energy deposition being considered in the millions - $ programs that we heard about at the recent meeting. In this regard, it is also worth pointing out that some surface charging of electronics takes place under bombardment by other ionizing radiations, so it is highly possible that the effect may already be included in existing lumped-parameter TREES measurements/data.

It is instructive to estimate what the magnitude of the charging might be. The canonical threat is something like 10^{14} H atoms per cm^2 sec. Taking the net yield of charged particles emitted from the surface as 10^{-2}, we get 100 nanocoulombs per cm^2 each second. Over a 1 m^2 area, it's as if the object is emitting one milliamp.

I believe it would be useful to learn how this exterior charging scales with the energy of a neutral H or D or Li beam. I expect that a little library investigation would show that there is a maximum at hundreds of kilovolts, which changes completely the kind of accelerator technology needed to make space weapons (provided, of course, that chargeup of surfaces represents a real threat to ICBM's and other putative targets).

PHOTOMETRICS, INC.

APPENDIX VIIa

MEMORANDUM

DATE: 26 January 1981

TO: H. A. Cohen, AFGL/PHG FROM: I. L. Kofsky

SUBJECT: Long-Focus, Fast Cameras Available at Stallion Site, White Sands Missile Range

I have investigated the "GEODSS" optical satellite tracking capabilities at WSMR for potential application to imaging the particle beams from BERT-2. The array of cameras, which are normally applied in military satellite surveillance, would appear to be unmatched by those at other potential rocket launch sites. Some of these video cameras were used to image PRECEDE, and R. Sluder arranged for their operation at SCSR-I. Individuals in charge of the two independent facilities are listed after the technical data.

Available Cameras – Specifications

A. Lincoln Lab Experimental Test Site – largely developmental.

2 each
31 inch diameter
f/5 165 in $f\ell$, 1° field or
f/2.5 83 in $f\ell$, 2° field

14 in diameter, coaligned w/31 inch unit
f/1.7 7° field.

Image plane has 700 lines across field
Noise equivalent radiance ~ 2 kR at f/2.5
Scan rate 0.5°/sec maximum
Tracking under computer control, no current real-time connection to any radar capable of tracking a WSMR rocket. However an automatic (image analysis-based) tracker is due to go on line shortly
Astronomical mount for telescopes
Low Light Level video imagery
Elaborate computer control and image processing.

B. GEODSS Site – to be operational April 1981 (Provisional data)

3 each Same dual system, except the larger telescope has a 40 inch aperture. Also no radar connection. Photometric calibration somewhat questionable.

TOTAL: 5 dual telescopes/cameras.

Technical

The angular velocity of A31.603's (SCSR-I) trajectory from Stallion is shown in the attached graph. The rate of change of angle is always a factor > 2 less than the maximum allowable for manual or automatic tracking. If BERT-2 has a similar trajectory it would be readily followed by these narrow-field cameras.

Taking 700 lines across the 1^{o} field for a high contrast target (Lincoln data), we find a spatial "resolution" of ~6 meters when the rocket is at 200 km from the camera. While 6 meters is worse than the resolution we'd want, and on the edge for checking Strickland-Jasperse's ideas, I doubt that faster telescopes will be identified near any practical rocket launch site. The nominal seeing limit at that range due to atmospheric turbulence is 2 meters.

Brightness limitations of the glows may force the use of the f/2.5, 2^{o} field option. In this case lateral spatial resolution becomes 12 meters at 200 km rocket range. Berger-Jasperse-Strickland single-particle theory indicates a narrow ~5 keV electron beam grows to ~ 50 m in diameter in the E (and F) region.

The 1^{o} field does not encompass the full electron beams deposition at any altitude above ~120 km. Multiple small-field cameras would allow imaging of the rocket region at several positions along the beam. Multiple images of the same area permit coadding to improve signal/noise. In sum, good use can always be made of each of the 5 cameras.

Cost of achieving real-time tracking of the camers by WSMR rocket-tracking radars is not yet determined.

PHOTOMETRICS, INC.

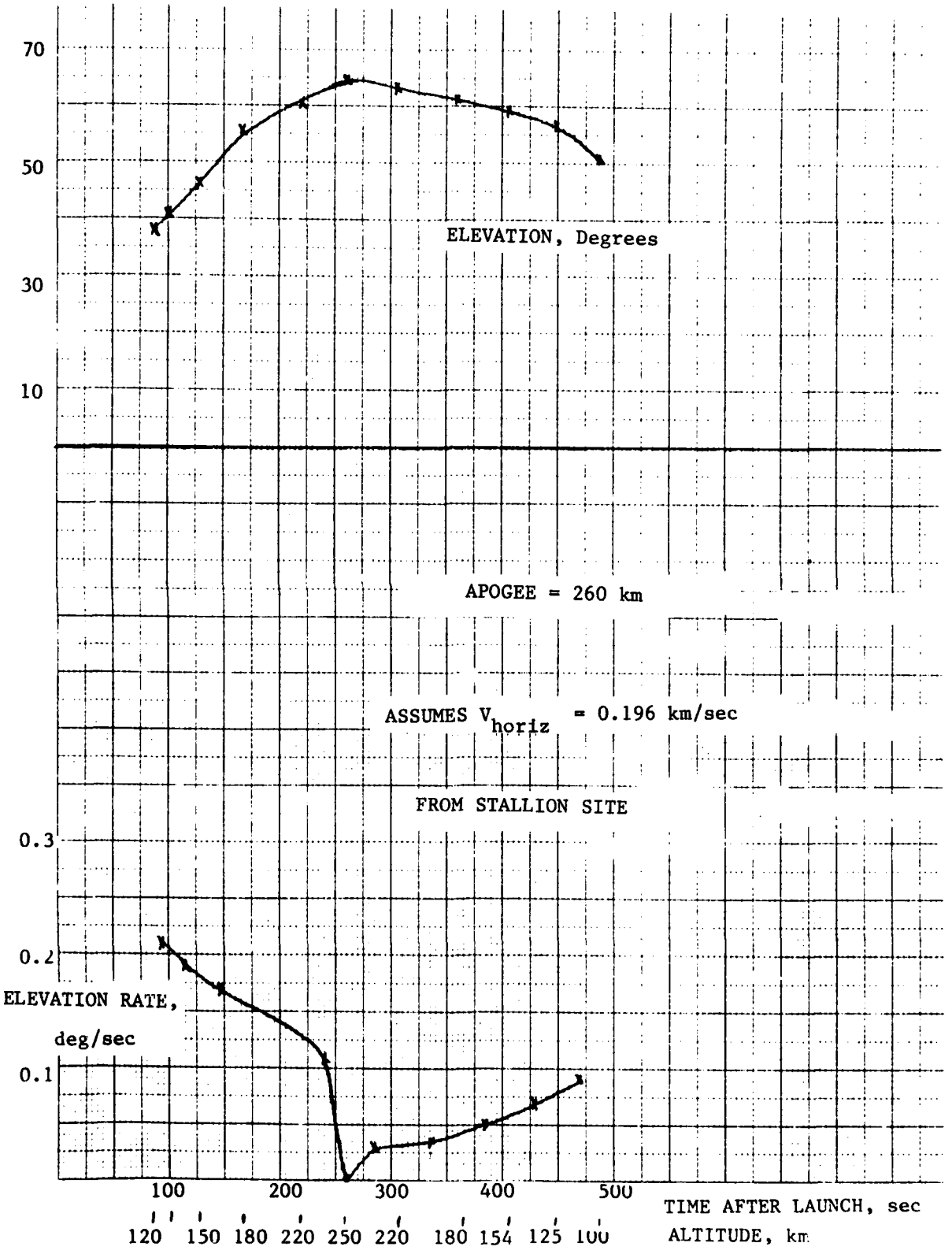

PHOTOMETRICS, INC.

APPENDIX VIIb

MEMORANDUM

DATE: 23 February 1981

TO: H.A. Cohen, AFGL/PHG FROM: I.L. Kofsky

SUBJECT: Visit to GEODSS Stallion Site, NM, 6 Feb 81 (night)

Please refer to memorandum of 26 Jan 81 for background on the application of the Lincoln Laboratory experimental and USAF operational cameras for imaging BERT-2 electron and ion beam excited glows.

Contacts: Richard Ramsey, LL
David Beatty, who tracked one camera-telescope for PRECEDE-II, 23 Dec 77
Howard M. Rathjen, Site Manager for TRW.

As the TRW site was not yet in operation, I was unable to arrange an evening tour. TRW is making a big marketing issue of their running GEODSS astrometrical cameras, have printed up a slick six page brochure promoting new business. I judge it will be necessary to go through Air Force channels to get useful cooperation from them.

The TRW cameras (there are 2 40 inchers, rather than the 3 I stated in my previous memo) have much higher tracking rates (3-6°/sec) than Lincoln's, and can follow the rocket easily. Lincoln (½°/sec) can also follow if the trajectory is similar to SCSR-I. The TRW cameras have about 1/10 the exposure "speed" of Lincoln's, as they have a weaker and less noisy image amplifier for compatibility with automatic moving-image tracking computers. They scan at 1.8 Hz (not 30).

The two Lincoln cameras have a 2:1 electronic zoom that has the effect of increasing (worsening) the effective f/number by a factor 2 to gain a factor 2 in magnification. Its automatic image follower is still "in preparation" (contact: Dr. Andrew Wandrop Jr, x7843).

Important: LL's current video receiver has considerable image blooming, which is a benefit in tracking stars and satellites (image dimension providing a direct measure of stellar magnitude) but a severe drawback if the lateral dimensions of the air-fluorescence streak is to be determined to test Strickland-Jasperse's beam energy deposition model. Fortunately the camera is to be replaced soon by a CCD array. I will follow up with Lincoln.

PHOTOMETRICS, INC.

APPENDIX VIII

MEMORANDUM

DATE: 30 December 1980

TO: H.A. Cohen FROM: I.L. Kofsky

SUBJECT: Interactions between Charged-Particle Beams and the Earth's Atmosphere -- Technical Issues and Required Measurements

Scenario. A capability to eject from space vehicles high-currents of ~3 - 3000 keV electrons, ions of various masses, and also neutral atoms will be developed in the next decade. Questions exist about the propagation and stability of these particle beams as they interact with the atmosphere and magnetosphere, as outlined here. Our discussion will focus on the issues of longitudinal and transverse transport of the initial beam energy, with a view toward military applications, rather than on use of charge ejection for geophysical characterization per se (as exemplified by electron echo, E-parallel-to-B, "anomalous resistivity" and RF wave generation experiments). Recommendations for optical and other diagnostic measurements on ejected beams follow an outline of currently identified technical problems.

1. Issues

1.1 Potential DoD Applications

The major currently-perceived DoD applications of ejected particle beams, other than direct spacecraft-system damage, are

- mapping of the geomagnetic field, by measurements in conjugate areas
- simulating the excitation of the atmosphere by energetic charged particles emitted from nuclear explosions, which produces radiation at various infrared wavelengths that presents increased background and clutter to IR surveillance systems (the "Excede" concept)
- serving as antennas for VLF-ELF radiation, potentially for communication with submarines (the conducting path substituting for a long metallic wire)
- producing directly ionospheric "blackout," electromagnetic wave-reflecting layers, and also false infrared targets

- triggering aurora, which has the effect of producing the aforementioned blackout and redout phenomena.

The first two applications relate to mitigation and production of effects on military systems of strategic high-altitude nuclear explosions. For example, a knowledge of the geomagnetic field configuration and the boundary of closed field lines would be needed to plan location of explosions that would result in excess ionospheric electron densities near the conjugate region, to produce radiofrequency communications and radar blackout. The Excede concept, which is funded by the Defense Nuclear Agency, is relatively straightforward; spectrometers and radiometers onboard the charge-ejection rocket measure the spectral yield in wavelength bands of detection-discrimination systems.

The antenna application is still in the concept stage, and to our knowledge has not received official support from DoD. It was tried, with indifferent results, on NASA rocket 27.010 AE (08 Apr 78), by frequency-modulating a 4 kV, 60 ma beam. Direct production of radiocommunications or radar blackout requires ~megawatts of deposited energy, and so appears impractical (please refer to the accompanying memo dated 23 Dec 80). On the other hand, the concept of producing a short-lived reflecting or refracting ionospheric layer for over-the-horizon communication or radar probing, or a false infrared-emitting target that might impair performance of an IR launch or satellite detection system, may prove to be of future interest. The idea of "spoofing" or "decoying" infrared surveillance or tracking systems with moving patches of radiating atmosphere has particular initial appeal.

Triggering of aurora (precipitation into the atmosphere of ~5 keV electrons) by introducing instabilities and turbulence in the magnetosphere is also an experimentally untried concept, although much theoretical work has been done. Further attempts to introduce instabilities by releases of plasma clouds – in particular, with barium ions – are scheduled (Firewheel is an example).

We note that further findings about the properties of the particle beam-atmosphere interaction may elicit other applications of this technology. The applications listed above are merely those that have so far surfaced.

1.2. Technical Issues

At present no accurate prediction can be made of the energy and spatial distribution of beams traversing the magnetosphere or ionosphere. Additionally there is only rudimentary understanding of the disturbances they produce in the ionosphere-magnetosphere, for example by exciting return currents. In brief, reliable descriptions of where the beam energy will go, how much infrared-radiation

and radiofrequency power it (and the disturbed ionosphere) will generate, and how much it will be accelerated or decelerated by electric fields, cannot now be made.

1.2.1 Beam Origin

In many cases an ejected beam of particles of a single charge is not monochromatic before "interacting" with the atmosphere or magnetosphere, for the following reasons. A discharge of some kind usually develops to assist the back flow of ambient plasma in maintaining the vehicle at the typical ~100 V potential (unless the spacecraft is artificially neutralized, as noted below); thus excess slow electrons are injected into the flux tube along with the beam. If, as postulated for moderate- to high -current conditions, there develops a beam-plasma discharge of the type clearly identified in laboratory low-pressure tanks, the beam will be "heated"; that is, it will contain not only secondary electrons of energy comparable to the ionization potential of N_2, O_2, and O, but also be spread about the initial accelerator potential toward both higher and lower energies. The effect of the two heating phenomena is shown in the figure attached.

In short, neutralization and secondary-production processes in the vicinity of the ejection vehicle degrade the "initial" beam. This degradation can be minimized by ejecting charge of the opposite sign, or better still plasma, from the spacecraft. Nonetheless it is necessary that the input energy spectrum be known to remove confusion between "source" - and "interaction" -generated processes.

1.2.2 Linear Processes

There exist at least six theoretical models of individual-particle transport in the atmosphere, which consider multiple Coulomb scattering by atomic nuclei, production of secondary electrons (ionization) by direct impact, and magnetic confinement. Most recently, one of these models, developed under support of AFGL, has predicted a factor 3 less lateral spreading than the various others (paper SA 56, EOS 61, 1060 (1980)). There appears to be sufficient uncertainty in some of the basic interaction cross-sections, and in the computational methods and approximations, to result in this large a discrepancy.

The occasional delay of electron echoes from magnetic mirroring at the conjugate hemisphere (seen in the ARAKS program) represents a second type of uncertainty, which is perhaps due to deceleration by magnetospheric electric fields.

1.2.3 Nonlinear Processes

As noted in Section 1.2.1, nonlinearities in the neighborhood of the particle accelerator have the effect of spreading the distribution of energies of the beam particles. By "nonlinearities," we mean physical phenomena that impact the beam's energy and spatial distribution not proportionately to the current and primary acceleration voltage, or to atmosphere-ionosphere parameters such as neutral species and ion density and local magnetic field strength and gradients. Discharges, space charge limiting, and ionosphere depletions are all examples of nonlinear phenomena.

At issue is the extent to which nonlinear processes affect the trajectory of the beam at distances from the spacecraft large compared to some characteristic "origin" dimension: the volume of ionosphere from which the neutralizing charge originates, the range to the first focusing node ($\sim$ 35 m in the ionosphere for 10 keV electrons) or perhaps the spacecraft's length.

Transverse and longitudinal spreading due to mutual repulsion represent one type of nonlinearity. Ab initio calculations are inexact because of the shielding provided by the ambient and beam-induced ionosphere. In near-relativistic beams – for example, of $\geq$ 1 MeV electrons – the magnetic force between charged particles in large part compensates the lateral electrostatic repulsion.

Beams of sufficiently high current and energy deposition rate heat the local atmosphere to "blowout," to make a short-lived low-pressure channel for propagation of later-arriving particles. This principle is applied in beam-weapon systems. While it would appear improbable that the power levels needed to achieve this extreme condition would be soon reached by space-borne accelerators, heating begins to deplete or even (by convection) enhance the deposition path when the fractional ionization density reaches 10^{-4}. The charge passing a unit area needed to achieve this condition is 2×10^{13} 100 keV electrons/cm^2 or 2×10^{12} 3 keV electrons/cm^2. That is, about 1 microcoulomb – 1μA for 1 sec – passing through a 1 cm^2 area of air deposits sufficient energy to heat and so expand the volume, changing the ambient air density encountered by the later-arriving particles.

2. Measurements

2.1. Onboard

A characterization of the particle beam's energy spectrum and angular and spatial distribution before it begins to interact with the atmosphere is needed in order to clarify and quantify the interaction

processes. That is to say, the "input" function must be measured or otherwise known if the interaction phenomena are to be sorted out from the phenomena that accompany beam production and ejection from the spacecraft.

What this means is, that measurements on the beam should be made from the spacecraft as well as from remote stations. Specifically, the usual measurements of backscattered electron and ion energy spectra, vehicle potential, return current distributions, plasma densities and temperatures, and RF spectra, along with extensive optical diagnosis (more on this momentarily) would be made from the spacecraft. If practical these in situ and remote-sensing measurements would also be made from daughter vehicles, tethers, or long booms, to map out conditions near the accelerator.

For example, the energy spectrum in the beam could be sampled by probes of dimensions much smaller than the Larmor radius placed, say, 20 meters from the ejection spacecraft proper. A measurement that provides somewhat similar but definitely less precise data is the spectrum of continuous and discrete x-rays excited in small (again compared to the Larmor radius) high-Z targets by the beam particles. The bremsstrahlung and line radiation intensity, appropriately unfolded, provides a measure of the beam's spectral distribution (as in the recent tank experiments by Jost et al).

Electron beams are not self-luminous, and thus not observable optically until they impact ambient (or spacecraft-generated) atoms. Geometries can be envisaged in which the atmosphere below an orbiting spacecraft or sounding rocket, where the beam impacts, could be viewed from onboard – in particular, Space Shuttle could readily achieve this capability.

Some ions, on the other hand, would be self-luminous by virtue of their emission from metastable states excited in the discharge of the source. The velocity distribution in the ejected ion beam could be determined by Fabry-Perot interferometry of these emission lines. This measurement, which is also within the capability of Shuttle (optical Fabry-Perot interferometers are planned for ionospheric wind measurements, for example), would determine the distribution in speeds of ejected ions, which are expected to be "spread" because of space charge repulsion.

Several of the remote measurements on the beam noted in the subsection following could be made from onboard, or from daughter vehicles or shuttle "free fliers," as will become apparent from the discussion. Additionally, there is a possibility for observations from vehicles guided to intercept the beam path to measure in situ the free electron density distribution produced by the energetic charged particles; as this type of operation is expensive and chancy, we do not consider it further here.

2.2 Remote Measurements

2.2.1 Imaging

As the critical measurement type is images of the air fluorescence excited by the beam, we discuss this topic first. To date, the cameras deployed for this purpose have been with one or two exceptions (principally, the GEODSS units) less than optimum in sensitivity and angular resolution. What is needed is an angular resolution that will permit measurement of the beam's "diameter" and (more strictly applicable) transverse radiance distribution each ~ 5 meters. More than one camera (or time-sharing of one large camera) might be needed to accommodate the full length of the energy-deposition streak, which is typically 20,000 meters. In a sense, the spacecraft or sounding rocket should be moved to the location of such telescope-cameras, rather than attempting to procure the camera(s) for the beam-interaction experiments.

Specifying the camera further, we would require 1) radar tracking to maintain the beam in the narrow field needed to achieve this order of resolution; 2) image intensification in the image plane; 3) a focal length of at least 1 meter to spread the image sufficiently across this plane; 4) radiometric calibration. Also needed is thorough calibration of the spread function of the camera system, and of its hysteresis (image-sticking) properties. From the measured spread function as a function of irradiance or fluence at the image plane, and the initial data, the "width" of the beam can be deconvolved.

We note also that the camera(s) should have sufficient sensitivity to record the end-point range of the beam. This is important because the aforementioned "hot" primary electrons have increased penetration. Radiometric calibration permits the brightness distribution in the streak's long direction to be determined. From this brightness distribution the initial energy distribution in the beam can be deconvolved (in principle, at least).

To summarize, the prime measurement is quality imagery. The beam should be located where precision optical measurements can be made by $1- 10M-class telescope-cameras. The camera is not an adjunct of the experiment, but rather is the heart of it.

2.2.2 Other Optical Diagnostics

The spectral distribution of the air excited by the beam provides another measure of its energy distribution. A second prime instrument would be a slitless wavelength-dispersing spectrograph, oriented so that the beam itself forms the slit (much like was

done with chemical release trails). This instrument would also be radar tracked to hold the beam in a single position and so build up signal/noise. The spectral range should extend from 0.35 to 0.45μm, to encompass the main features of the N_2^+ First Negative and N_2 Second Positive band sequences. The ratio in these features is a measure of the "temperature" of the beam. (This is the issue currently being worked on by M. Chamberlain of PhotoMetrics, for potential application to SCEX.)

This measurement could also be made with telescope filter photometers, as has to some extent been done in the Excede series. The higher throughput of these instruments is in part compensated by their limited number of spectral features resolved (two, or three).

The spectrograph should also have low scattered light, to permit measurement of any "plasma" continuum radiations from the beam volume. Further, the spectrometer or telescoped photometers would view serially along sections of beam, to isolate differences in spectrum as a function of penetration altitude.

We note that various other spectral features also transfer information about particle energy distributions. Most of these, however, either lie in wavelength regions attenuated by the atmosphere (the UV features of the N_2 triplet mainfold) or are not sufficiently spectrally isolated for absolute radiometry (most N_2 First Positive bands). This issue of selecting bands merits further consideration, particularly in light of the improving sensitivity of instruments that respond to infrared wavelengths transmitted by the atmosphere.

Additionally, many beam instabilities are accompanied or even manifested by brightness or irradiance "flicker" at frequencies under ~100 Hz. Ground photometry should have sufficient light-collecting area to resolve these temporal variations, preferably by viewing at individual positions along the beam (in N_2^+ First Negative band light).

2.2.3 Other Instruments

Instruments for diagnosis of backscatter from the atmosphere below the spacecraft or from the conjugate hemisphere have been applied in the Araks and Electron Echo experiments, and need little further description. As an example, electron spectrometers onboard the ejection spacecraft would be set up to measure the "echo" from downward-directed pulses of electrons or ions, so as to determine the backscatter intensity and velocity distribution. Daughter vehicles carrying similar spectrometers and plasma density/

temperature probes would determine the lateral distribution of the backscatter, that is, the drift or diffusion across the magnetic field lines. Another important measurement that should be made onboard (and where possible on daughter vehicles) is the angular distribution of the backscattered particles, to determine pitch angle degradation.

As is well known, the radiofrequency spectrum of the beam is a further critical diagnostic measure. Because of absorption (filtering) by the ionosphere, the RF data to date are at present somewhat ambiguous. More and better receivers are needed to achieve proper diagnosis.

Radar reflection is a further measure of ion-cloud parameters. However, since the data are usually so difficult to interpret, further planning would be needed to consider the effectiveness of this technology.

2.2.4 Laboratory Tank Experiments

A coherent program of measurements on beam-atmosphere interactions would entail a series of simulations and scaled-experiments in a large vacuum tank. This principle, which is certainly self-evident, has been adopted by NASA for its Shuttle beam-ejection programs.

3. Summary

We have outlined the perceived DoD applications of intense particle beams interacting with the atmosphere and magnetosphere, identified the principal propagation issues, and reviewed briefly the types of measurement needed to clarify the physical processes. Characterization of the "input" beam is needed to quantify the interaction. The principal diagnostic remains optical imaging (and spectroscopy, which also involves imaging), which for full effectiveness requires telescope-cameras of throughput considerably higher than generally applied in the past. Measurements from onboard the spacecraft and/or daughter vehicles complement those made from ground stations.

Attachment

PHOTOMETRICS, INC.

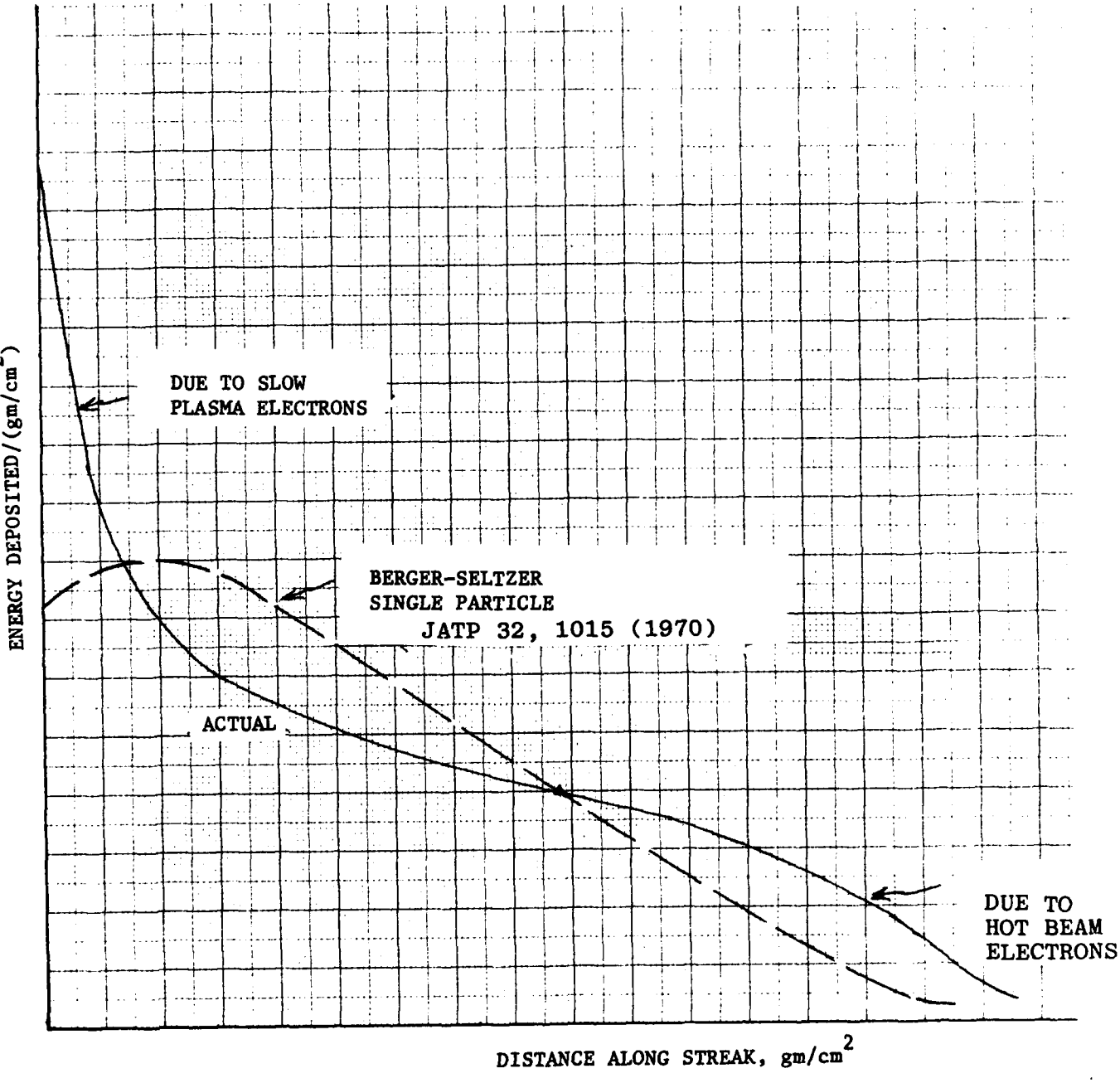

APPENDIX IX

PHOTOMETRICS, INC.

MEMORANDUM

DATE: 23 December 1980

TO: H.A. Cohen FROM: I.L. Kofsky

SUBJECT: Artificial Ionosphere Enhancements Produced by Deposited Electron or Ion Beam Energy

1. Plasma density increases and their effects on communication at all frequencies -- HF in particular -- was a major issue in nuclear explosion effects up to perhaps 5 years ago. Gradually it was recognized that the path and link redundancy of the DoD communications network made "strategic" nuclear bursts designed for this purpose ineffective. The matter is not now under active consideration, the only element of it still thought important being F-region plasma irregularities, which impact UHF-VHF satellite communications (hence barium releases by DoD). I doubt that interest could be developed for the small-scale enhancement of the E or F region that, practically speaking, could be produced (see 3), below).

2. On the other hand there might be interest in a short-lived artificial ionosphere off which over-the-horizon communications or radar waves could be bounced. AFGL is actively working in OTH radar detection.

3. The energy needed is beyond that achievable in practice. To cover even so small an area as $(31\ km)^2 = 1000\ km^2$ to the necessary D-region density of 10^5 electrons/cm^3 in a 20 km altitude layer takes 1 megawatt. Specifically

a) electron density $= \sqrt{\frac{\text{ion pair production rate}}{\text{effective recombination coefficient } \alpha}}$.

$\alpha = 10^{-6}\ cm^3/sec$ in the D region; therefore

production rate $= (10^5)^2 \times 10^{-6} = 10^4$ pairs/cm^3 sec.

b) Power input into the $20 \times 10^5 \times 10^3 \times 10^{10}\ cm^3$ volume =

$$\frac{10^4 \text{ pairs}}{cm^3 \text{ sec}} \times \frac{34 \text{ eV}}{\text{pair}} \times 1.6 \times 10^{-19} \frac{\text{W sec}}{\text{eV}} \times 2 \times 10^{19}\ cm^3 = \underline{\underline{10^6 \text{ watts}}}.$$

The enhancement is largely recombined about 20 sec after the beam has been turned off; it also takes about this time to build up, so that 10^6 watts must be input for at least 20 sec.

END

FILMED

9-84

DTIC